UNIVERSITY OF OKLAHOMA

GRADUATE COLLEGE

WELLBORE CLEANOUT IN INCLINED AND HORIZONTAL WELLBORES – THE EFFECTS OF FLUID RHEOLOGY, INCLINATION, AND SOLIDS DENSITY.

A DISSERTATION

SUBMITTED TO THE GRADUATE FACULTY

in partial fulfillment of the requirements for the

Degree of

DOCTOR OF PHILOSOPHY

By

SOHAM PANDYA

Norman, Oklahoma

2019

Downloaded from SHAREOK. Persistent Handle URL: https://hdl.handle.net/11244/321402

WELLBORE CLEANOUT IN INCLINED AND HORIZONTAL WELLBORES – THE EFFECTS OF FLUID RHEOLOGY, INCLINATION, AND SOLIDS DENSITY.

A DISSERTATION APPROVED FOR THE

MEWBOURNE SCHOOL OF PETROLEUM AND GEOLOGICAL ENGINEERING

BY

Dr. Ramadan Ahmed, Chair

Dr. Prakash Vedula

Dr. Subhash Shah

Dr. Catalin Teodoriu

Dr. Saeed Salehi

© Copyright by SOHAM PANDYA 2019

All Rights Reserved.

To those who inspired this work

and to those who will read it.

ACKNOWLEDGMENTS

The inspiration provided by people close to me has made this research a success. I would like to take this opportunity to thank my mentors, family, friends, and supporters of this research.

I would like to express my deepest appreciation to the committee chair, Dr. Ramadan Ahmed for his strong guidance and illuminating suggestions. He has been encouraging throughout my doctorate tenure and steered me in the right direction. Dr. Subhash Shah has the attitude and substance of a genius and his mentoring has been vital to my growth as a researcher. His guidance towards my Masters thesis laid a foundation and encouragement for me to pursue doctorate research. I thank him immensely for teaching me skills that have helped me contribute to the field of research in terms of technical writing and technical presentations.

Member of my dissertation committee has always been an encouragement through their work of research. Dr. Teodoriu Catalin has been a great advisor and his feedback has been always helpful in the advancement and betterment of the research. A special thanks to him for being supportive and providing special assistance during any unforeseen circumstances that could have been obstructive in research. Dr. Saeed Salehi has provided meaningful guidance to this research with his inspiring questions and constructive criticism. I would like to thank him for providing useful suggestions and fine-tuning of dissertation and presentation format in addition to technical information included in the research. This research involved the understanding of fluid dynamics and flow turbulence in addition to the oil and gas knowledge. Dr. Prakash Vedula has taught me the technical aspects of flow dynamics and particle flow in turbulence and I sincerely thank him for his time.

I would like to extend a special thanks to Jeff McCaskill for his technical support with lab equipment and providing me insights on the functional design of the experiment.

This acknowledgment would not be complete without thanking my family and friends, who supported me throughout my doctorate endeavor and encouraged my enthusiasm towards research. I deeply appreciate my parents and sister for their unending love and support and for providing for all my needs, financially and morally. They have served as an inspiration to me and encourage me to be the best at everything. A special thanks to my wife, Nidhi Desai-Pandya, who has supported me emotionally with her words of motivation throughout my doctorate tenure and for her patience and understanding. I would finally like to thank my friends who have always shown encouragement throughout my doctorate tenure.

Last but not the least, I would like to express my gratitude to Mewbourne School of Petroleum and Geological Engineering at the University of Oklahoma for supporting me through with scholarship and financial aid that has helped me maintain my focus in research.

TABLE OF CONTENTS

ACKNOWLEDGMENTS v

TABLE OF CONTENTS vii

LIST OF TABLES xi

LIST OF FIGURES xii

ABSTRACT xvi

CHAPTER 1 – INTRODUCTION 1

1.1 Problem Statement 2

1.2 Hypothesis 7

1.3 Objectives 7

1.4 Scope of the study 8

1.5 Structure of the dissertation 9

CHAPTER 2 – THEORY 11

2.1 Eccentricity in Annulus 13

2.2 Bed Erosion Mechanisms 16

2.3 Flow Patterns During Solids Bed Erosion 18

2.4 Effects of Various Parameters 22

2.4.1 Wellbore geometry 23

2.4.2 Wellbore Inclination 24

2.4.3 Fluid Velocity and Flow Regime 26

2.4.4 Fluid Characteristics 27
2.4.5 Solids Properties 29
2.5 Turbulence in Bed Erosion 31
2.5.1 Turbulent Shear Stress 33
2.5.2 Turbulent Velocity Profile 36
CHAPTER 3 – LITERATURE REVIEW 38
3.1 Solids Transport Under Steady-State Conditions 38
3.2 Bed Erosion Under Transient Conditions 43
3.3 Mechanistic Hole Cleanout Models 45
3.4 Computational Fluid Dynamics (CFD) in Bed Erosion 51
CHAPTER 4 – BED EROSION – EXPERIMENTAL STUDY 57
4.1 Design of Experiments 57
4.2 Experimental Setup 58
4.2.1 Support Assembly 58
4.2.2 Hoisting system 58
4.2.3 Test Section 60
4.2.4 Separator 60
4.2.5 Mixing System 60
4.2.6 Pumping System 60
4.2.7 Instrumentation and Data Acquisition System 61

4.3 Test Materials 61
4.4 Test Procedure 62
4.5 Definition of Parameters 65
4.6 Results and Discussion from Experimental Study 68
CHAPTER 5 – DIMENSIONAL ANALYSIS 77
5.1 Buckingham Pi Theorem (Dimensionless Parameters) 78
5.2 Model Development 79
5.3 Model Validation 82
5.4 Sensitivity Analysis 85
5.5 Model Implementation 90
CHAPTER 6 – CFD FOR PARTIALLY BLOCKED ANNULUS 95
6.1 CFD Model Description 96
6.1.1 Geometry 96
6.1.2 Meshing / Grid Generation 99
6.1.3 Governing Equations and Model Selection 104
6.2 Simulation Details 107
6.2.1 Setup and Post-Processing 107
6.2.2 Simulation Matrix 115
CHAPTER 7 – ANALYSIS AND MODELING 117
7.1 Velocity Profiles 118

7.2 Shear Stress at Bed Interface 122

CHAPTER 8 – CONCLUSIONS AND RECOMMENDATIONS 131

8.1 Conclusions 131

8.2 Recommendations 132

NOMENCLATURE 133

GREEK LETTERS 136

ABBREVIATIONS 138

REFERENCES 140

APPENDIX A – DERIVATION OF PI GROUPS 151

APPENDIX B – VELOCITY PROFILES FOR DIFFERENT FLUIDS AT VARIOUS BED HEIGHTS AND FLOW RATES 155

APPENDIX C – VELOCITY CONTOUR PLOTS – CONSTANT FLUID 158

APPENDIX D – VELOCITY CONTOUR PLOTS – CONSTANT FLOW RATE 160

APPENDIX E – BED SHEAR STRESS PROFILES FOR DIFFERENT FLUIDS 164

LIST OF TABLES

Table 4.1: Test matrix 61

Table 5.1: Π-Groups as formulated using Buckingham Pi method 79

Table 5.2: Values of constants (A to E) as used in Eq. (5.3) 80

Table 5.3: Correlation matrix – Effects of various parameters on $\boldsymbol{\Pi_1}$. 85

Table 5.4: Baseline values for sensitivity analysis 86

Table 6.1: Mesh statistics 101

Table 6.2: Skewness ratio range and corresponding cell quality (ANSYS® Meshing User's Guide) 103

Table 6.3: Properties of fluids used in the simulations 108

Table 6.4: Details of all boundaries defined in all flow models 111

Table 7.1: Input variables used in CFD Simulations 117

Table 7.2: Correlations for regression coefficients $\boldsymbol{\alpha_x}$ and $\boldsymbol{\beta_x}$. 129

LIST OF FIGURES

Fig. 1.1: Proppant bed formation after hydraulic fracturing (Li & Luft, 2014) 3

Fig. 2.1: Tagging of solids plug-in a vertical well section 11

Fig. 2.2: Eccentricity vs hole inclination (Data: Elsayed and Nasr El-Din, 2006) 15

Fig. 2.3: Eccentricity effect on annular pressure drop gradient 15

Fig. 2.4: Forces acting on a particle on the bed interface 16

Fig. 2.5: Forces acting on a solid particle in various well sections 18

Fig. 2.6: Schematic views of flow patterns and corresponding concentration profiles 20

Fig. 2.7: Solid transport mechanism in vertical and deviated wells (Bern et. al. 2003) 21

Fig. 2.8: Solids concentration in annular suspension flow for different sizes of drill pipe within 0.127 m (5-in.) hole. (data source- Becker & Azar, 1985) 24

Fig. 2.9: Effect of solids density of transport ratio (data source – Li & Wilde, 2005) 30

Fig. 2.10: Turbulent flow and eddy behavior 31

Fig. 2.11: Instantaneous velocity with time at any arbitrary location in turbulent flow 32

Fig. 2.12: (a) Velocity profile and (b) stress profile for turbulent and laminar flow 34

Fig. 2.13: Particle moving upward due to eddies 35

Fig. 2.14: Layers in a turbulent flow regime 36

Fig. 3.1: Cuttings concentration vs laminar fluid velocity (Tomren, 1986) 39

Fig. 3.2: Cuttings concentration vs hole inclination (Tomren, 1986) 39

Fig. 3.3: Effect of rheology and inclination on MTV (Ford et al., 1990) 41

Fig. 3.4: Sand holdup vs superficial velocity (Sayindla et al., 2017) 42

Fig. 3.5: Moving bed and streaks at the interface as observed by Kelessidis and Mpandelis (2004) 45

Fig. 3.6: Forces acting on the center of the particle protruding out of the bed. 46
Fig. 3.7: Critical transport comparison (Clark and Bickham, 1994) 49
Fig. 3.8: Mesh systems for concentric and eccentric annuli (King et al. 2000)..... 53
Fig. 3.9: Normalized velocity profile versus radial position (0=pipe; 1=well) 54
Fig. 3.10: Normalized velocity profile versus radial position for power-law (PL) and yield power-law (YPL) type fluids (0=pipe; 1=well) 54
Fig. 3.11: a) velocity contours and b) apparent viscosity contours for eccentric annulus with and without inner pipe rotation. (King et al., 2000) 55
Fig. 3.12: CFD Results vs Lab Data (Bilgesu et al., 2002)..... 56
Fig. 4.1: Schematic of the experimental setup (Pandya et al., 2019)..... 59
Fig. 4.2: Wellbore cleanout setup in an inclined position (Pandya et al., 2019) 59
Fig. 4.3: Rheograms of polymeric fluids (Data source: Pandya et al., 2019)..... 63
Fig. 4.4: Particle size distribution of HDP and LDP used in this study..... 64
Fig. 4.5: Typical Bed Erosion Curve 66
Fig. 4.6: Bed height calculation (Pandya et al., 2019)..... 66
Fig. 4.7: Bed erosion curves for different particle densities, cleanout fluids, and inclination angles. (Pandya et al., 2019) 71
Fig. 4.8: Bed profiles in inclined test section with different fluids: a) Fluid 1; and b) Fluid 3 (Pandya et al., 2019) 71
Fig. 4.9: Cleanout efficiencies of a) Fluid 1, b) Fluid 2, and c) Fluid 3 at various inclinations for high and low-density proppants at different flow rates (Pandya et al., 2019). 72
Fig. 4.10: Secondary flow pattern observed during erosion of HDP with Fluid 2 and at 60° inclination (Pandya et al., 2019). 73

Fig. 4.11: Comparison of the current measurements with model predictions of Ozbayoglu et al. (2004) 74
Fig. 4.12: Cleanout efficiency ratio versus inclination angle (Pandya et al., 2019) 76
Fig. 5.1: a) inner pipe completely covered; b) inner pipe partially covered (Pandya et al., 2019)81
Fig. 5.2: Cross plot for modeled prediction and experimental results of bed height. (Pandya et al., 2019) 82
Fig. 5.3: Bed-erosion curves from experimental data (Adari et al.) and predicted curves (from correlation) for 87° inclination. 84
Fig. 5.4: Effect of various parameters on calculated bed height through model. 89
Fig. 5.5: Effect of power-law rheological parameters on apparent viscosity of the fluid..... 90
Fig. 6.1: Flow geometries as generated in DesignModeler for four scenarios simulated..... 97
Fig. 6.2: Schematic of entrance length in pipe flow. 97
Fig. 6.3: Velocity profile and pressure gradient along the length of CFD model..... 98
Fig. 6.4: Meshing structures for four scenarios simulated. 100
Fig. 6.5: Pressure gradient vs element size of grids generated for bed heights. 102
Fig. 6.6: Skewness ratio distribution for each mesh case 102
Fig. 6.7: Comparison of pressure gradient from CFD simulation and analytical model. 104
Fig. 6.8: Different flow boundaries defined in all flow geometries..... 109
Fig. 6.9: Velocity contour plot a) across the axial length and b) at the outlet 113
Fig. 6.10: Flow velocity contour for the entire cross-sectional area of flow 114
Fig. 6.11: Flow velocity contour for the entire cross-sectional area of flow 114
Fig. 6.12: Bed shear profile at the solid-fluid interface. 115
Fig. 7.1: Location within geometry used to obtain flow parameters 118

Fig. 7.2: Cross-sectional velocity profile in the absence of bed 118

Fig. 7.3: CFD simulation of near-bed velocity profiles of different fluids at 5.05 L/s and 50% bed height (Pandya et al. 2019) 119

Fig. 7.4: Velocity profile for various bed heights using Fluid 1 at a flow rate of 5.05 L/s 120

Fig. 7.5: Velocity contours for Fluid 1 varying flow velocity and bed height 121

Fig. 7.6: Velocity contour plots for different fluids with various bed height at 9.46 L/s 122

Fig. 7.7: Bed shear stress profiles for Fluid 3 at various bed heights and flow rates 123

Fig. 7.8: Average bed shear exhibited by various fluids at different bed heights and mentioned flow rate. 124

Fig. 7.9: Rate of normalized bed height & normalized bed shear. 127

Fig. 7.10: Cross-plots between CFD bed shear and Kozicki's model 130

Fig. D1: Velocity contour plots for different fluids with various bed height at 5.05 L/s. 160

Fig. D2: Velocity contour plots for different fluids with various bed height at 6.31 L/s. 161

Fig. D3: Velocity contour plots for different fluids with various bed height at 7.57 L/s. 162

Fig. D4: Velocity contour plots for different fluids with various bed height at 9.46 L/s. 163

Fig. E1: Bed shear stress profiles for Fluid 1 at various bed heights and flow rates. 164

Fig. E2: Bed shear stress profiles for Fluid 2 at various bed heights and flow rates. 165

Fig. E3: Bed shear stress profiles for Fluid 3 at various bed heights and flow rates. 166

ABSTRACT

Recent technical improvements in the drilling process have allowed drilling of high inclination and horizontal wells with longer laterals. The frequency of such wells has increased over time due to their advantage of increased contact area with the reservoir. However, the complexity of these wells results in more well completion problems such as deposition of solids in the wellbore and increased Non-Productive Time (NPT). The reduction of NPT depends on factors influencing the mechanism of solids transport. The dominance of gravity over buoyancy forces the solids to settle vertically downwards irrespective of the direction of the flow. However, the distance required for solids to settle downwards is significantly reduced in directional and horizontal wells. Moreover, the fluid flow in these wells has a reduced velocity component in the vertical direction. The substantial reduction of the vertical component of fluid velocity, which prevents solids from settling, results in rapid solids deposition and bed build up. Also, the forces acting on the flow protruding particle of the bed determine the erosion mechanism of solids bed formed in inclined and horizontal wells.

This study undertakes an experimental approach to solve the problem of optimization of wellbore cleanout process in deviated and horizontal well sections. In addition, Computational Fluid Dynamics (CFD) approach is incorporated to interpret and explain experimental observations. Experimental investigations were carried out using a large-scale flow loop. Bed-erosion experiments were conducted in an eccentric annulus (140 mm × 60 mm annular geometry and 10.36 m long section) to study the effects of several influencing factors (fluid rheology, inclination, and solid density) on wellbore cleanout efficiency. The effects of these factors were analyzed in terms of normalized bed erosion curves (reduction of bed height with time) and cleanout efficiency (percentage removal of solids weight).

Experimental results demonstrated that high-viscosity fluids are superior cleanout medium at low inclinations due to their better solids suspension capability while low-viscosity fluids have greater erosion capability and thereby perform well at high inclinations and horizontal configuration. CFD simulations show that low-viscosity fluids have significantly greater local velocity in the vicinity of the bed than highly viscous fluids, even though the viscous fluid exhibit a higher bed shear stress. The analysis indicates that the local fluid velocity is more important than bed shear stress in eroding the bed. Besides this, the density of solids was found to have a moderate effect on the hole cleaning process, and solids with higher density were slightly more difficult to remove from the wellbore section.

Furthermore, experimental results are analyzed by developing a dimensionless relationship between various influential parameters. The correlation developed is capable of upscaling the lab-scale model to field scale. This was validated by comparing the results obtained from the model with those measured by other studies. The maximum error in the prediction of this model is less than 20%. In general, the model can be directly applied in field scenarios with considerable accuracy within the specified ranges of dimensionless groups.

CHAPTER 1

INTRODUCTION

Advancements in drilling technology have allowed the oil industry to drill horizontal and inclined wells at a high rate of penetration. Such highly directional wells are preferred over conventional vertical wells due to their increased contact area with the reservoir. Moreover, such wells have the ability to tap a very thin reservoir that may otherwise be inaccessible or costly to access using vertical wells. Several directional wells can be drilled from a single pad to access the reservoir in any direction thereby decreasing the overall well costs significantly. Increased demand in drilling and completion of these directional and horizontal wells has resulted in process optimization to reduce the non-productive time occurred at the rig site and thereby, maximizing the profits. One of the major sources of non-productive time is the duration required to clean the wellbore. Although hole cleaning is considered a non-productive operation, it is essentially unavoidable and required for efficient drilling and proper completions. Once, the well is in production, wellbore cleanout may be required to remove the accumulated sand or other debris in the hole. Hence, reducing the time required for hole-cleaning becomes essential.

The solid's transportation behavior during cleanout significantly impacts the efficiency of cleanout. Solids, due to their dense nature and by the force of gravity, tend to settle down vertically. The distance these particles would travel before reaching the borehole wall is very minimum in directional and horizontal well configurations. Moreover, the vertical component of velocity is also substantially reduced thereby making the settling even faster. The continuous settling of these solids forms a bed in inclined and horizontal wellbores. Formation of such beds not only cause many types of flow problems in the well but also has an adverse effect on the

downhole equipment. Hence, it becomes essential to remove the solids from the wellbore in a timely and efficient manner.

This research is focused on solving this issue of optimizing the hole-cleaning process in horizontal and inclined wellbores by studying the bed erosion experimentally and use CFD for hydraulic analysis of the erosion process. A large-scale flow loop was utilized to conduct bed-erosion tests and understand the effect of several parameters such as fluid rheology, inclination angle, the density of solids and flow parameters on the efficiency of the hole cleaning process. A sensitivity study of these parameters can result in a quick calculation strategy that may allow for faster cleanouts in the field by optimization of certain parameters. Computational Fluid Dynamics (CFD) is a technique that allows flow characterization in complex geometries such as a partially blocked eccentric annulus. Unlike the transient nature of experiments, the CFD model developed was targeted to study the bed shear at different bed heights. Therefore, the CFD study involved several steady-state flow simulations in an eccentric annular configuration with varying bed height.

1.1 Problem Statement

Solids such as drilled cutting, drilled plug debris, post frac proppant and produced sand can easily settle on the low-side of a horizontal well thereby reducing the annular clearance for downhole tools. Fig. 1.1 is an image documented by Li & Luft (2014) that shows the formation of proppant bed in dune shape after hydraulic fracturing job in a horizontal lateral of a well. Formation of bed due to the settling of solids may obstruct the movement of downhole tools during completion and workover operation and in worst scenarios get the tool stuck. Such problems often require expensive fishing operations. Depending on the severity of a stuck tool,

fishing failure may lead to sidetracking or well abandonment. Moreover, the formation of solids bed hampers hydrocarbon recovery (Brown, Bern, & Weaver, 1989). These problems emphasize the need to perform efficient wellbore cleanout operations that would resolve these issues. Coiled tubing has been considered a more viable option than workover rigs to achieve efficient hole-cleaning.

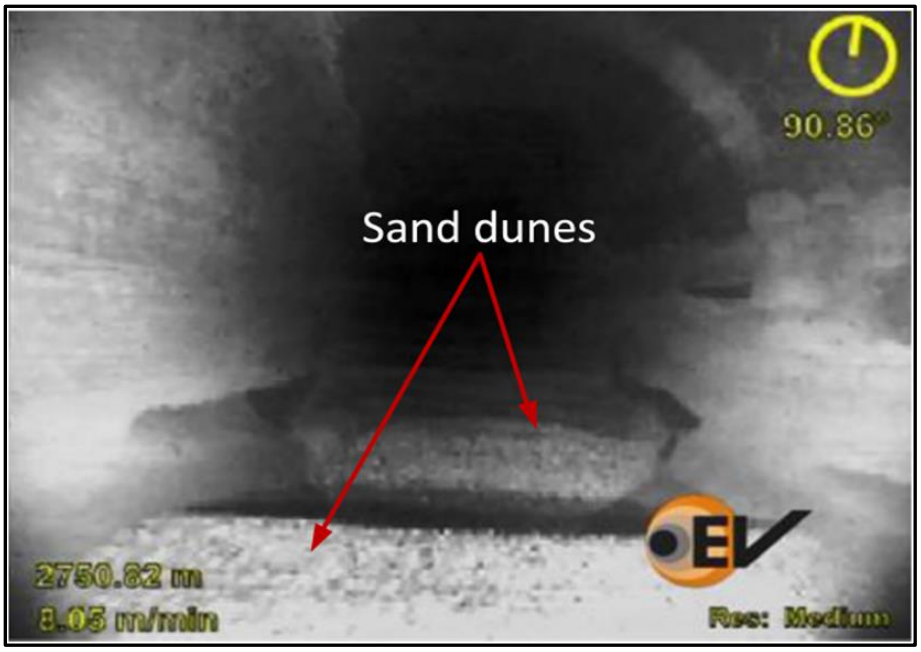


Fig. 1.1: Proppant bed formation after hydraulic fracturing (Li & Luft, 2014)

Approximately 50% of all CT interventions comprise of wellbore cleanouts to remove debris such as produced sand or residual proppant from hydraulic fracturing treatments (Rolovic et. al. 2004). This is attributed to many reasons including the ease of mobility and reduced field setup time (rig up/rig down). Additionally, lack of pipe connections in CT reel makes it much safer to operate a CT rig with a lesser concern for leaks and spills. It also minimizes the tripping time as running the tubing in the hole does not require making or breaking connections.

Although CT has certain major advantages over workover rigs in terms of hole-cleaning, it does provide some restrictions in terms of maximum tubing size available to be mobilized on well sites. Coiled tubing is reeled on a drum creating a setup of spool that can be conveniently transported to well sites. However, large size tubing can result in excessively large diameter of spool that would logistically restrict the mobilization of such fleet to well sites. On the contrary, deployment of a much smaller sized coiled tubing increases the annular clearance in the wellbore thereby reducing flow velocity available for solids removal. Smaller tubing would also generate more friction and subsequently higher surface pressures. Hence, the maximum flow rate available for fluid circulation with smaller tubing is limited to a lower range. This eliminates the possibility of increasing flow rates for optimized cleanout and control over the annular velocity. In horizontal sections of complex well profiles, CT tends to lay eccentrically on the low side of the lateral. This generates flow stagnant zones on the lower side and makes hole-cleaning a more challenging issue (Nazari et al., 2010; Thomas et al., 1982). The available literature comprises majorly of steady-state experimental work resulting in numerous empirical correlations and some rules-of-thumb (for instance, circulating 2-3 times the annular volume for sufficient cleanout) to achieve efficient cleaning. Often, these correlations are specific to certain configurations and cannot be applied universally.

The efficiency of hole-cleaning can be optimized by controlling various influencing parameters. However, it remains a challenge to create set values for these parameters and quantify their interdependent effect on wellbore cleanout process. Flow rate has the most significant and direct impact on solids removal. Higher flow rate results in better clean out efficiencies (Azar & Sanchez, 1997). Theoretically, any fluid when pumped at excessively high flow rate can erode the bed and remove most of the solids. However, limited pump capacity and pressure ratings of

tubing restrict the maximum flow rate at which the fluid can be circulated. Similarly, a higher density of fluids has a positive impact on hole cleaning by reducing the effective weight of the solid particle (Martins & Santana, 1992). The density of circulation fluid imposes the restriction of maximum equivalent circulating density (ECD) of fluid that can be pumped downhole. Excessive fluid density increases the hydrostatic pressure of the fluid column in the well. This is further limiting in longer laterals attributing to higher frictional pressure losses associated with the length of these wells. This is highly undesirable during the drilling process, especially if hydrostatic pressure exceeds the formation fracture pressure. Control of fluid viscosity provides an effective way to optimize wellbore cleanout. However, the influence of rheological properties on hole cleaning is complex and not completely understood. Unlike fluid properties, solids properties are found to have less influence on hole cleaning. A dense particle can settle from suspension into a stationary bed relatively easily, making it difficult to remove from the wellbore. Particle size has the least impact in terms of efficiency of hole-cleaning. Results reported in the literature on this aspect have contradictory conclusions.

It is essential to quantify the nature of solids accumulation in the wellbore and remove these solids efficiently before a tool can be lowered into the well. Entire well trajectory can be broadly classified into a vertical, inclined and horizontal section. The removal of solids from vertical wells is relatively easier when compared to horizontal wells. Particles are transported by the flow stream in vertical well if adequate annular fluid velocity and fluid viscosity are maintained. Hence, the hole-cleaning process can be reasonably controlled in vertical section as fluid particles settle in a direction opposite to the flow. However, particle transport mechanism in inclined and horizontal sections vary significantly as compared to a vertical section. Reduction in the vertical fluid velocity component in an inclined section enhances the settling of solids on the

low-side of a wellbore. After the formation of a solids bed, the forces acting on the bed determine the movement of the bed particles. The bed may tend to slide downwards as a single entity in inclined sections demonstrating the avalanching effect (Li & Luft, 2014). Moreover, once the solid particles reach the inclined wall, depending on the properties of the fluid and solids, they can form a concentrated high-density slurry. With time the slurry develops as a dense layer on the low-side of the annulus with a layer of clear fluid above it. Subsequently, the dense layer flows downwards along the inclined wall and creates a secondary flow which is similar to the Boycott effect (Boycott, 1920). Boycott observed that particle settling is more rapid in an inclined tube than in a vertical one. The secondary flow development tendency reduces as the inclination increases to a horizontal orientation, even though bed formation is prominent in horizontal section due to the lack of the vertical component of fluid velocity to offset the deposition of particles. Therefore, due to the severity of solids settling in inclined and horizontal wellbores, it becomes essential to study the solids transport mechanism in these well sections.

Wellbore cleanout in inclined and horizontal sections is usually a turbulent flow problem (Diplas et al., 2008; Heyman et al., 2013). A theoretical solution to a turbulent flow problem is difficult to obtain due to the fluctuations of flow parameters such as fluid velocity and pressure. This is attributed to the inherent difficulty of studying the near-bed velocity profile within the turbulent regime. Moreover, there is a lack of research studies pertaining to erosional studies. Most of the literature involves studying hole-cleaning under a steady-state condition in which the rate of solids removal is in equilibrium with the rate of solids deposition, thereby maintaining a constant solids concentration within the section. The industry has been trying to tackle the problem of hole-cleaning for more than 50 years. Although some major advancements have been made, the

cleanout mechanism is not yet completely understood and is still a major problem especially in inclined and horizontal wells.

1.2 Hypothesis

The current research focuses on quantifying the effects of various parameters on the efficiency of hole cleaning. It is hypothesized that bed erosion is an exponential decay process. The profile of the decay curve is governed by parameters that influence the hole-cleaning process. The same trend is anticipated for the average bed shear obtained from CFD simulation. Classic sediment transport studies (Wilson, 1987; Meyer-Peter and Müller, 1948; Engelund, 1981) consider the strong dependence between the rate of bed erosion and bed shear stress. This hypothesis is based on similar dependence between these parameters during sediment transport in open channel flows such as a case of flow over river-bed. Another hypothesis of the study is that the Kozicki's friction factor correlation can be extended to turbulent flow model by adapting the shape factor concept for partially blocked annuli.

1.3 Objectives

The overall objective of this research is to optimize the wellbore cleanout process by better understanding the mechanisms of bed erosion. Specific objectives are as follows:

i. Understand and quantify the effects of the major influential parameters on the hole-cleaning mechanism.
ii. Develop a generalized bed erosion model to predict a reduction in bed height with circulation time.
iii. Simulate steady-state flow over fixed bed height using computational fluid dynamics (CFD) model.

iv. Examine and interpret experimental results using CFD simulations of the velocity profile and bed shear stress.

1.4 Scope of the study

This study intends to understand the wellbore cleanout mechanism by conducting a combination of experimental investigation and CFD simulations. The experiments were conducted in a 10.36 m (34 ft) long annular test section using three fluids with different rheological properties. The fluids were pumped at flow rates ranging from 5.05 L/s (80 gpm) to 7.57 L/s (120 gpm) while varying the angle of inclination (45, 50, 60, 70, 75 and 90°). The selection of these parameters was based on current industry practices. The inclinations selected for the experimental investigation were the most difficult to clean according to the previous studies. Cleanout fluids utilized in the study were water (Fluid 1), 10 lbm/Mgal or 1.2 g/L guar (Fluid 2), and 20 lbm/Mgal or 2.4 g/L guar (Fluid 3).

Guar based fluids were mixed using guar gum liquid gel concentrate. The concentrate used in this study had a polymer activity of 4 lbm/gal (480 g/L) of slurry. Guar gum is essentially a galactomannan based naturally occurring polymer extracted from cluster bean of a guar plant. Chemically, guar gum comprises of a combination of galactose and mannose polymeric chains. Monomers of both sugars have a chemical formula of $C_6H_{12}O_6$ but are structurally different. The molecular weight of the polymeric chain can range from 0.5 to 8 million grams per mole. Guar gels are commonly used as an additive in various oilfield operations particularly in stimulation and wellbore cleanout. The predominant use of guar is attributed to its ability to form strong hydrogen bonds with water molecules. It generates a hydro-colloid and remains stable in solution over a pH range of 5-7. Thus, it is chiefly used as thickener and stabilizer. Solids used in the bed

erosion experiments were 20/40 mesh (600 microns) ceramic proppant with two different specific gravity (2.5 and 3.2).

Computational fluid dynamics model is utilized to simulate bed erosion under turbulent flow regime assuming steady-state flow condition. A wall with roughness equal to the particle size is incorporated in the model in lieu of the bed interface. Results are obtained at a certain distance away from the inlet in the CFD model to ensure stable and fully developed flow. Results obtained from steady-state simulations are paired with the results obtained from experimental investigation to make a reasonable comparison.

1.5 Structure of the dissertation

This entire dissertation is divided into 8 chapters.

- Chapter 1 describes the need to carry out this study and underlines the hypotheses and objectives of this study.
- Chapter 2 details the theory behind particle transport within eccentric annulus in horizontal and inclined wellbores. This section will also summarize the different flow patterns that arise due to various particle transport mechanisms and the conditions that result in them. Finally, the effect of individual parameters and the significance of turbulence in hole-cleaning is explained.
- A summary of numerous previous studies conducted to investigate bed erosion has been described in Chapter 3. These studies are divided into three major sections. First, experimental studies conducted to study hole cleaning under steady-state and transient conditions are summarized. This is followed by literature focused on investigating the hole-cleaning mechanism through the development of mechanistic models based on force

balance. Lastly, the application of CFD models and results reported by various studies in the literature.

- The description of the experimental setup, test procedure, and data analysis are presented in Chapter 4. Experimental results, data analysis, and discussion on these results are also included in this chapter.
- Chapter 5 describes the approach taken to develop a dimensionless relationship using the data obtained from experiments. It also compares the data predicted by the correlation to the data obtained by other studies to validate the model.
- The application and use of computational fluid dynamics are explained in detail in Chapter 6. It includes the detail of the model developed to study flow over a uniform solids bed and input parameters used in the model. The results obtained from the CFD study is also presented in this chapter.
- Results obtained from CFD are correlated with the experimental data in Chapter 7.
- Chapter 8 summarizes the conclusions and recommendations for future research.

CHAPTER 2

THEORY

Solids build-up and subsequent formation of a stable bed in the annulus can be attributed to several reasons. However, irrespective of the cause of bed formation, it becomes essential to quantify the required degree of hole-cleaning before designing and conducting a hole-cleaning job. Many practices are commonly undertaken in the field to predict the severity of solids accumulation in different well sections. The most conventional and frequently applied technique in vertical sections is to lower the tubing down the hole and circulate fluid at the required rate until surface measurement of pipe weight decreases rapidly. This procedure is commonly known as 'tagging' a plug/solids column and is schematically represented in Fig. 2.1.

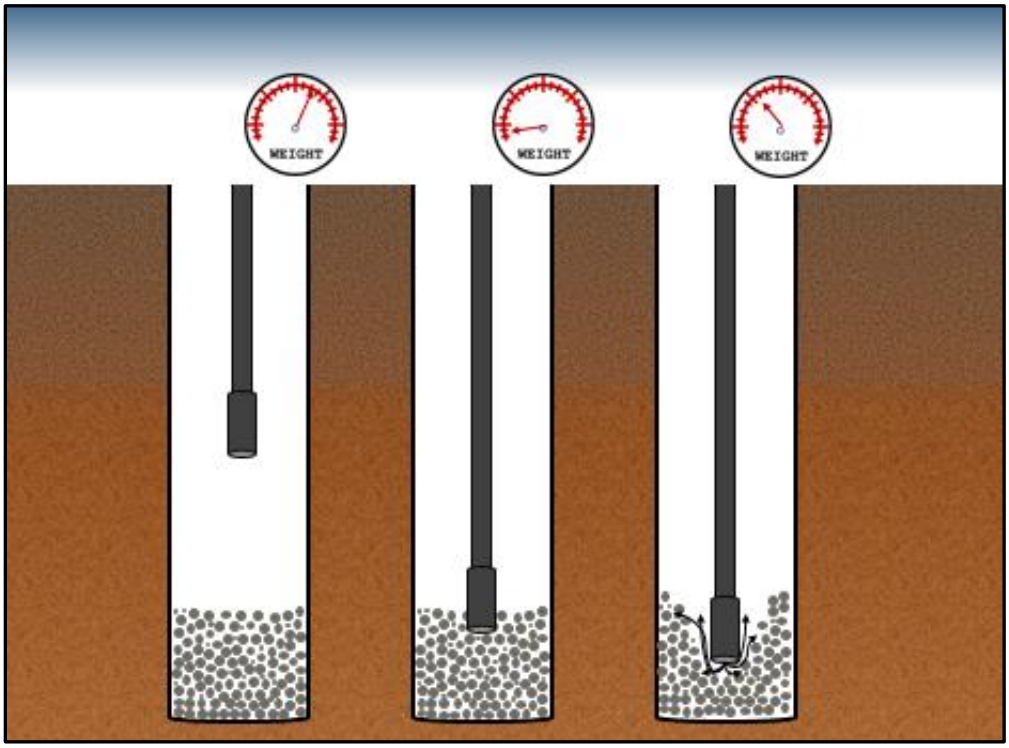


Fig. 2.1: Tagging of solids plug-in a vertical well section

The instant drop in pipe weight during a trip-in run is due to the sudden normal force exhibited by solids bed/plug on the pipe. The necessary amount of solids to be removed from the wellbore can be obtained based on the depth at which tag is recorded, the wellbore configuration (open hole) or annular configuration (cased hole) and predicted/known physical properties of the solids in the hole.

The detection of solids buildup is relatively challenging in horizontal and highly inclined sections as the solids settle on the low-side and may only partially block the cross-sectional area. The partially blocked cross-sectional area does not result in a rapid reduction of pipe weight recorded at the surface, which can lead to inaccurate quantification of deposited solids. On the contrary, it is the gradual reduction in pipe weight in horizontal and inclined sections that is usually indicative of bed build up. This gradual reduction is attributed to the frictional resistance of the bed as the pipe is forced to run through/over it. The buildup of solids bed is only a probable reason for gradual pipe weight reduction. It could also be attributed to other factors such as the generation of higher friction due to contact between the longer length of pipe resting on the low-side of casing in the lateral. A more reliable indicator of solids build-up in a horizontal lateral is a combination of gradual pipe weight reduction during trip-in and encountering overpull (higher tension in the pipe) during the trip-out process. This overpull is the result of the increased weight of solids being dragged along with the pipe. However, such operations involving generation of forced overpull possess a higher risk of stuck-pipe, loss of bottom-hole assembly or even pipe failure if pull force exceeds the tensile limits of the pipe.

Other common indicators of predicting the presence of solids bed could include conducting an injection test to verify that perforations are not covered by bed and reduction of solids

concentration in the return line during hole-cleaning/drilling operations that could indicate deposition of solids back in the well. Secondary indications, such as surface pressure, rate of penetration and flow rate in return line can help verify the deposition of solids during the drilling process. A strong indicator of bed formation would be when the return mud flow rate and density are less than expected. Similarly, a decrease in drilling rotary speed, reduced rate of penetration and unpredicted excessive bit wear can be indicative of accumulations of solids near the depth of bit.

The most infallible method of quantifying and visualizing the formation of solids bed in the wellbore is to lower a downhole camera to obtain photographic images (Fig. 1.1). Downhole cameras allow real-time visualization of bed formation with identification of possible low clearance zones in the annulus. Despite its high performance and reliability, it is uncommon to lower downhole cameras due to its high cost. Another restriction of using cameras is the limited visualization capability especially when a wellbore is filled with non-transparent drilling and completion fluids. Therefore, the most cost-effective and feasible technique to identify and quantify solids bed is to run-in a pipe and circulate fluid through it to prevent any problems related to excessive over-pull as mentioned earlier. This process forces the inner pipe to rest on the low-side of the well, thereby, generating a partially blocked annular flow geometry.

2.1 Eccentricity in Annulus

Eccentricity, usually expressed as a percentage, is the displacement of the center of the inner pipe with respect to the center of the hole or casing. A 100% eccentric annular profile refers to the scenario when the inner pipe completely rests on the low-side of the outer pipe. A 0%

eccentric (or concentric) profile refers to the case in which the centers of both inner and outer pipe coincide. Mathematically, eccentricity is defined as:

$$\varepsilon = \frac{e}{r_o - r_i} * 100 \quad (2\text{-}1)$$

where ε is eccentricity; e is the offset distance between the centers of inner and outer pipes; r_o is the radius of the outer pipe; r_i the radius of the inner pipe.

Eccentricity is one of the critical factors affecting solids removal from the low-side of an inclined wellbore. A fully eccentric annulus creates flow stagnant zones on the low-side thereby making bed erosion challenging (Thomas et al., 1982; Nazari et al., 2010). Although a very uncommon scenario in wellbore geometry, negative eccentricity (in which the inner pipe is drifted to the upper side of the wellbore) results in favorable conditions for efficient hole cleaning as it allows high-velocity flow in the low-side of the wellbore to erode the bed. Elsayed and Nasr El-Din (2006) studied the eccentricity change in annular profiles with the increase in inclination. It can be observed from their study (Fig. 2.2) that eccentricity increases exponentially with the increase in wellbore inclination. Assuming the curves follow the projected trend, the eccentricity tends to be at 100% prior to 90° deviation. This result is consistent irrespective of the weight on bit applied in case of drill-string or weight of bottom-hole assembly for the case of completion strings.

The effect of eccentricity on annular fluid flow behavior was studied by several researchers. Since no exact mathematical solution is developed from these studies, approximate solutions are presented in some studies (Luo and Pedan 1987; Escudier et al. 2001). Extending on these studies, Singh and Samuel (2009) conducted numerical simulations using CFD software to analyze the effect of eccentricity on annular pressure drop gradient for Newtonian fluid. One of

the most critical factors that affect the hole-cleaning efficiency is the annular velocity profile. The velocity profile itself depends on the annular cross-sectional area available for fluid flow and the eccentricity.

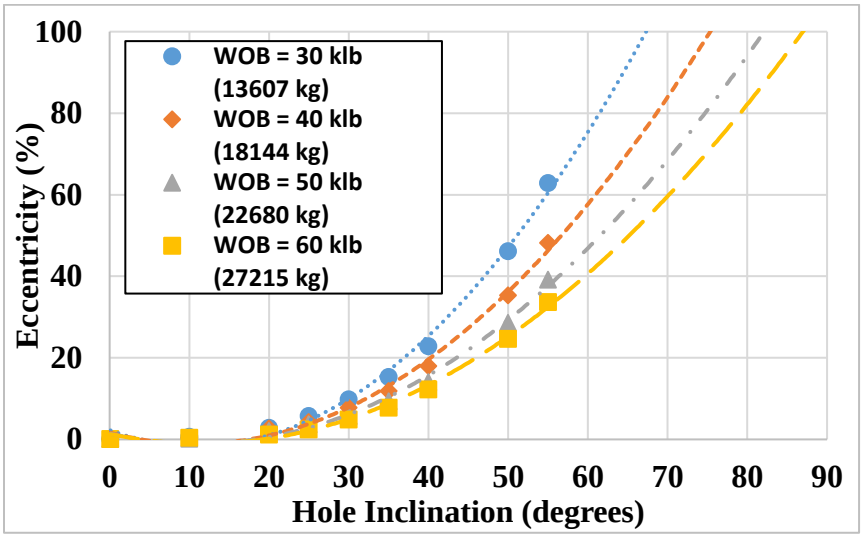


Fig. 2.2: Eccentricity vs hole inclination (Data: Elsayed and Nasr El-Din, 2006)

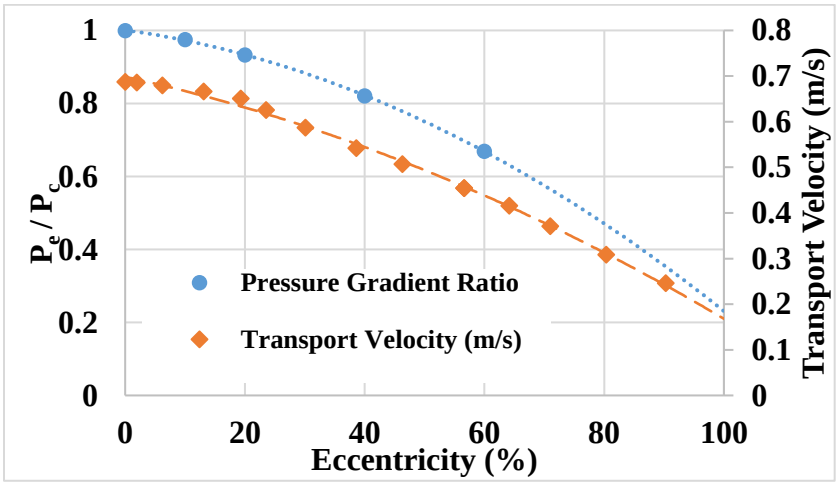


Fig. 2.3: Eccentricity effect on annular pressure drop gradient (Data: Singh and Samuel , 2009 and Annung, 2010)

Fig. 2.3 represents the effect of eccentricity on the ratio of eccentric to concentric annulus pressure loss gradient. The reduction in pressure loss gradient with the increase in eccentricity is evident from the results of the simulation. This decrease in pressure gradient results in

insufficient bed shear stress and prevents bed erosion. The results suggest that hole cleaning efficiency reduces when shifting from a concentric to an eccentric annulus.

2.2 Bed Erosion Mechanisms

The bed erosion process is majorly controlled by the magnitude and direction of forces acting on solid particles at bed interface (Fig. 2.4). These forces primarily consist of gravity, buoyancy, drag and lift. These forces regulate the flow dynamics and transport patterns in various wellbore section. The resulting flow patterns are discussed in the next section. Additionally, turbulence in the flow results in the generation of eddies that aids in particle suspension into the flow stream. It also hinders the re-deposition of particles already in suspension back into the stable bed. Although turbulence plays a major role on the particle in suspension, its intensity is very low close to the bed interface due to damping effects. Hence, turbulence plays a limited role in lifting the particles from a stationary bed, especially at higher inclinations. Gravitational force is a function of the mass of the particle. Thus, it is expressed as:

$$F_{gravity} = mg = \rho_s V_s g == \frac{1}{6}\pi d_s^3 \rho_s g \tag{2.2}$$

where m is mass of the solid particle; ρ_s is absolute solid density; V_s is the volume of the particle; d_s is solid's diameter; g is acceleration due to gravity.

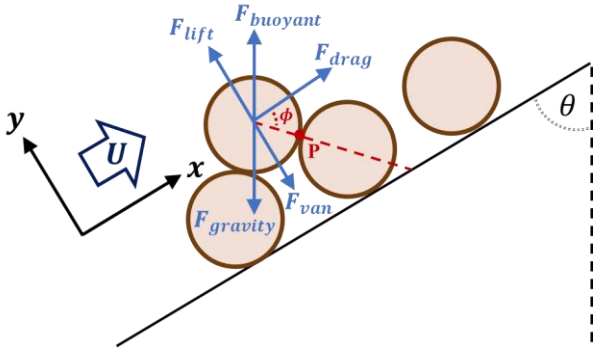


Fig. 2.4: Forces acting on a particle on the bed interface

The buoyant force exerted by a fluid acts in the upward direction such that it opposes the weight of particle in fluid:

$$F_{buoyant} = m\left(\frac{\rho_f}{\rho_s}\right)g = \frac{1}{6}\pi d_s^3 \rho_f g \tag{2.3}$$

where ρ_f is fluid density.

The hydrodynamic lift force acts in a direction perpendicular to average flow velocity and it tends to uplift solid particles from the stationary bed. The drag force is the frictional force acting on the particles parallel to the direction of fluid flow. The hydrodynamic lift and drag on the solid particle are expressed as:

$$F_{lift} = \frac{1}{2}C_L \rho_f u^2 A_p \tag{2.4}$$

$$F_{drag} = \frac{1}{2}C_D \rho_f u^2 A_p \tag{2.5}$$

where C_L is the lift coefficient; C_D is the drag coefficient; A_p is the projected area of the particle over the bed surface; u is fluid velocity. The drag and lift coefficients are determined from empirical correlations. During wellbore cleanout, the lift, drag, and buoyant forces act towards transportation of solids downstream of the flow while gravity acts to deposit the particles in the bed.

Particle settling in vertical sections occurs in the axial but opposite direction to flow if drag force exhibited by the fluid cannot offset the effective particle weight. In deviated sections, settling occurs in a combination of vertical and lateral direction since the lateral component of gravity ($F_{gravity} sin\theta$) plays a major role. The hydrodynamic lift, turbulence/eddies, and other non-Brownian diffusion mechanisms help maintain solids in suspension. At high well inclinations

(more than 45°), these mechanisms become less contributing when compared to gravity. At these inclinations, fluid gravity plays a dominant role in depositing particles on the wellbore.

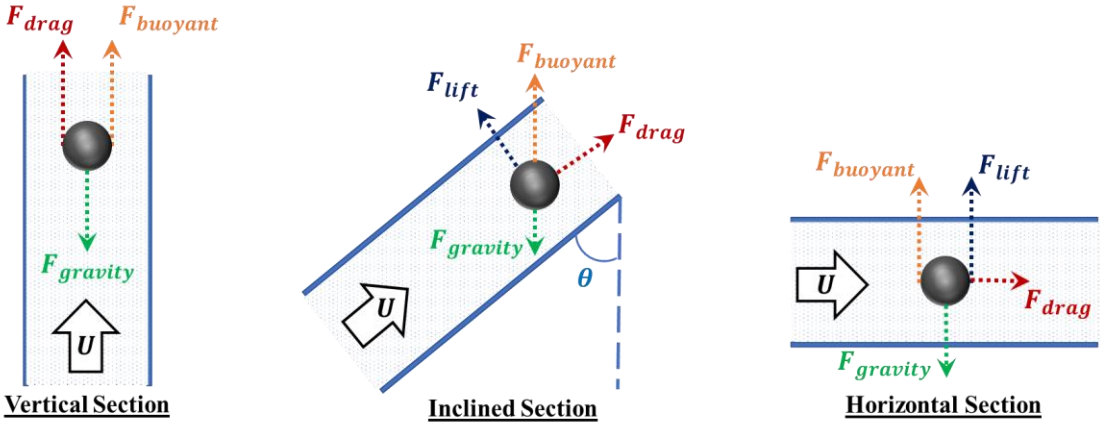


Fig. 2.5: Forces acting on a solid particle in various well sections

2.3 Flow Patterns During Solids Bed Erosion

Fluid flow during wellbore cleanout process is mainly a flow of two-phases, solids and liquid, predominantly as a slurry. The slurry primarily contains of smaller sized particles that are denser than the fluid medium and hence tend to settle. The settling tendency of particles in a downward direction due to gravity along with other forces acting on them results in complex flow patterns. Due to the complexity of the flow patterns, the majority of hole cleaning studies rely on visual observations of different flow phenomena. Visual observations possess an inherent human bias in the identification of gradual transitions of flow patterns. Few of the very first classification studies categorized flow patterns into a "non-deposit flow regime" majorly consisting of solid suspensions and a "flow regime involving deposits" during which the deposition of particles is visually evident. Another method of classification between different patterns can be done as follows (Fig. 2.6):

- Homogenous flow (Fig. 2.6a): Such a flow occurs when there is absolutely no presence of stationary or moving solids bed. Solids transport in vertical wells is an example of homogenous flow. However, very high annular flow velocities are required to maintain solids in a homogenous suspension in inclined and horizontal wells. Flow rates required to attain homogenous flow are very high and rarely achieved in the field.

- Heterogeneous flow: Unlike the homogenous flow pattern, heterogeneous suspension flow can be attained in the field with possible flow rates. In a horizontal flow section, a gradual concentration gradient of solids particles develops in the axially perpendicular direction. Low-side of the flow area is dominated by a high concentration of solid particles (Fig. 2.6b)

- Heterogeneous and Sliding bed flow: Upon further reduction in flow velocity, the solids tend to settle more frequently, thereby forming a packed bed of solids. However, the flow velocity is sufficiently high to move the bed as one single entity. The solids concentration in this bed is less than the maximum bed packing level (Fig. 2.6c). An upper layer of heterogeneous suspension is still prevalent in this flow pattern.

- Saltation and Stationary Bed Flow: Once the flow velocity is too low to enable particle motion, a stationary solids bed is formed at the very bottom of the flow area. Above this layer, there exists a moving bed layer that moves as a whole bed (Fig. 2.6d). Such flow also results in dunes formation in certain cases and under certain inclinations. Movement of particles just over the stationary bed is often termed as ‘saltation’. The rest of the flow area is dominated by a heterogeneous flow, though its concentration gradient in the vertical direction is much greater than those observed in the other flow patterns.

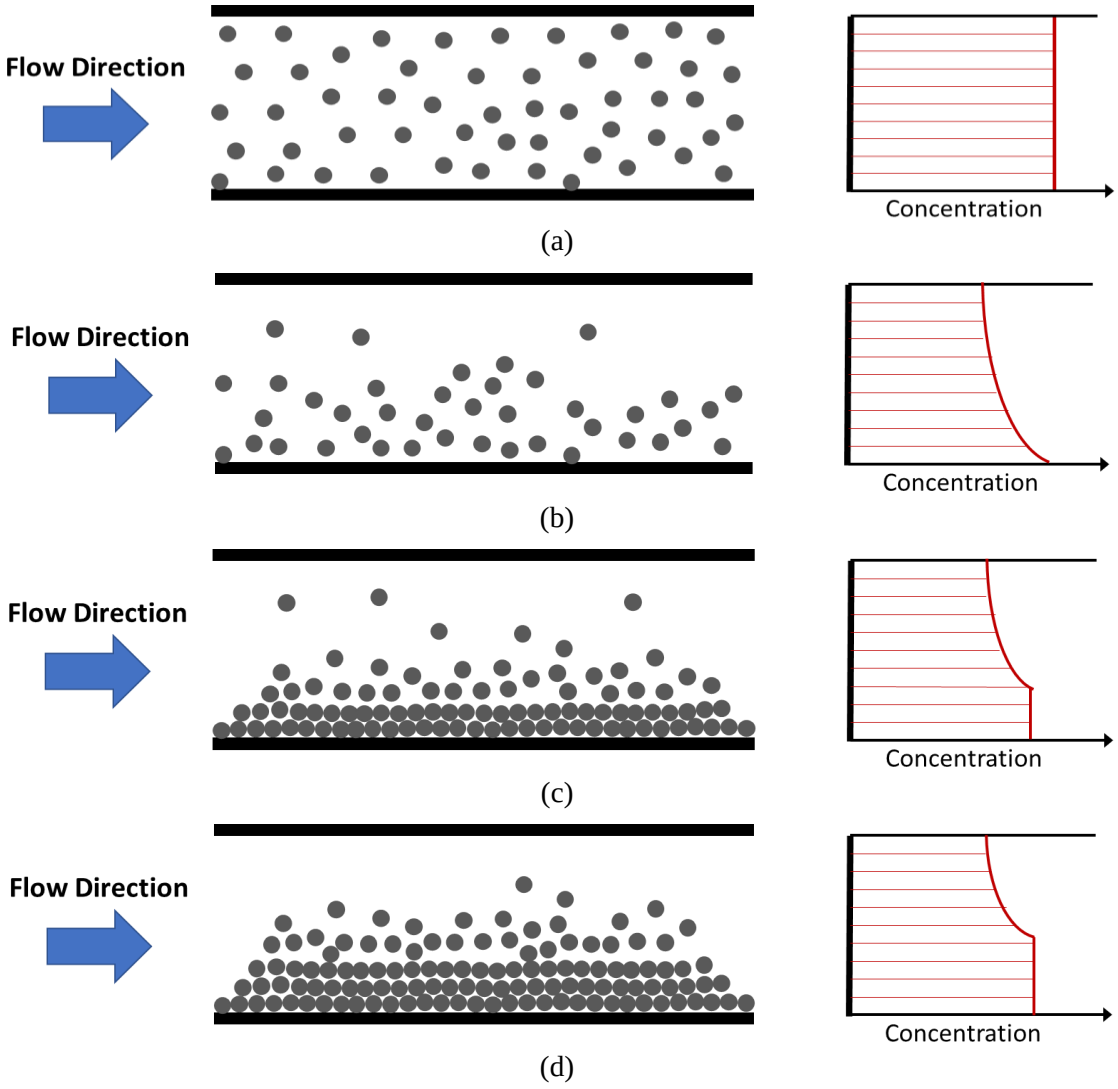


Fig. 2.6: Schematic views of flow patterns and corresponding concentration profiles

Saltation occurs when solids travel for only a short distance in the flow stream due to the in upward lifting forces (hydrodynamic lift, buoyancy, turbulence, and viscous forces). Once the particles encounter sufficient lift forces or turbulence, they are suspended into the flow stream. The drag force then imparts momentum onto these suspended particles thereby allowing the fluid to carry it forward. However, once solid particles are in the flow stream, lift force and turbulence diminish; as a result, the particles re-deposit on the bed. The cycle repeats until the particle is removed from the required lateral section.

Theoretically, at extremely high flow rate, any fluid can clean the hole. Unfortunately, excessive flow rates cannot be used in wells due to dynamic downhole pressure limitation. As a result, the annular fluid velocity needs to slightly exceed the solids bed buildup conditions in sensitive formations with a narrow pressure window. With limited annular velocity, solids beds form on the low-side of the hole in high angle holes. If the circulation rate is very low, solids are unlikely to be removed from the wellbore. Upon increasing the flow rate, the bed becomes progressively eroded. Solid particles traveling on the bed interface undergo saltation and form dunes or large ripples. The bed then starts to move slowly and solids are cleaned from the wellbore. This mechanism of bed movement is a more noticeable feature of hole cleaning with low viscosity fluids.

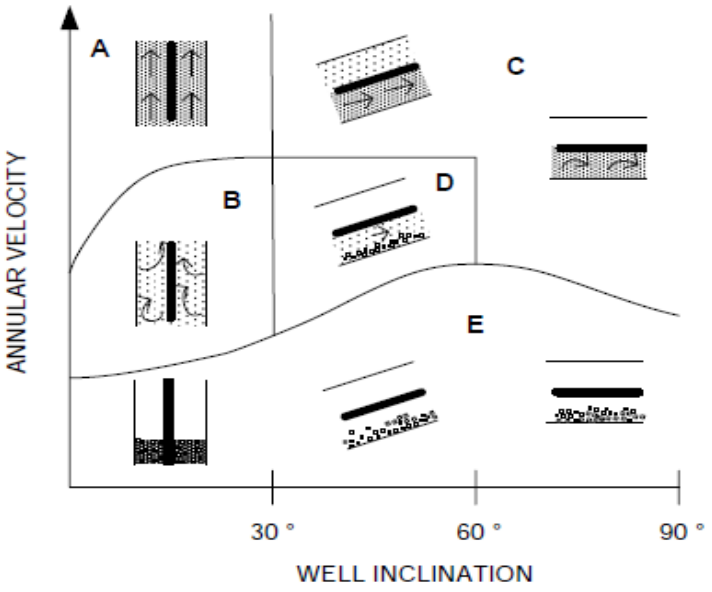


Fig. 2.7: Solid transport mechanism in vertical and deviated wells (Bern et. al. 2003)

Fig. 2.7 exhibits different regimes in solids transport mechanisms as described by Bern et. al. (2003). In holes with inclination less than 30 degrees, the solids are effectively suspended by the fluid and the beds do not form. In such cases, conventional transport calculations based on

vertical slip velocity can be used to estimate hole cleaning efficiency. Beyond 30 degree inclinations, the solids can easily form beds on the low-side of the hole, which can slide backward down the well, causing pack-off. Solids which form on the low-side of the hole can either move as a sliding or moving bed or may be transported as dunes or ripples.

There are several mechanisms that could possibly play a major role in the solids transport process within a particular flow pattern. However, the governing mechanism is the one which dominates the flow at a particular wellbore inclination. Two mechanisms (rolling and lifting) are often considered to analyze the critical/incipient condition for initiating the movement of a flow protruding particle.

2.4 Effects of Various Parameters

As mentioned previously, the effects of critical parameters that affect hole cleanout and their interactions with each other needs to be understood to optimize the wellbore cleanout process. These critical parameters can be widely categorized into three groups:

- Operational parameters – Operational parameters usually have a profound effect on hole-cleaning. Wellbore geometry, inclination angle, pipe eccentricity, and flow velocity are examples of operational parameters. The effect of pipe eccentricity has been discussed in Section 2.1.
- Fluid properties – The second category of parameters essentially includes rheology and density of fluid. Fluid properties can be easily controlled and modified in the field during a cleanout operation. While this makes fluid properties a resourceful tool for wellbore cleanout, its impact on the process of bed erosion is very complicated. Hence, it is important to examine the influence of fluid properties on the cleanout mechanism.

- Solids properties – Solids properties that have an influence on bed erosion are solids size and density. However, previous studies indicate that these factors have a relatively moderate effect on bed erosion when compared to other factors.

2.4.1 Wellbore geometry

Annular area available for slurry flow and subsequent removal of solids is a function of casing size or open-hole diameter and the outer diameter of the inner tubing. Completion strategies or borehole geometries with larger diameters make it challenging to achieve adequate flow velocity required for efficient hole-cleaning. Conversely, inner pipe with a large diameter would aid in attaining high velocities and better cleanout. Even though a large-diameter inner pipe makes it feasible to pump cleanout fluids at a higher velocity, it increases substantially the tubing friction pressure. Despite its advantage, the application of a large-diameter inner pipe has certain drawbacks and limitations. For a constant inner casing diameter, a large inner pipe would result in higher annular friction pressures as it creates a narrow and restricted flow area between the casing and the pipe. Implementation of larger OD coiled tubing (CT) has further limitations from logistical and safety perspective. CT is transported to field in the form of a spool that consists of the tubing coiled around a drum. Large tubing requires a large reel over which tubing can be spooled. This increases the cost of transportation of spool to the field that may not be possible in all cases. Hence, optimization of completion strategies should be taken into consideration the wellbore geometry.

Becker & Azar (1985) analyzed the outcome of change in drill-pipe diameter on the concentration of solids in suspension flow (not forming a stable bed). The study suggested that volumetric solids concentration increases to a certain extent with an increase in pipe diameter (if

other relevant parameters are maintained constant). It was observed that torque applied to the drill pipe due to solids concentration is proportional to the outer diameter of the inner pipe. It was pointed out that steady-state was not achieved when tests were conducted with 0.09 m (3.5-in.) pipe in all except 30° inclination. A similar study (Jalukar 1993) suggested that the velocity required to initiate solids movement increases with the hydraulic diameter of the annulus. This effect was insignificant when inclination was between 30° and 45°.

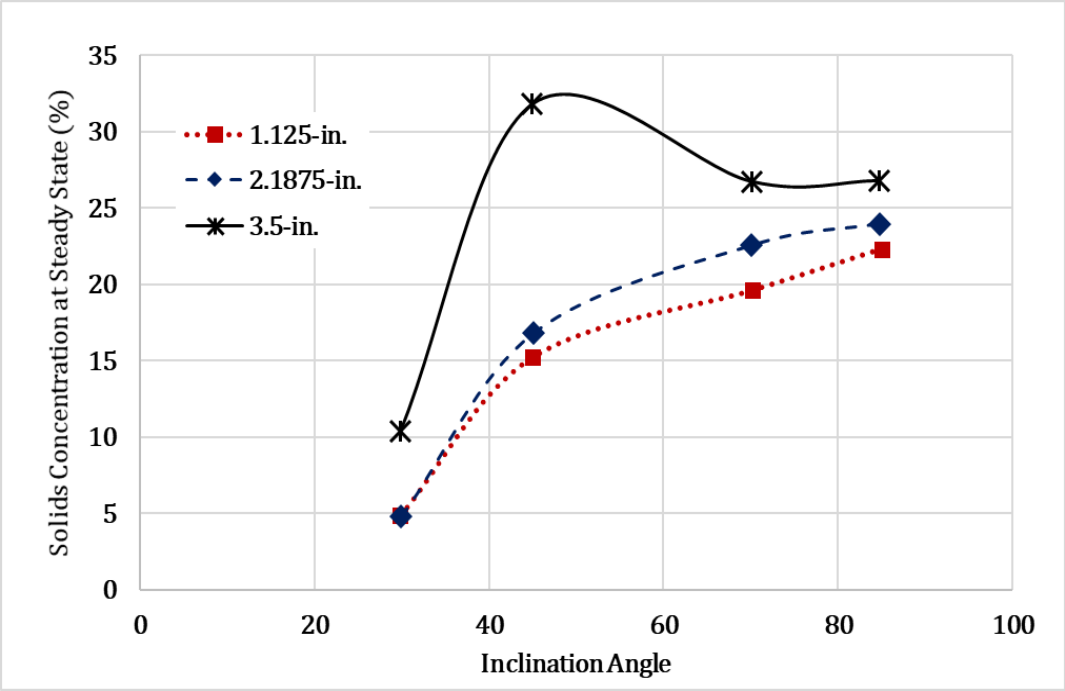


Fig. 2.8: Solids concentration in annular suspension flow for different sizes of drill pipe within 0.127 m (5-in.) hole. (data source- Becker & Azar, 1985)

2.4.2 Wellbore Inclination

The wellbore inclination is an important parameter affecting solids transport. Erosional mechanism and transportation behavior of solids is different under various range of inclinations. Three distinct inclination range have been identified depending on the associated solids transport mechanism as follows:

i. Low (0 to 30°)

ii. Intermediate (30 to 60°)

iii. High (60 to 90°)

In the absence of fluid flow, the bed tends to slide downward in the inclined section and accumulates at the 'heel'. In the presence of fluid flow, the sliding can be prevented if the bed shear stress applied by the fluid is sufficiently high. In order to maintain solid suspension, flow velocity should be considerably increased in the intermediate inclination range. Otherwise, solid beds form and slide downward since the gravitational force acting on solids bed exceeds the combined effect of bed shear stress applied by fluid and static friction force acting on the interface of bed and wall. The sliding creates a secondary flow, which is similar to the Boycott effect. This phenomenon is prevalent in this range of inclination. The secondary flow is enhanced by the density difference between the bed layer and low-density suspended layer, which is flowing above the bed.

Tomren et al. (1986) conducted 242-bed erosion tests under various inclinations, pipe/hole eccentricity, and fluid flow regimes. The formation of a stationary bed was predominant at inclinations greater than 35°. Ford et al. (1990) defined the term Minimum Transport Velocity (i.e. minimum velocity to initiate particle movement from the stationary bed) and investigated the effects of different operational parameters. The experimental results suggested that Minimum Transport Velocity (MTV) required to initiate solids movement by rolling mechanism increases with hole angle until it reaches a point of inflection after which it starts to reduce. The critical angle (point of inflection) has been found to be in the range of 40° to 60° from vertical. The solids beds in this range of angles were unstable and the authors reported local agitation of particles.

2.4.3 Fluid Velocity and Flow Regime

Annular flow velocity is the most critical and important design parameter in order to obtain maximum bed erosion. Large annuli require high flow rates to achieve the required fluid velocity. Many experimental based studies have been conducted to determine the influence of fluid velocity on bed erosion process. A high fluid velocity exerts higher shear stress on the solids bed, which improves the rate of bed erosion. Moreover, high velocity also increases the fluid drag and lift forces that help in the movement of suspended solids across longer flow length. A common observation in many of these studies was that a critical velocity exists, below which the solids tend to form a stable bed on the low side of an inclined annulus (Li & Walker, 1999).

Bed erosion is highly dependent on the cross-sectional velocity profile within the wellbore. The velocity profile, in turn, depends on fluid rheology and hence, the shear stress applied at the fluid-solid bed interface. In practical terms, a fluid can be either in a laminar or a turbulent flow regime, depending on the combination of the inertial forces and frictional forces. A dimensionless ratio of inertial and viscous forces, called Reynolds number, determines the fluid flow regime.

$$Re = \frac{inertial\ force}{viscous\ force} = \frac{\rho_f U d_h}{\mu} \tag{2.6}$$

where Re is the Reynolds number; U is the mean velocity of fluid; $d_h$is the hydraulic diameter; μ is the dynamic viscosity of fluid.

Laminar flow occurs within a lower range of Reynolds number, in which the viscous force is dominant over the inertial force, and it is characterized by smooth and constant fluid flow

behavior. Turbulent flow occurs at high Reynolds numbers, and this flow regime is dominated by inertial forces. This leads to the generation of chaotic eddies, vortices and other instabilities in the flow.

In laminar flow, the fluid molecules follow the path of streamlines. These streamlines do not cross each other. The combined effect of smooth and stable flow in the laminar flow regime plus the no-slip condition inhibits the lifting of particles from the solids bed. On the contrary, a large number of eddies are developed when the fluid is well within the turbulent regime. The size of eddies can vary from very large ones crossing several streamlines to much smaller ones that are limited to near the walls. In terms of fluid kinematics, these eddies superimpose on the main flow stream and reshape it. The fluid element experiences rotation due to the momentum transfer from eddies that cross the streamline they follow. Implications of generating turbulent eddies in fluid flow and its effect on wellbore cleanout mechanism are discussed in detail later.

It is also important to point out the flow conditions occurring within a boundary layer. Irrespective of the flow velocity and flow regime, boundary layer occurs at the solid-liquid interface having a characteristic of sharp velocity reduction to zero. This is often termed as “no-slip” condition. In simpler words, no-slip condition states that the fluid adheres to the surface of the solid in a boundary layer.

2.4.4 Fluid Characteristics

Fluid characteristics are extremely important in effective cuttings transport behavior. Fluid rheology is a characteristic that requires the most attention. Fluid must be designed in a way to incorporate the highest pump rate with the smallest possible friction pressure. High viscosity fluids perform better in vertical or near-vertical wells whereas highly deviated and horizontal

wells benefit more from low viscosity fluids. Li & Walker (1999) found similar results from their experiments. The authors compared three different fluids (water, HEC, and Xanthan polymer). It was concluded that for the vertical/near vertical wellbore, hole cleaning is more efficient if high-viscosity fluid is pumped under laminar flow condition than low-viscosity fluid under turbulent flow condition. The shear stress at the solids bed and liquid interface, for a near-horizontal wellbore, plays the key role in transporting solids. Low viscosity fluids help generate high shear rate at the tubular walls and develop a turbulent flow pattern more readily. The turbulence helps suspend particles in the flow stream.

Li & Wilde (2005) studied the cleanout efficiency with various bio-polymers. These bio-polymers had high Low Shear Rate Viscosity (LSRV) and were shear thinning in nature. These fluids exhibit relatively low-viscosity at the fluid-solid interface due to high shear. As a result, the turbulent velocity profile develops and helps the lifting of the particle into the flow stream. The fluid element in the flow stream is exposed to a relatively low shear rate as compared to the wall and hence maintains high viscosity. Due to this, once the particles are picked up from a stationary bed, the viscous fluid is able to carry them to a longer distance before they re-settle. It was recommended that the LSRV should be higher for better suspension capabilities. To summarize, high viscosity fluids are better in carrying the suspended particles whereas low viscosity fluids are more efficient in lifting the particles from a stationary bed. However, high viscosity fluids can be more costly and complex as compared to low viscosity fluids.

The increase in fluid density increases solids suspension capacity of fluid by reducing the settling velocity of the suspended particles (i.e. increasing buoyancy). Despite the fact that fluids with higher density increase buoyancy, they increase bottom hole pressure. Another disadvantage

with ‘weighted’ fluids is the tendency of the weighting material to settle out of the fluid phase, which is known as ‘sag’. One of the major functions of drilling fluid is to exert hydrostatic pressure to control the well, and hence fluid density cannot be altered for improving hole cleaning.

2.4.5 Solids Properties

The properties of solid particles being eroded from the bed and transported to the surface might not be entirely known in some cases, especially drilling. Therefore, an accurate prediction of solids properties becomes essential to model efficient hole-cleaning. The sphericity of particle is often neglected in cleanout studies, but it has been found to be an important factor affecting the static and hydrodynamic forces acting on solid particles. The viscous shear force acting on a particle is more consistent in the case of a perfectly spherical particle. Additionally, maximized surface area per volume ratio attributed to the sphericity of the particles helps transport them much easier than non-sphericity particles. Moreover, the fluid-induced rotation on spherical particle slightly hinders the inertia or ability to move as it spins. Not only are the non-sphericity particles difficult to lift from a stationary bed, but they also continuously accelerate and decelerate or even stop as they rotate along their own axes. Hence, for the same amount of distance transported, the non-sphericity particles require more time of circulation and more energy to be imparted by the fluid.

The density or specific gravity of solid particles have a direct impact on the weight of the particle. The weight of the particle and solid-liquid density difference predominantly determine the subsequent lifting of a particle from a stationary bed. A heavier particle is more difficult to transport. Li & Wilde (2005) carried out experimental tests with four types of 20/40 mesh

proppant having different densities. Fig. 2.9 represents the transport ratio of these particles plotted against relative in-situ fluid velocity in 127 mm × 38.1 mm annulus with water used as cleanout medium. The specific gravity of proppant tested varied from 1.25 to 3.56. High-density solids deposited easily to form solids beds. The solids were easier to transport in a vertical wellbore than in a horizontal one. Highly viscous fluids performed better in vertical wellbores whereas low-viscosity fluids such as water performed better in horizontal sections.

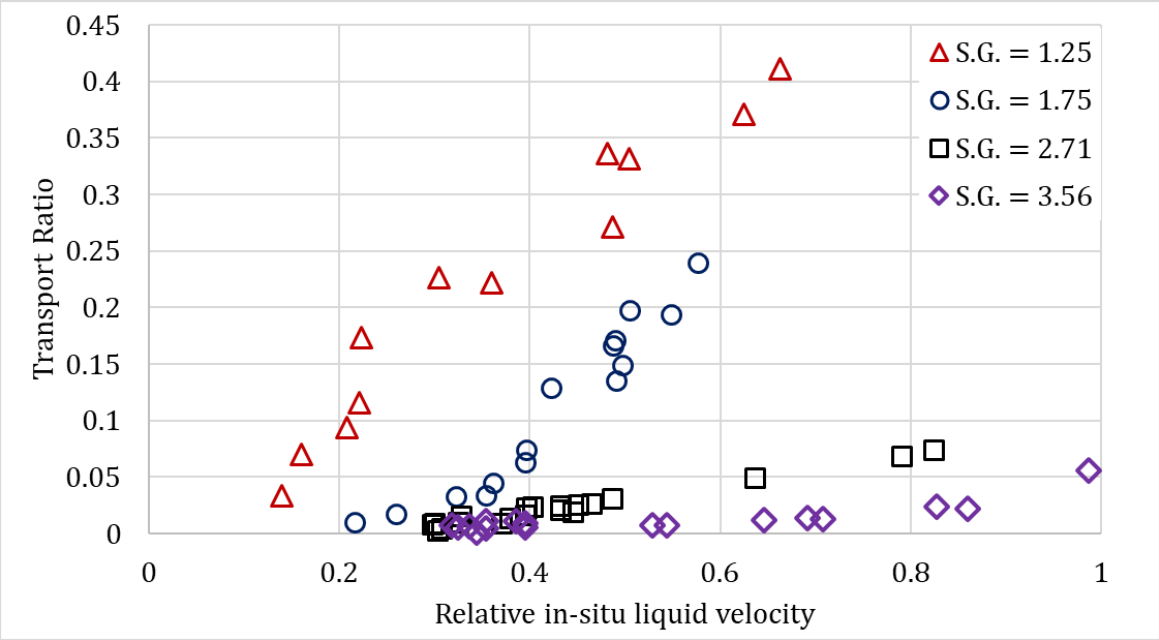


Fig. 2.9: Effect of solids density of transport ratio (data source – Li & Wilde, 2005)

A number of studies (Larsen 1990; Li & Wilde 2005) have been conducted to examine the effect of particle size on hole cleaning. Larsen (1990) tested cuttings with different size distributions: large (7 mm), medium (4.45 mm) and small (2.3 mm). Smaller cuttings were difficult to transport at high inclinations. However, on reducing the inclination, small cuttings of uniform shape were easier to clean. Li & Wilde (2005) investigated three different particle sizes and observed that velocity required to prevent solids from settling (critical velocity) increases with

particle size (up to 0.5 mm). On further increasing the particle diameter, the critical velocity decreases.

2.5 Turbulence in Bed Erosion

Most of the hole cleaning occurs under turbulent flow regime. This makes it vital to understand how turbulence affects the motion of solid particles in the annulus from the moment they are dislodged from the bed. However, this topic is relatively underdeveloped despite the immense work conducted by previous studies (Arnipally et al., 2018; Csuka and Olšiak, 2016; Hartnett and Kostic, 1990; Gnambode et al., 2015; Gavrilov and Rudyak, 2016; Capecelatro and Desjardins, 2013; Dodge and Metzner, 1959; Bizhani and Kuru, 2019). This is attributed to the fluctuations occurring due to eddies that make turbulence a very complex phenomenon. Consequently, field engineers rely more on empirical or semi-empirical correlations developed for different scenarios to evaluate hole-cleaning efficiency.

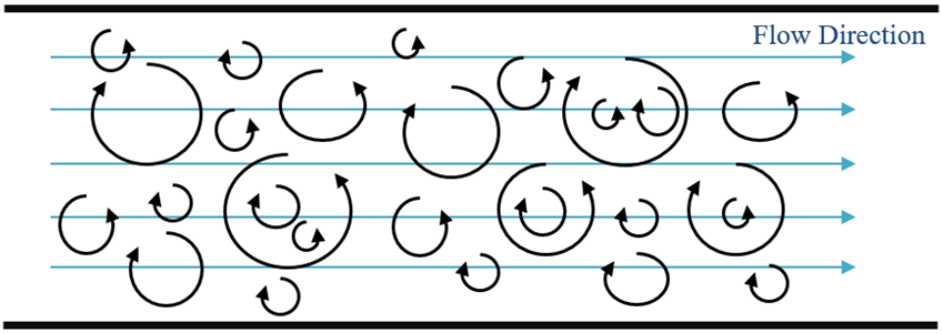


Fig. 2.10: Turbulent flow and eddy behavior

Momentum transfer across streamlines in laminar flow is majorly through the viscous forces. Conversely, in turbulent flow regime, rapidly developed swirls or eddies are responsible for momentum transfer. Eddies, or the swirling flow pattern, occurring in the turbulent flow of fluid is characterized by random fluctuations (Fig. 2.10). A significant amount of momentum is

transferred due to these fluctuations. The mass and momentum transfer across different fluid regions in turbulent flow is much more rapid as compared to that by viscous diffusion in laminar flow. This increases in the rate of mass and momentum transfer results in energy loss that leads to a higher value of friction factor.

Turbulence is not restricted to only unsteady-state flow. Even though the fluid flow may be steady, it may involve eddies which cause steady fluctuations in local velocities, temperature and pressure. In turbulent flow, the instantaneous velocity (u) at any time is not stable and tends to fluctuate about an average value (Fig. 2.11). The velocity profiles can be mathematically decomposed into an average $\langle u \rangle$ and fluctuating velocity (u´). such Thus: u = $\langle u \rangle$ + u´. Similar decomposition can be applied to velocities in other coordinates and other parameters such as temperature and pressure.

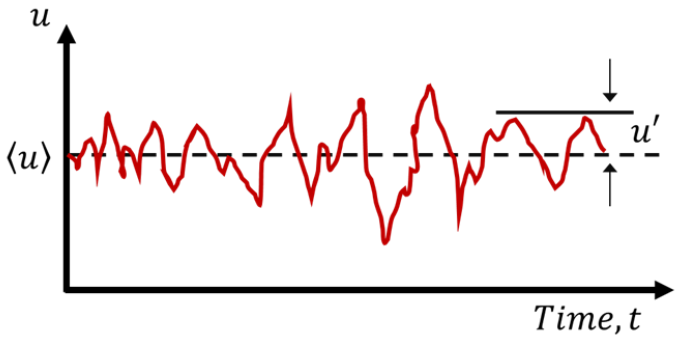


Fig. 2.11: Instantaneous velocity with time at any arbitrary location in turbulent flow

For flow analysis, the instantaneous variables are averaged over a sufficiently large time interval. Subsequently, the average of fluctuating components throughout the large time interval is zero. However, the average values of instantaneous variables are independent of time. The magnitude of fluctuations are usually of a lower order, but the large frequencies of fluctuations make them an effective method of mass, momentum, and energy transfer. As mentioned previously and from

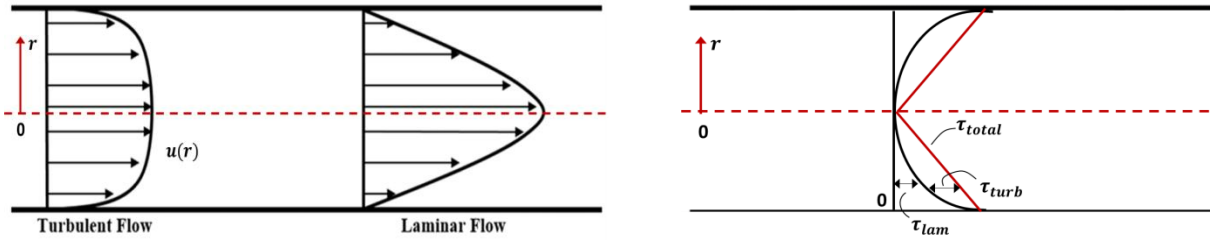
various sources of literature, average fluid velocity plays an integral and dominant role in proper solids removal. This chaotic movement due to fluctuations can result in significant pressure across a fluid particle in the flow stream and must be considered when analyzing the effect of average fluid velocity on hole-cleaning.

2.5.1 Turbulent Shear Stress

Previous experimental studies have concluded that shear stress due to turbulence is much larger than that by laminar flow and hence, laminar flow calculations for the same cannot be extended to turbulent flow regime. In order to understand shear stress caused by eddies, it can be beneficial to study it in two distinct parts: the laminar and turbulent component of the total shear stress. Laminar component accounts for the inter-layer momentum transfer. Conversely, turbulent shear stress is related to the momentum transfer due to inter-layer mass transfer. Mathematically, total shear stress can be described as (Kudela, 2010):

$$\tau_{total} = \tau_{lam} + \tau_{turb} \tag{2.7}$$

Fig. 2.12 presents the average velocity profile and magnitude of shear stress components in turbulent and laminar pipe flows. It should be noted that the average velocity profile of turbulent flow follows a logarithmic profile while laminar flow displays a parabolic profile. Additionally, an important aspect of turbulent flow velocity is that it has a sharp decrease in velocity near the wall (no-slip condition). A substantial amount of momentum is transferred from the center of the pipe towards the pipe walls in case of turbulent flow as compared to laminar flow. Within the boundary layer, the velocities closer to the wall are much higher in turbulent flows than laminar flows. However, as the magnitude of turbulence increases, this boundary layer gets thinner and the momentum can be directly applied to particles, moving them back into the flow stream.



(a) (b)

Fig. 2.12: (a) Velocity profile and (b) stress profile for turbulent and laminar flow

Fig. 2.13 illustrates momentum transfer occurring in turbulent flows due to eddies. Assume a flow in horizontal pipe with particle movement from a low-velocity layer (y_2) to an adjacent high-velocity layer (y_1) in an upward direction through a differential area dA due to velocity fluctuation v'. The mass flow rate crossing through this area is $\rho v' A$. This momentum transfer causes a slight reduction of average velocity above dA. Consequently, the horizontal velocity of fluid-particle crossing the domain dA is increased by u'. The force acting on a fluid volume above dA due to this momentum transfer is equal to the rate of change of momentum (Eq. 2.8).

$$\delta F = (\rho v' dA)(-u') = -\rho u' v' dA \tag{2.8}$$

Hence, the shear force per unit area or the turbulent shear stress at any point can be expressed as:

$$\tau_{turb} = \frac{\delta F}{dA} = -\rho \overline{u'v'} \tag{2.9}$$

Although the average velocity in horizontal ($\overline{u'}$) and vertical ($\overline{v'}$) directions are zero as mentioned earlier, the average values of their products are not zero ($\overline{u'v'} \neq 0$). On the contrary, experiments have revealed that their average is a negative value. The product of fluid density and these non-zero fluctuating velocity products are known as Reynolds stress or turbulence stress.

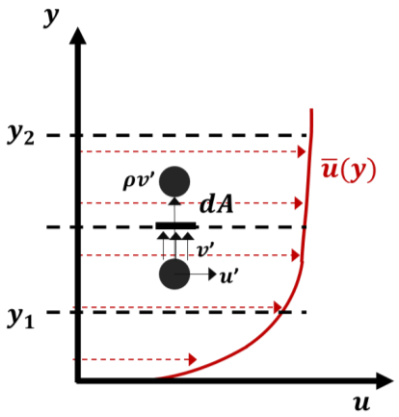


Fig. 2.13: Particle moving upward due to eddies

Momentum transfer through turbulence is very analogous to momentum transfer through molecular diffusion during which particle collide with each other. Therefore, for simplicity, it can be represented in terms of eddy viscosity (μ_t) or turbulent viscosity as

$$\tau_{turb} = -\rho\overline{u'v'} = \mu_t \frac{\partial \bar{u}}{\partial y} \tag{2.10}$$

Combining this with Eq. 2.7 yields,

$$\tau_{total} = (\mu + \mu_t)\frac{\partial \bar{u}}{\partial y} \tag{2.11}$$

Eddy diffusivities are comparatively much greater than molecular diffusion on the core flow region of a turbulent flow. As the profile moves towards the wall, the eddies lose their intensity and diminish significantly at the wall due to the no-slip condition. This is the reason why the core velocity profile is much flatter in the core region and the velocity gradient reduces rapidly close to the wall.

2.5.2 Turbulent Velocity Profile

As presented in Fig. 2.14, turbulent flow regime comprises of four separate layers categorized by the distance from the wall:

1. Viscous sub-layer, dominated by viscous shear
2. The buffer layer, in which turbulent effect start getting significant
3. Overlap layer includes both viscous and turbulent shear
4. The outer layer or core region, dominated by turbulent shear

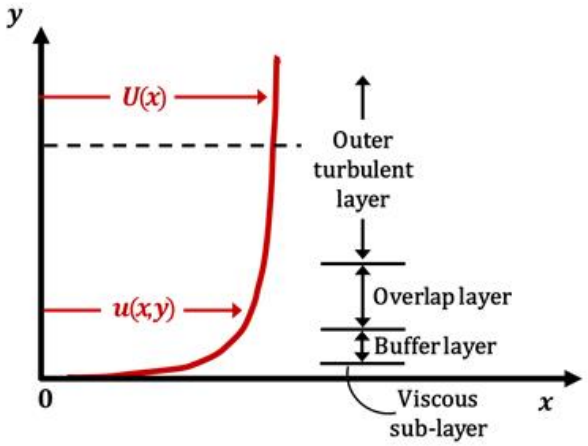


Fig. 2.14: Layers in a turbulent flow regime

Let U be the time-averaged velocity in the x-direction. Layer closest to the wall is a viscous sub-layer in which the viscous effects are dominating. The velocity profile in this layer approximately equates that of a laminar flow regime and is nearly linear with a streamline flow. Next layer closer to the core flow is called a buffer layer. Although the flow is still dominated by viscous stresses, the turbulent effects start becoming significant in this layer. Above this is an overlapping layer (often termed as the transition layer) in which viscous effects and turbulent effects both play an important role. The core of the flow, also called outer layer. Developing an analytical model for the entire turbulent flow regime (similar to the laminar regime) is difficult

because flow characteristics are quite different in each layer. Identification of key parameters, developing functional analytical forms of turbulence and applying experimental data has been found to be the best approach to obtain the turbulent velocity profile.

CHAPTER 3

LITERATURE REVIEW

Wellbore cleanout has been a very important topic for oil and gas research. Many studies have been conducted to examine the movement of solids during cleanout operation from various perspectives. This chapter presents a review of important experimental studies performed by various researchers in the past. These studies are usually conducted using a specific flow loop and modifying test variables. The experiments are performed to study two major categories of solids transport – steady-state and transient. Steady-state transport is a process when the amount of solids removed is equal to the amount of solids generated (usually through drilling process in the field), thereby maintaining a constant concentration of solids in the flow loop. Transient transport is bed erosion during which there is a reduction of solids bed in the flow loop until it becomes constant. The constant bed height (equilibrium bed height) is achieved when fluid is unable to erode the bed any further. There is no generation or injection of solids in the test loop during transient erosion process. This research is conducted to study the transient nature of bed erosion. The challenge of optimizing wellbore cleanout has also been targeted by developing a generalized model.

3.1 Solids Transport Under Steady-State Conditions

One of the earliest investigations to understand the effects of different factors on hole-cleaning was conducted by Tomren et al. (1986). Results indicate that greater annular velocities are vital for efficient cleanout process, especially in directional wells (Fig 3.1). Increase in inclination from vertical to horizontal with steady cuttings generation rate during drilling decreases the cleanout efficiency of the fluid. Rapid buildup of solids bed and faster downward sliding were

observed when inclination was between 40° to 50° (Fig. 3.2). The critical inclination varied with flow rate. Additionally, muds with higher viscosity were better in removing drilled cuttings out of the well than fluids with low viscosity.

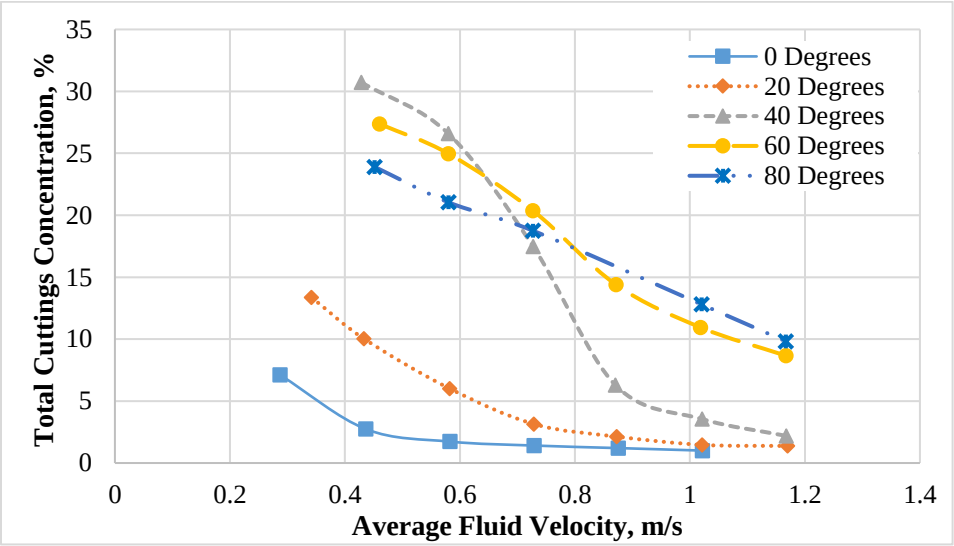


Fig. 3.1: Cuttings concentration vs laminar fluid velocity (Tomren, 1986)

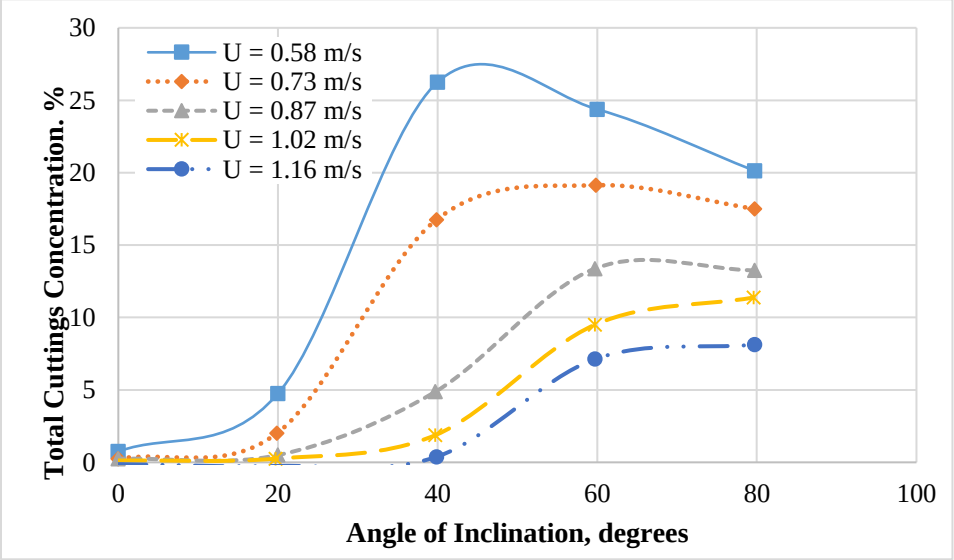


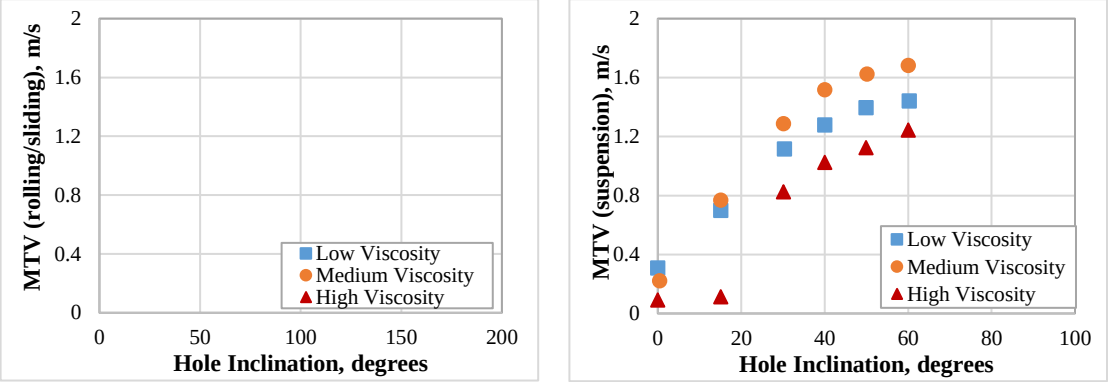
Fig. 3.2: Cuttings concentration vs hole inclination (Tomren, 1986)

Another steady-state cleanout study (Larsen 1990), conducted to investigate the critical velocity required to prevent deposition of cuttings during drilling demonstrated the impact of well

inclination and flow rate on cuttings removal. The angle of inclination and annular flow rate were found to have maximum impact on the cuttings removal process. Low-viscosity muds performed better than high-viscosity muds in high inclinations. This is attributed to their relatively higher velocity in the narrow clearance between the drill pipe and casing. Wall shear acting on the fluid slows down the velocity of the fluid in narrower section creating a stagnant zone in the low-side of the annulus.

An earlier study (Ford et al. 1990) used a borehole simulator to identify the slurry flow patterns occurring during a cleanout operation. Although all transport mechanisms described in Chapter 2 were descriptively defined, two major mechanisms (rolling-sliding and suspension) were identified. In the first mechanism, drilled cuttings are transported out of the wellbore through the rolling-sliding mode of transport occurring on the low-side of a borehole. In the second one, drilled cuttings are transported as suspension within the flow stream. A Minimum Transport Velocity (MTV) was defined as minimum velocity to prevent the formation of any static or downward moving bed in the annular section during slurry flow. For the case of the rolling-sliding mechanism, MTV is defined as the velocity required to develop separated or continuous dunes/moving beds. Contrastingly, for cuttings transported through suspension, MTV is the velocity required to develop sand clusters or transport solids through the process of saltation and suspension. At extremely small inclinations (< 30°) cuttings bed exhibited a tendency of downward sliding and making it almost impossible to generate stable cuttings bed. However, based on general observations, it was concluded that MTV required to transport the solids by sliding-rolling mechanism increased initially with inclination before reaching a maximum value, and subsequently decreasing (Fig. 3.3). The critical angle or the point of inflection for this trend

was found to be in the range of 40° to 60° from vertical. The solids bed at these critical angles were unstable and the authors reported local agitation of particles.



(a) (b)

Fig. 3.3: Effect of rheology and inclination on MTV (Ford et al., 1990)

Larsen (1997) experimentally investigated the influence of fluid rheology, inclination angle, eccentricity, fluid flow rate, and solids size on the Critical Transport Velocity (CTV). The CTV is defined as the minimum average flow velocity needed to sustain suspension of solids or prevent its settling. An empirical correlation that predicts CTV has been developed. The study reported the range of CTV (0.9–1.2 m/s) for typical cleanout operations. A similar flow loop study (Sanchez et al. (1999) was conducted to investigate the effect of drill pipe rotation on wellbore cleanout during directional drilling. Results demonstrated a significant impact of pipe rotation on wellbore cleanout. The cuttings concentration reduction was found to be a function of drillstring rotation, inclination angle, and flow rate. Pipe rotation enhanced bed erosion by reducing the residual cuttings concentration in the annulus and the erosion time. Later, an experimental study (Ozbayoglu et al. 2004) showed the most dominant effect of fluid velocity on cleanout efficiency. The extension of the study (Ozbayoglu et al. 2008) concluded that a stationary bed is generated when bulk velocity is less than 1.83 m/s (allowing for solids to settle). A similar approach was adopted by Duan et al. (2008) using different fluids and three particle

sizes. Low-viscosity fluids were more efficient in eroding larger particles whereas viscous fluids were more efficient in cleaning fine particles. Rotational speed of inner pipe further enhanced cleaning of smaller solids. Although the qualitative results were in agreement with that obtained by Ozbayoglu et al. (2008), quantitative data obtained by Duan et al. (2008) deviated significantly (up to 80%).

A more recent study (Sayindla et al. 2017) examined the process of cuttings transport with a continuous sand injection to investigate hole cleaning efficiency in horizontal test section using oil-based (OBM) and water-based (WBM) drilling mud. Fig. 3.4 relates sand holdup of oil-based and water-based muds at fluid velocities of 0.50, 0.75, 1.0 and1.2 m/s and no drill pipe rotation and rotation of 150 RPM. Observations suggested that OBM has better cleaning performance than WBM without drill string rotation. With drill pipe rotation, cleanout efficiency of both fluids is very similar. The sand holdups in both cases were reduced with the introduction of pipe rotation. This is attributed to the additional velocity component acting on the bed in the form of tangential flow combined with axial flow.

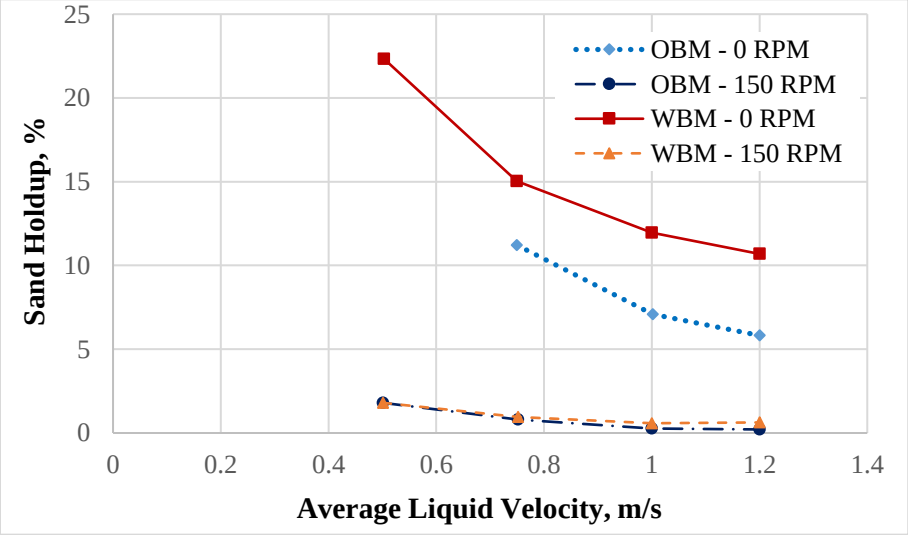


Fig. 3.4: Sand holdup vs superficial velocity (Sayindla et al., 2017)

3.2 Bed Erosion Under Transient Conditions

An early bed erosion study (Zamora and Hanson 1990) developed a set of 28 ‘rules of thumb’ to be followed for efficient cleanout. These rules were based on the experimental investigations conducted in test flow loops with test variables including inclination, wellbore geometry, fluid type, solids bed, flow velocity, and its profile, flow regime, fluid rheology, fluid density, sweeps, and pipe rotation speed. It was observed that intermediate inclination angles (30° to 60°) were most difficult to clean as the developed bed tends to slide downwards or ‘avalanche’ opposite to the flow direction. The range of upper and lower limits of factors influencing bed stability was narrowed down to type, shape, and size of solids forming the bed, rheology, and density of fluid utilized in hole-cleaning and the wall roughness. However, the extent to which these factors contributed to bed stability or the demarcation of the range of these parameters was not discussed conclusively. Within the range of 40° to 50° inclination, ‘boycott’ settling was an additional phenomenon that accelerated bed formation. During the downward sliding of bed, a cross-sectional density gradient generates across the annular area thereby causing pressure imbalance. This causes the convection mechanism to move light density fluid on the up-side forming a thin layer near the upper wall and the concentrated bed to slide downward. Hole cleaning parameters considered for optimal hole-cleaning in one section of the wellbore may not be adequate to other sections of the same well. Ideally, these parameters should be varied as different sections of well are to be cleaned out. This may not be practically possible in each case. For this purpose, it was recommended that fluid properties should be designed to target hole-cleaning in inclinations of 35° to 55° as these are the most difficult inclinations to clean.

Later, a more comprehensive bed erosion study (Adari 1999) was conducted using a large-scale flow loop. The study developed an exponential decay function to predict the reduction in bed

height with circulation time. The relationship is valid for a certain range of flow parameters. The experiments were limited to high viscosity weighted drilling muds for the flow rate range of 12.62 – 31.54 L/s. Most of the cleanout operation is conducted with less viscous fluids, especially in horizontal wells with longer laterals. Therefore, the relationship developed by Adari cannot be directly implied in such cases.

Walker and Li (2000) summarized the influence of solid size and fluid rheology on the bed erosion process. Flow tests pertaining to the effect of fluid rheology suggested that Xanthan Gum (Xanvis) and Hydroxyethyl Cellulose (HEC) based fluids with a relatively higher viscosity than water exhibit better suspension capability but lack the efficiency in eroding the bed. Higher flow rates may result in excessive pressure loss which can be detrimental for the cleanout operation. Therefore, it was recommended to pump higher viscosity fluids under laminar flow regime to efficiently remove solids from the vertical section of the well. Additionally, particle size range between 0.15 mm and 7 mm were investigated and it was observed that solid size distribution with a particle size of 0.76 mm was the most difficult to erode. The results obtained by Walker and Li were consistent with observations made by Martins et al. (1992) who had conducted a similar study.

A flow loop study on (Kelessidis and Mpandelis 2004) on slurry flow pattern observed the formation of non-stationary progressive beds at lower flow rates (Fig. 3.5). Increase in the flow rate resulted in erosion thereby reducing the bed height with time. At even higher flow rates, movement of the solids was characterized as a dispersed bed in which solids did not settle completely but were transported in streaks at the low-side of the annulus.

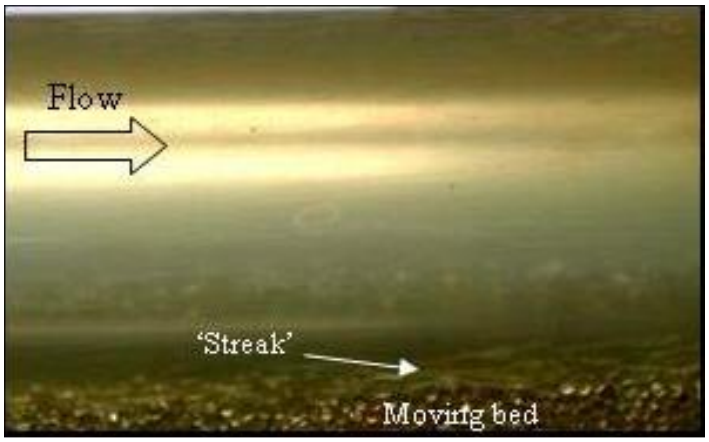


Fig. 3.5: Moving bed and streaks at the interface as observed by Kelessidis and Mpandelis (2004)

3.3 Mechanistic Hole Cleanout Models

Since the expansion of the applications of directional and horizontal drilling, a number of mechanistic hole cleanout models (Espinosa & Candia, 2011; Ahmed et al. 2001; 2003; Duan et al. 2008; Gavignet & Sobey 1989; Martins & Santana 1992; Ford et al. 1996; Clark and Bickham 1994) have been developed. Development of mechanistic models to study the wellbore cleanout process involves analysis of forces acting on the bed interface using mass and momentum balance equations. Mass balance is applied to the different phases considered in the cleanout system and momentum balance is applied to the different layers within the system. Solutions to these equations are obtained by applying relevant mathematical or physical assumptions (boundary conditions) depending on whether the target model is one-layer, two-layer or three-layer. One-layer model defines the cleanout mechanism as the flow stream in which the only mode of transport is the suspension. Two-layer model results in solids transport occurring in two distinct layers. The bottom layer comprises of a stationary or moving (as a single entity) solids bed. Another layer of clean fluid/fluid with suspended solids exists above the bed. In addition to the above-mentioned layer, the three-layer model includes a moving/dispersed bed as a third

layer that exists between stable bed and suspension layer. The literature in this manuscript focuses majorly on one and two-layer models since the study conducted considers a reduction of stable bed and suspension layer.

One of the first cleanout models was developed by Clark and Bickham (1994) that describes solids transport mechanism over the entire well trajectory (from top of well to bottom-hole assembly). This model is developed to calculate the minimum transport velocity required to either settle/lift particles in vertical sections or initiate particle movement by rolling/lifting in deviated and horizontal sections. Fig. 3.6 represents a schematic diagram of bed interface at an inclination angle, θ, from vertical.

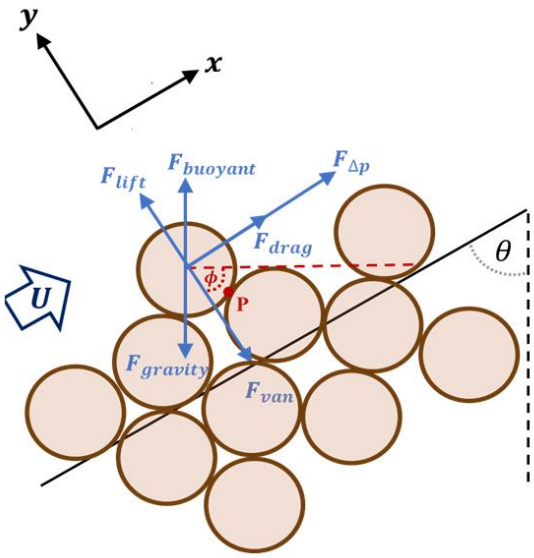


Fig. 3.6: Forces acting on the center of the particle protruding out of the bed.

A few of these particles protrude out of the bed. Higher well inclinations generate conditions such that complementary of inclination angle becomes less than the angle of repose of solid bed ($\theta < 90\text{-}\phi$). Such conditions result in a stable bed and movement of solids through rolling and lifting mechanism. The minimum flow rate to dislodge a solid particle from the bed can be calculated if the dynamic forces acting of the center of gravity of particle can be calculated in

terms of local average velocity, U. The gravitational center of the particle encounters various forces acting by the interparticle interaction and through fluid flow. Static forces imparted on the particle are – buoyant force ($F_{buoyant}$), gravity ($F_{gravity}$) and plastic force due to the thixotropy of fluid (F_p). Similarly, dynamic forces acting on the solid particle includes drag force (F_{drag}), lift force (F_{lift}), and the force due to the frictional pressure gradient ($F_{\Delta p}$). The solid particle is held stationary by a reactive (friction) force that is essentially a sum of vectors of fluid drag and force due to the pressure gradient. The equilibrium conditions required to initiate rolling mechanism of the particle can, therefore, be estimated by balancing the moment at the contact point, P.

$$|y|\left(F_{drag} + F_{\Delta p}\right) + |x|\left(F_{lift} - F_p\right) + l\left(F_{buoyant} - F_{gravity}\right) = 0 \tag{3.1}$$

where the gravitational and buoyant moment arm length (l) is calculated as:

$$l = |x|\left(sin\theta + \frac{cos\theta}{tan\phi}\right) \tag{3.2}$$

The origin is considered to be at the center of the particle in consideration. The complementary angle of the angle of repose, ϕ can be geometrically expressed as $\phi = \tan^{-1}(x/y)$. Initiation of particle rolling requires a condition that the sum of dynamic forces should exceed the sum of static forces. Increase in dynamic forces can be typically attained by enhancement in the flow velocity. A similar procedure can be followed to obtain the criteria to determine the onset of the lifting of the solid particle within deviated and horizontal wellbores. The lifting of the solid particle will occur once it starts the movement in vertical (y) direction. Once the particle is entrained into the flow stream, the axial relative velocity imparts the drag force on the solid particles and transports it up to some distance before the particle falls back in the stable bed when the relative velocity diminishes due to the acceleration of the particle. Considering the

momentum balance for equilibrium condition, the sum of all the forces acting in y-direction can be represented as:

$$F_{lift} - F_P + \left(F_{buoyant} - F_{gravity}\right).sin\theta = 0 \quad (3.3)$$

It is observed through the equation that as the well profile approaches vertical ($\theta \rightarrow 0°$), lift force acting on the particle tend to be equal to plastic force ($F_{lift} \rightarrow F_p$). The solution for Eq. 3.3 can be obtained with the help of auxiliary equations (by expressing various forces in terms of velocity) resulting in the calculation of the critical velocities required for rolling and lifting. Neglecting the plastic force, critical velocity equations for rolling and lifting mechanisms are described in Eqs. 3.4 and 3.5, respectively.

$$u_{roll} = \left[\frac{4\left[d_p g\left(\rho_s - \rho_f\right)(cos\theta + sin\theta tan\phi) + dP/dx\right]}{3\rho_f(C_D + C_L tan\phi)}\right]^{\frac{1}{2}} \quad (3.4)$$

$$u_{lift} = \left[\frac{4\left[d_p g\left(\rho_s - \rho_f\right)(sin\theta)\right]}{3\rho_f(C_L)}\right]^{\frac{1}{2}} \quad (3.5)$$

where, $\frac{dP}{dx}$ is the pressure gradient $\left(= \frac{4\tau_w}{D_{hyd}}\right)$.

The results obtained through these equations were validated with experimental data obtained by various studies. It was observed that the equations tend to under-predict the values of critical flow rate for both concentric and eccentric annulus and at all inclinations. The inconsistency in predicted and actual data was attributed to the difference in methods of data collection. The critical flow rate during experiments was recorded when the first movement of any particle in the bed was 'visually' observed. However, the model developed is based on the average particle size.

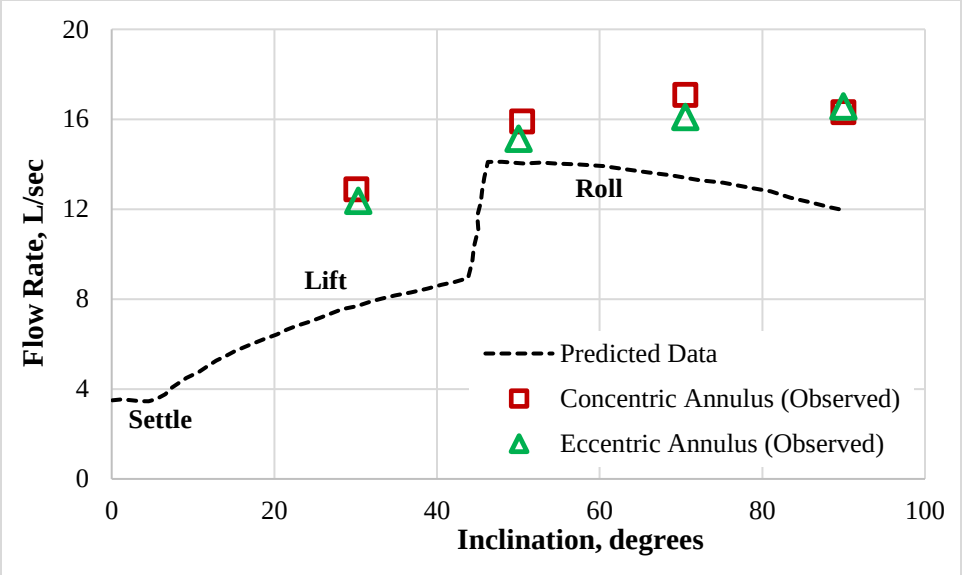


Fig. 3.7: Critical transport comparison (Clark and Bickham, 1994)

A relatively precise hydraulic model was established by Ahmed et al. (2001; 2003) to predict the rate of bed erosion. The model was formulated by a combination of hydrodynamic equations and classical mechanics. The study was focused on the evaluation of forces imparted on a particle in the bed and consequently, to optimize the parameters affecting its movement. Rate of bed erosion was represented as a function of instantaneous acceleration experienced by the solid particle as it is dislodged from its position in the bed. The hydraulic model developed was able to predict bed erosion with considerable accuracy when compared to data obtained during experimentation. Moreover, this literature elucidates accurate methods for drag and lift force calculation for different scenarios. It was concluded that the rate of solids erosion, (E_r), can be expressed in terms of solids density, velocity and bed porosity.

$$E_r = \rho_s(1-\phi_p)\left(\frac{dh}{dt}\right)_{bed} \tag{3.6}$$

where,

ρ_s = particle density

ϕ_p = bed porosity

Eq. 3.6 can be reduced in terms of instantaneous acceleration experienced by the solids particle (a_p) with an assumption that net force acting on it is constant during the process of erosion. The derived equation (Eq. 3.7) consists of entrainment function (ε_t) which is related to annular geometry, particle size, bed packing and considers the time required for particle entrainment into the flow stream.

$$E_r = \frac{1-\phi_p}{2}\rho_s a_p \varepsilon_t \tag{3.7}$$

The outcomes from this study suggested that rolling and lifting of particles can occur simultaneously with one phenomenon dominating the other depending on circumstances such as inclination, velocity fluid rheology, etc. This is in strong agreement with the conclusion made by other researchers such as Duan et al. (2008).

The hydraulic models described so far are developed by incorporating localized flow parameters such as bed shear stress or/and local velocity of the fluid near solids bed. Converting and expressing these local parameters in terms of field scale parameters such as pump flow rate can induce considerable error towards the calculation of these parameters. A more realistic mechanistic model can be developed if there is a better understanding of the nature of the interaction between the solid phase and liquid phase during the hole cleaning process. Interaction of these phases in a multi-phase system can be bi-directional wherein the solid sediments can affect the turbulence in the fluid phase and vice versa (Bagchi & Balachandar, 2003). Many attempts have been made in the past to study such interactions pertaining to sediment transport in the rivers and other flow channels (Best, Bennett, Bridge, & Leeder, 1997; Carbonneau & Bergeron, 2000; Gore & Crowe, 1989; Wiberg & Rubin, 1989). Due to the difference in the characteristics of the processes, the studies were restricted to water as the fluid medium and did not capture the effect of rheology on the transport. Another limitation of mechanistic models is

its applicability to turbulent flows. As mentioned earlier, mechanistic models result in a local fluid velocity acting on a particle. However, in a turbulent flow regime, the local velocity at any point is not constant and fluctuates from its average value. Therefore, it is imperative to account for velocity fluctuations to accurately study the localized hole cleaning mechanism.

3.4 Computational Fluid Dynamics (CFD) in Bed Erosion

Availability of high capacity computer processors and their ability to run complex algorithms in a fraction of seconds has led to the development of CFD models to study hole-cleaning mechanisms. CFD approach is usually implemented to solve more complex flow problems by obtaining a solution to the Navier-Stokes (N-S) equations in a discretized spatial domain. For turbulent flows, CFD simulations on wellbore cleanout can be carried out using three approaches: Direct Numerical Simulation (DNS), Large Eddy Simulation (LES) and Reynolds Average Navier-Stokes (RANS) simulation.

DNS method is targeted to solve the N-S and continuity equations exactly without any averaging of values to obtain a time-dependent solution. Very fine meshing is required to solve a complex problem through DNS simulation as it requires capturing all scales of turbulence with respect to initial and boundary conditions. Even though DNS models are very accurate for capturing very fine length and time scale, they are not computationally attractive due to the greater computational requirements. Additionally, these models possess several limitations pertaining to boundary layer specification, range of applicable Reynolds number, and solution resolution.

Unlike the DNS approach, LES method tends to explicitly resolve only the large-scale eddies while the effect of smaller eddies arising from Reynolds stress is modeled using a sub-grid model. The reason only large-scale eddies are solved exactly is that these eddies contain the

majority of the energy in the domain and hence, are more prominent in enduring turbulence. Contrastingly, smaller eddies contain much less energy and are majorly responsible for dissipating energy from the system. The multi-grid model helps ensure that net energy is conserved within the system from sustained turbulence to dissipative eddies. Since only the large-scale eddies are solved and small-scale motions are modeled, approximate models can be incorporated without compromising the accuracy. This significantly reduces the computational power required to solve LES models and hence, is relatively less expensive than DNS models. Since the sub-grid system of LES approximates the smaller dissipative eddies, it becomes tedious for the system to solve a model with a smaller number of fine grids. This is one of the major drawbacks of using LES models to simulate the hole-cleaning process as it becomes difficult to capture wall interaction effects with different phases.

RANS models solve the N-S equations for the average flow parameters and model the eddies across both large and small scales. This is done by decomposition of turbulent variables into time-averaged (mean) value and instantaneous (fluctuating) value along with averaging flow equations in time scale. The instantaneous flow velocity can be mathematically represented as the sum of time-averaged velocity and fluctuating velocity as follows:

$$u(t) = \langle u \rangle + u'(t) \tag{3.8}$$

The average velocity, U, is mathematically defined as:

$$\langle u \rangle = \frac{1}{T} \int_{t_0}^{t_0+T} u(t) dt \tag{3.9}$$

Here, the net average velocity fluctuation is always zero. Similar to Eqs. 3.12 and 3.13, other variables such as pressure and temperature can be decomposed using RANS model. Time-averaging of N-S equations helps get rid of fluctuating values and results in Reynolds stresses

that define the momentum transport. The additional term in the RANS momentum equation represents this stress tensor. The system of RANS equations has more unknowns than the original N-S equations. These unknown quantities make it an open system of equations to be solved. Boundary conditions are specified in order to obtain closure to this system of equations. This is the fundamentals of the RANS modeling approach. Due to its simplicity, RANS models are widely accepted in hole cleaning simulations despite it is being used as an approximate solution to a complex problem.

Investigation of solids transport using a three-dimensional numerical solver was first introduced by King et al. (2000). A set of different operating conditions were simulated to improve cuttings removal process during drilling using a software developed by Simulog. Variables studied include solids bed accumulation with respect to pipe eccentricity, pipe rotation, inclination. Finite volumes and finite elements meshes were used to obtain the solution of the N-S equations for Newtonian fluids. Certain adjustments were made to capture the behavior of non-Newtonian drilling fluids. The flow geometry model used to study the fluid flow in the annulus is presented in Fig. 3.8a.

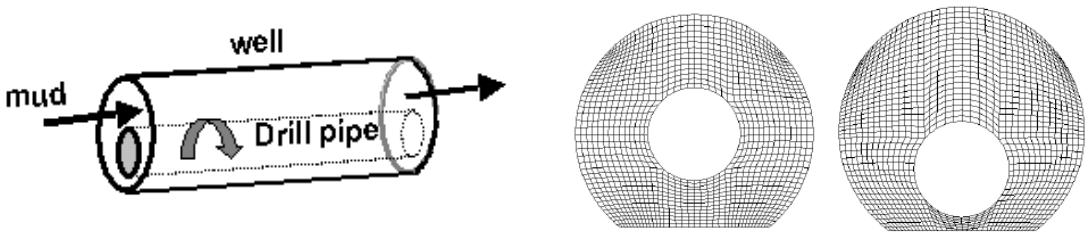


Fig. 3.8: Mesh systems for concentric and eccentric annuli (King et al. 2000)

Fig 3.8b is a representation of the cross-sectional mesh that was generated to model the solids removal process. Computational calculations were made at a total of 228,150 nodes across the

entire curvilinear mesh. Local velocities were predicted from the wall of the inner pipe to the center of the annulus and these predictions were compared against experimental readings obtained by Nouri et al. (1994) as plotted in Fig 3.9.

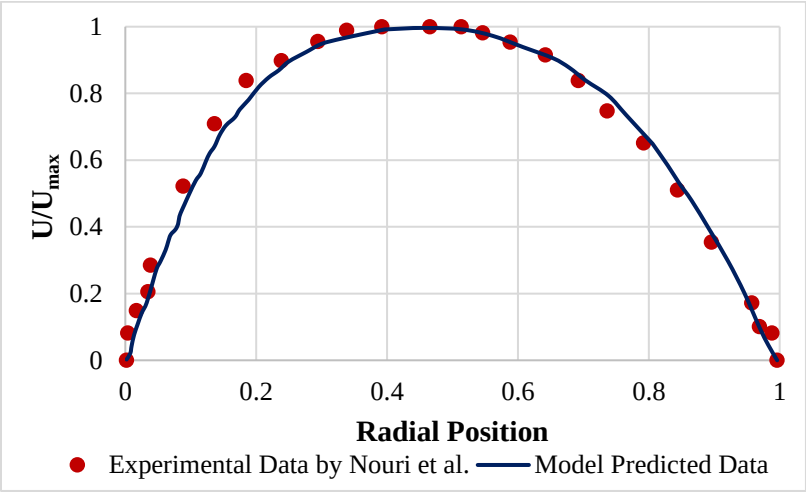


Fig. 3.9: Normalized velocity profile versus radial position (0=pipe; 1=well) (Nouri et al., 1994)

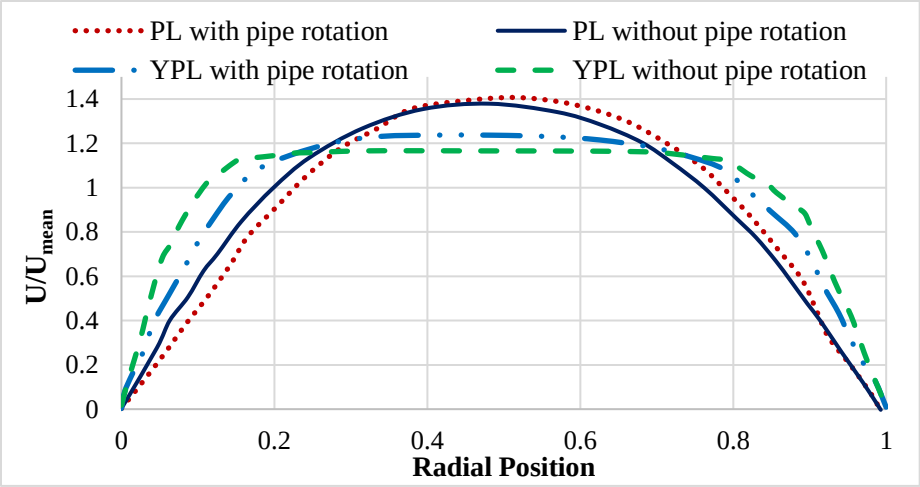


Fig. 3.10: Normalized velocity profile versus radial position for power-law (PL) and yield power-law (YPL) type fluids (0=pipe; 1=well)

Additionally, power-law and yield power-law type fluids were considered (Fig. 3.10). The yield stress inherent to yield power-law fluid tends to flatten the velocity profile in the center. Eccentricity in the annulus modifies the flow pattern by creating low-velocity zones in the

narrow areas of the annulus and higher-velocity zone in the wider part (Fig. 3.11a). The asymmetric nature of the velocity profile reduces hole-cleaning efficiency in eccentric annulus due to the formation of flow stagnant zones, especially with the absence of pipe-rotation. The apparent viscosity profile is similar to that of fluid velocity in which the maximum apparent viscosity is attained towards the pipe center (Fig. 3.11b). The high viscosity close to the center improves suspension capability of the fluid. However, low-viscosity at the pipe wall results in the rapid sedimentation of particles.

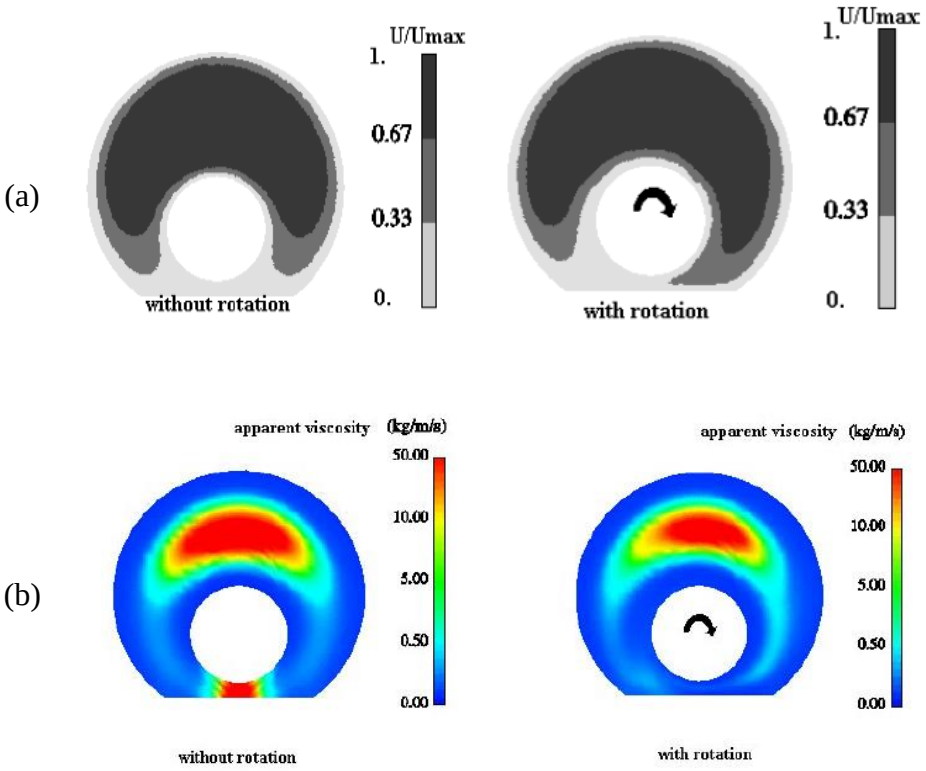


Fig. 3.11: a) velocity contours and b) apparent viscosity contours for eccentric annulus with and without inner pipe rotation. (King et al., 2000)

Bilgesu et al. (2002) used CFD tools to study solids transport efficiency as a 3-D steady-state process (Fig. 3.12). The multiphase flow model is implemented to study solid-liquid flow. Different power-law fluids and water were considered in the simulation. Results obtained

confirmed that increases in fluid density and flow velocity are beneficial for hole cleaning. However, any discussion on the segmented flow regime and the effect of turbulence was not made. The results obtained from the simulation were compared with experimental data and were found to be in good agreement.

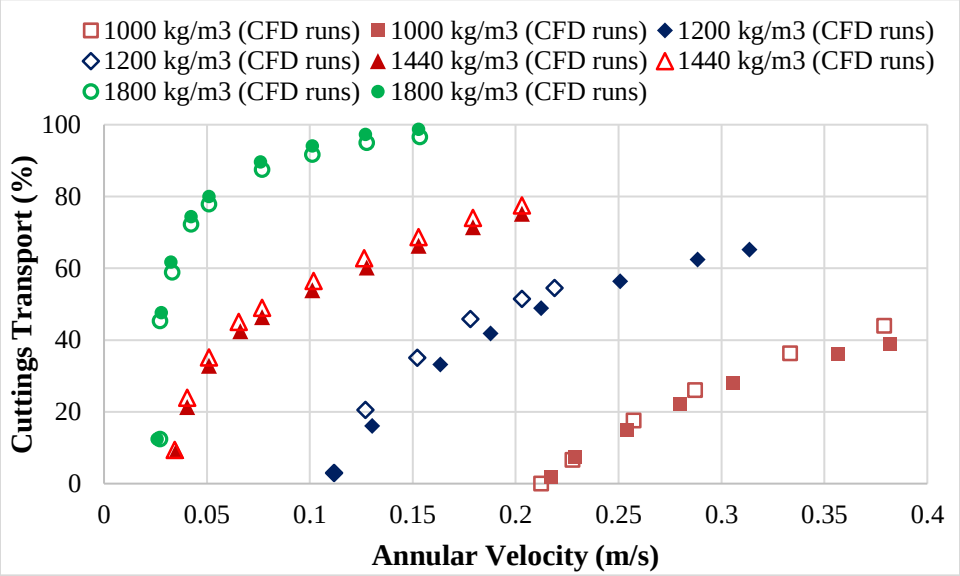


Fig. 3.12: CFD Results vs Lab Data (Bilgesu et al., 2002)

Many of the CFD models studied lack credibility in capturing the two-phase flow behavior of slurry flows. Additionally, several cleanout fluids are non-Newtonian in behavior. Hence, it is of utmost importance to adjust Newtonian models applied in simulations to capture the non-Newtonian effect. In summary, although the CFD models are a great tool to study hole-cleaning, it still requires a thorough understanding to make credible turbulent simulations.

CHAPTER 4

BED EROSION – EXPERIMENTAL STUDY

This chapter encompasses the details and results pertaining to the experimental study conducted at various inclinations and different flow parameters to study the bed erosion process. Detailed descriptions of individual components of the test setup and chronological test procedure have been presented in this chapter.

4.1 Design of Experiments

A systematic method based on the design of experiments concept was used to generate the test matrix for the experimental part of the research. The controllable input factors/dependent parameters are the ones that can be modified in the field. For the scope of this study, these parameters majorly involve the fluid properties and circulation time. On the contrary, uncontrollable or independent parameters, such as wellbore geometry and solid's properties, are not within the control of engineers but need to be considered in order to analyze the interaction with dependent factors. When an experiment has three or more variables, an interaction is a situation in which the simultaneous influence of two variables on a third is not additive. The selection of the range of all parameters incorporated in the research are based on the field applications. For instance, annular configuration consisting of a 127 mm ID outer pipe and a 60 mm inner pipe is a common occurrence during a typical cleanout operation. Similarly, the fluids used in this study were based on their frequent use in the field. Other parameters such as flow rate and solid's parameters are also selected to replicate typical field-case scenarios. Although, this ensures the direct application of results and subsequently developed model to the field, dimensional analysis was carried out to allow upscaling of lab setup to field setup.

4.2 Experimental Setup

The experiments were conducted in a 10.36 m (34 ft) long eccentric annular test section consists of a 5-inch fully transparent acrylic tube (OD = 140 mm and ID = 127 mm) and 2.375-inch inner steel tubing (OD = 60 mm). A schematic of the test section is shown in Fig. 4.1. Various components of the setup are described as follows.

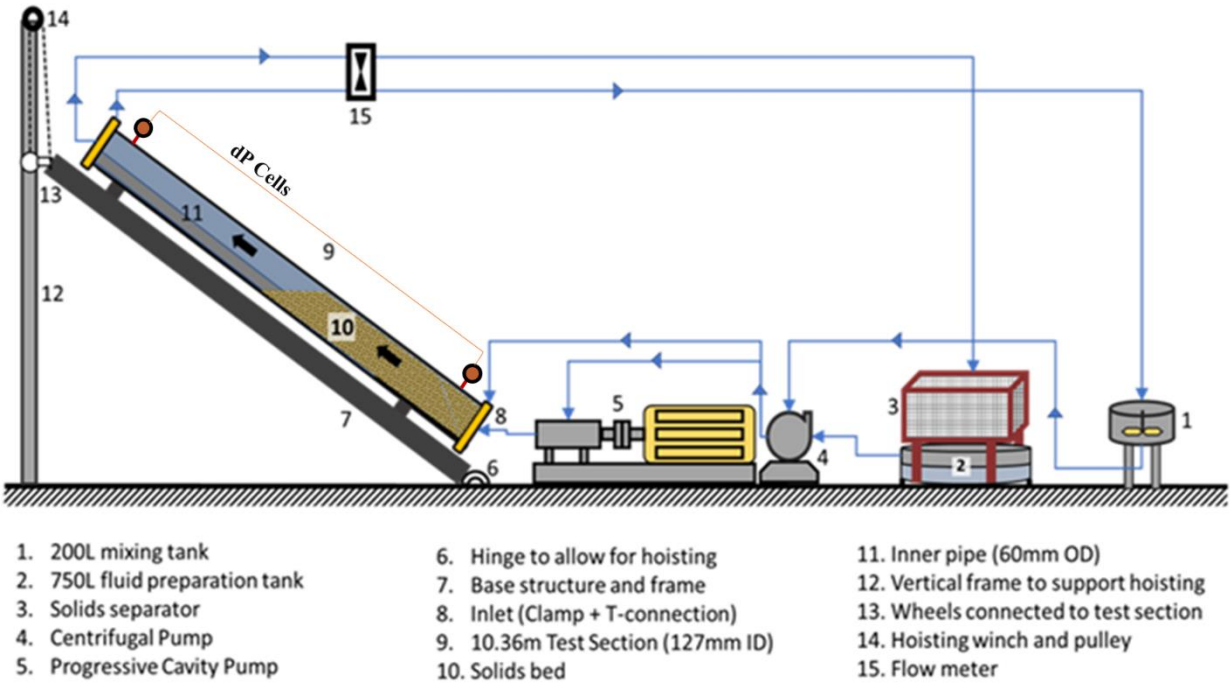
4.2.1 Support Assembly

The base assembly has been constructed to support the test section and ensure its stability under different operating conditions. A 3.65-m long and 1.52-m wide base frame is used as a base structure to mount two hinges placed 1.37 m apart and I-beams over it as shown in Fig. 4.2. This base frame is attached to a set of rollers to allow smooth linear movement of the test section during experiments involving inclination.

The test section is mounted on the 10.36 m long central I-beam using clamps and quick connectors to ensure a proper seal and smooth flow across the test section thereby preventing any flow disturbances. The discharge end of the test section is attached to a pulley-winch hoisting system allowing to raise the test section at the desired inclination. Two tracks fabricated from 10.36 m long channels are welded on both sides to allow for linear movement of cameras.

4.2.2 Hoisting system

The hoisting system comprises of a 9.75 m vertical hollow square beam with rollers placed inside to guide the vertical movement of the test section. The roller assembly consisted of two 152 mm diameter wheels coupled together with a 19 mm OD shaft. The free end of the central horizontal beam (the discharge end) is connected to a pulley mounted on top of the vertical beam using a steel rope that can be used to hoist the section to the desired inclination.



1. 200L mixing tank
2. 750L fluid preparation tank
3. Solids separator
4. Centrifugal Pump
5. Progressive Cavity Pump
6. Hinge to allow for hoisting
7. Base structure and frame
8. Inlet (Clamp + T-connection)
9. 10.36m Test Section (127mm ID)
10. Solids bed
11. Inner pipe (60mm OD)
12. Vertical frame to support hoisting
13. Wheels connected to test section
14. Hoisting winch and pulley
15. Flow meter

Fig. 4.1: Schematic of the experimental setup (Pandya et al., 2019)

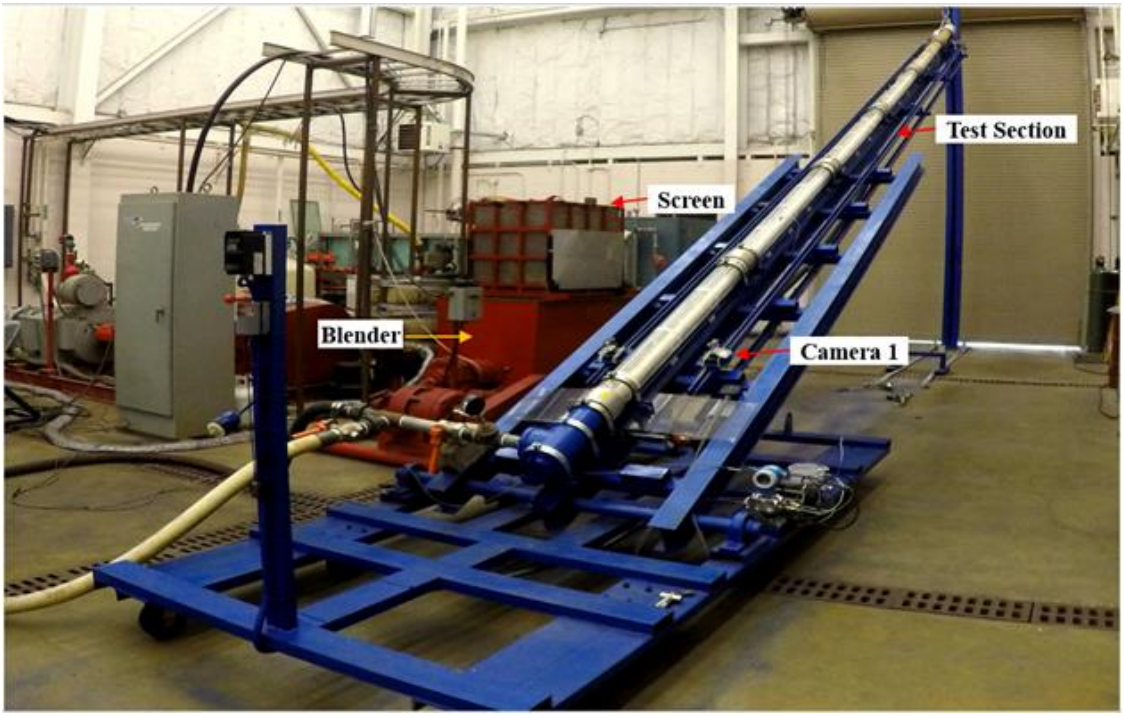


Fig. 4.2: Wellbore cleanout setup in an inclined position (Pandya et al., 2019)

4.2.3 Test Section

The test section comprises the outer transparent tube and inner steel tube. This pipe was painted white to aid better flow visualization. The flow through the pipe is restricted by welding blinds on both ends of it. Gate valves and t-connections are installed on the inlet and outlet sides of the test section to allow flow diversion from the test section to the remaining components of the flow loop.

4.2.4 Separator

The separator system consists of an in-house fabricated rectangular frame (3.5 ft × 2.75 ft × 3.25 ft) and a sieve (50 US mesh screen) that was used to collect solids removed from the test section. The fabricated separator was tested for handling solids at the maximum flow rate.

4.2.5 Mixing System

The mixing tanks and pumps were connected to the flow loop using 50 mm OD hoses. The required cleanout fluid was mixed and hydrated in a 750 L blender, which was also used as a circulation tank. The 200 L mixing tank was used to mix a slurry of proppant and water that was recirculated through the flow loop using a centrifugal pump to generate a stable bed in the test section. Progressive cavity pump connected in series with the centrifugal pump was bypassed during bed deposition to prevent any abrasion of the pump stator. The flow rate was changed using Variable frequency drives (VFDs) connected to the pumps.

4.2.6 Pumping System

Bed deposition was primarily performed using a centrifugal pump that was operated via a variable frequency drive (VFD). This pump was equipped with a motor having 25 HP power and

impeller rotating speed of 1770 RPM. A progressive cavity pump, having a 100 HP, 3 phase 60 Hz motor, 1780 RPM motor, was used in series with the centrifugal pump to perform bed erosion tests at high flow rates. The maximum achievable flow rate using this pump by itself was approximately 9 L/s at 4136 kPa.

4.2.7 Instrumentation and Data Acquisition System

A Coriolis mass flowmeter (Endress Hauser Proline Promass E 200) that was installed downstream of pumps measures the flow rate up to 1166 kg/min with an accuracy of ±0.25% of the reading, fluid density with an accuracy of ±0.0005 g/cc and temperature of the fluid with an accuracy of ±0.5 °C ± 0.005. A data acquisition system was used to transmit the recorded measurements to the main computer using a wireless logger. Chain and sprocket assembly installed on either side of the test section allowed camera movement to record bed height at different locations. Two cameras (video recording at 1080 p and 120 fps video) driven by an AC motor combined with a directional switch system was used to control the speed and direction.

4.3 Test Materials

Test Fluids: Three different cleanout fluids (Table 4.1) were incorporated to conduct bed erosion tests.

Table 4.1: Test matrix

Total number of bed erosion tests	72
Cleanout fluids:	Fluid 1 (Water) Fluid 2 (1.2 g/L guar gel) Fluid 3 (2.4 g/L guar gel)
Flow rates:	5.05, 6.31, 7.57 L/s (80, 100 and 120 gpm)
Inclination angles:	45°, 60°, 75° and 90° from vertical
Solids specific gravity:	2.5 for LDP and 3.2 for HDP
Solids size:	400 to 840 microns (20/40 US mesh)
Annular configuration:	Outer Casing: 140 mm OD and 127 mm ID Inner Pipe: 60.325 mm OD

Guar fluids were mixed using a gel concentrate that was diluted using a calculated volume of water and allowing sufficient hydration time. The hydration process helps in the proper generation of a hydro-colloidal slurry of polymeric fluid. A rotational viscometer (Fann Model 35) was used to characterize the rheology of polymeric fluids used in the study. It was found that fluid rheology can be best described using a power-law model (Fig. 4.3).

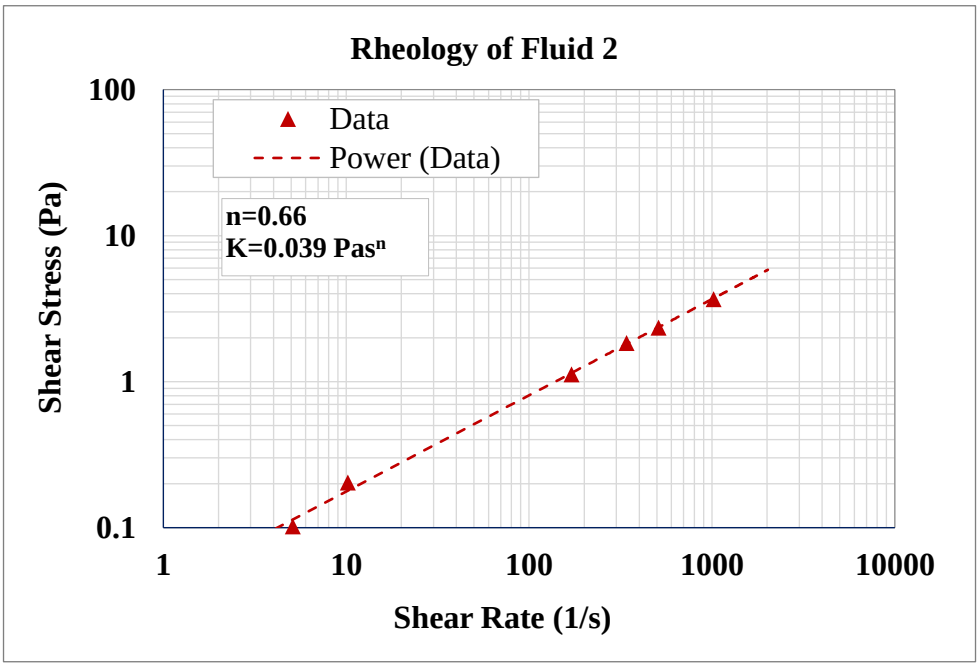
Test Solids: Solids used in this research were restricted to proppant with two different specific gravities majorly due to the ease of availability. High and low-density ceramic proppants were utilized in the bed erosion experiments. Proppants were assumed to have a considerable uniformity in terms of sphericity due to their ceramic nature of production. Particle size distribution was obtained using Laser Particle Size Analyzer. Fig 4.4 presents the size distribution of low (LDP) and high-density proppant (HDP). The results show that majority of the size particle distribution for both types of proppant (95% of LDP and 91% of HDP) fall between 20 US Mesh (400 microns) and 40 US Mesh (840 microns). The average diameters of LDP and HDP were 630 and 780 microns, respectively.

4.4 Test Procedure

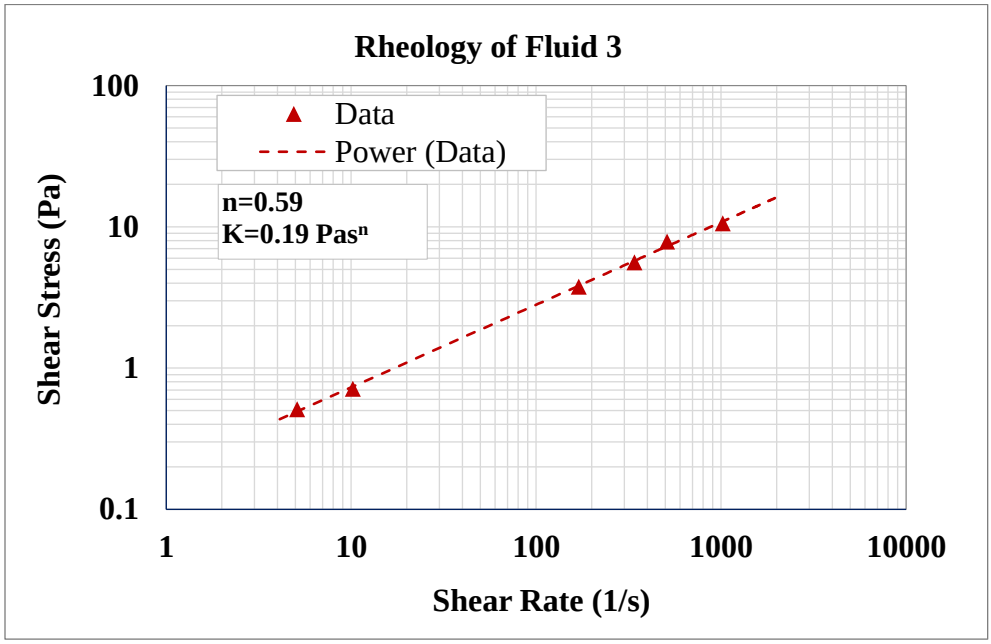
The experimental procedure can be chronologically divided in following steps – fluid mixing, deposition of bed, bed erosion, collection/drying of solids, and flushing of the test section.

4.4.1 Mixing of test fluid

For the preparation of guar-based fluids, a calculated amount of gel concentrate was mixed and diluted with tap water. The mixture was gently mixed for at least an hour or until the polymer was uniformly dispersed. The fluid was then allowed to hydrate for 60 mins before a sample was obtained and tested for the rheology.



(a)



(b)

Fig. 4.3: Rheograms of polymeric fluids (Data source: Pandya et al., 2019)

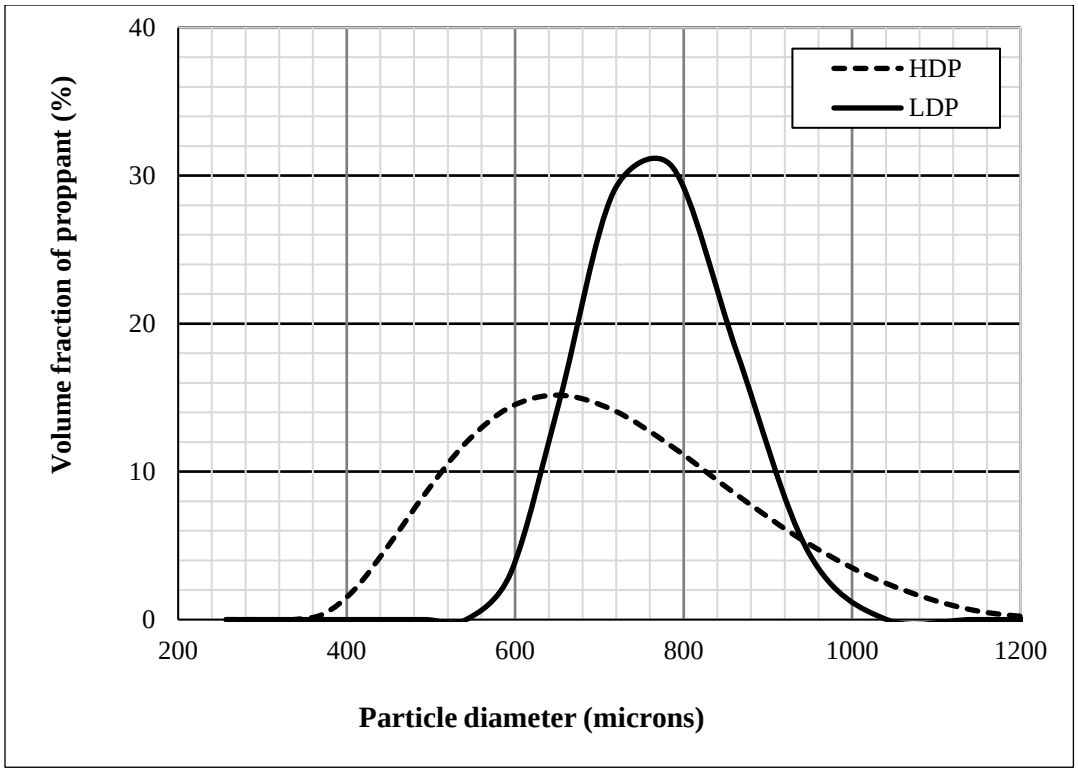


Fig. 4.4: Particle size distribution of HDP and LDP used in this study (Data source: Pandya et al., 2019)

4.4.2 Deposition of Bed

A slurry of proppant and water was circulated at lower flow rates through the test section in order to deposit the solids bed. The slurry was prepared by adding proppant at a very slow rate to water while it was circulated through the flow loop using a centrifugal pump. Uniform initial bed height was maintained for each test by adding a fixed amount of proppant in the slurry. Pilot bed deposition tests indicated that 77 kg of LDP was required to completely submerge the inner pipe with solids, thereby reproducing a case of poor hole cleaning. The equivalent weight for HDP was 90 kg. The slurry was maintained under constant slow agitation to ensure proper mixing without the influx of air. The flow was diverted into the bypass line and the test section was isolated once a stable bed height was obtained. All the flow lines were finally flushed with water at a high flow rate to remove any proppant remaining in them.

4.4.3 Bed Erosion

The tests fluid was initially circulated at a very low flow rate to displace the water from the test section that was used to deposit solids without agitating the bed. The test section was then hoisted to the desired inclination and an initial bed height reading was obtained at this point. The bed height was recorded at 42 points (21 on each side of the test section) and the average of these bed height readings was considered as the initial bed height. The flow of test fluid was increased to the desired rate in the bypass line. The flow was then diverted into the test section to initiate the bed erosion. The erosion continued for 30 mins and solids eroded from the test section were cumulatively collected in the separator. Average bed height was obtained after every 2 mins during the test.

4.4.4 Collection and Drying of Solids

The solids eroded from the bed, remove from the section and collected in the separator were removed and dried in an oven maintained at a temperature of 93°C. The weight of the dried solids was then measured and recorded as cleanout weight after 30 minutes (m_{30}).

4.4.5 Flushing of Test Section

As a final step, the test section was back-flushed using tap water at a high flow rate until all the remaining solids were removed from the test section and collected in the separator. The dry weight of the collected solids was recorded as the weight of flushed sand (m_{flush}).

4.5 Definition of Parameters

This section involves the description of the parameters defined to quantitatively assess the trends in the data obtained in the experimental study. Two distinct parameters are defined for this purpose.

4.5.1 Bed Erosion Curves

The bed erosion curves are presented in the form of normalized bed height versus circulation time (Fig. 4.5). The maximum circulation time for all the erosion tests in this study was 30 minutes. Normalized bed height (h_n) is defined as the ratio of the instantaneous bed height ($h(t)$) and the initial bed height (h_i). Each point on the curve is the average of bed heights recorded from 42 different points on both sides across the length of the test section. Bed measurements were obtained by visual observations from the slow-motion replay of recorded video. Based on the repeatability of 12 tests, the accuracy of these reading was determined to be ±5%.

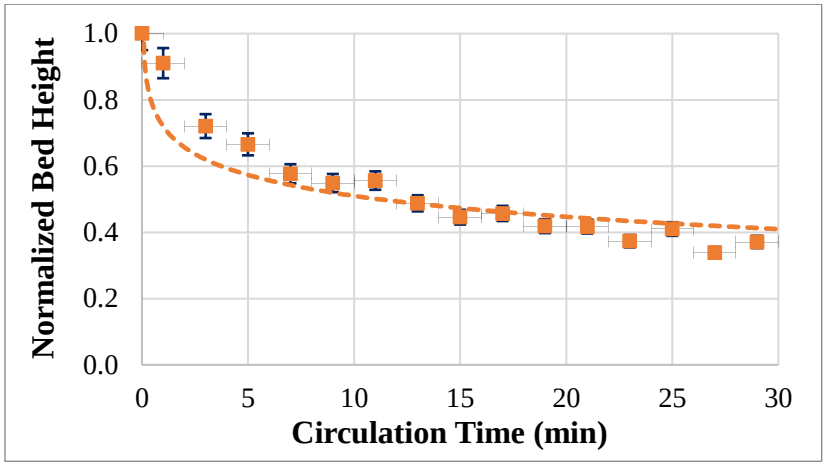


Fig. 4.5: Typical Bed Erosion Curve

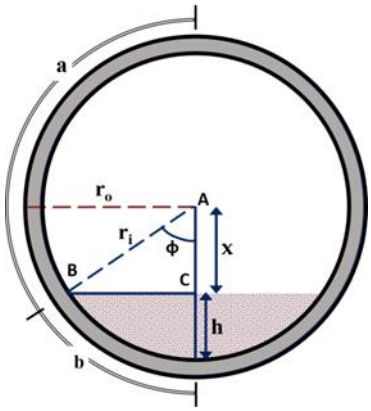


Fig. 4.6: Bed height calculation (Pandya et al., 2019)

$$h_n = \frac{h(t)}{h_i} \tag{4.1}$$

$$h(t) = r_i - r_o \cos\left(\frac{b}{r_o}\right) \tag{4.2}$$

$$b = \pi r_o - a \tag{4.3}$$

$$\phi = \frac{b}{r_o} \tag{4.4}$$

The definition of normalized bed height is related to other geometrical parameters such as r_i (inner radius of outer pipe), r_o (outer radius of outer pipe), a (circumferential reading from the top of pipe), b (circumferential reading from the bottom of pipe), and ϕ (central bed angle). Circumferential reading from the top was obtained visually and other parameters were calculated based on this reading using the above equations.

4.5.2 Cleanout Efficiency

The cleanout efficiency is a measure of the cumulative weight of solids removed during bed erosion process. It is mathematically defined as the ratio of the dry solids weight collected in separator after 30 minutes of cleanout test (m_{30}) and the combined dry solids weight collected at the end of cleanout test and back-flush $(m_{30} + m_{flush})$.

$$Cleanout\ Efficiency = \frac{m_{30}}{(m_{30}+m_{flush})} \tag{4.5}$$

The combined weight of solids removed during the cleanout process and solids removed during back-flush is slightly different from the feed weight because an average of approximately 1.8 kg of solids was lost (i.e. not recovered by the sieve).

4.6 Results and Discussion from Experimental Study

A total of 72 distinct bed erosion tests were conducted throughout the experimental study. The test variables (Table 4.1) included in the experiments are flow rate, fluid type, inclination angle and specific gravity solid.

4.6.1 Rheological Characterization

Three fluids with varying viscosity but similar density were used as cleanout fluids during bed erosion. Fluid 1 represents a Newtonian fluid. Fluids 2 and 3 are guar gel-based fluids with a non-Newtonian (power-law model) rheological behavior. The rheological measurements of these fluids (Fig. 4.3) were determined at ambient conditions using a standard Model 35 Fann viscometer.

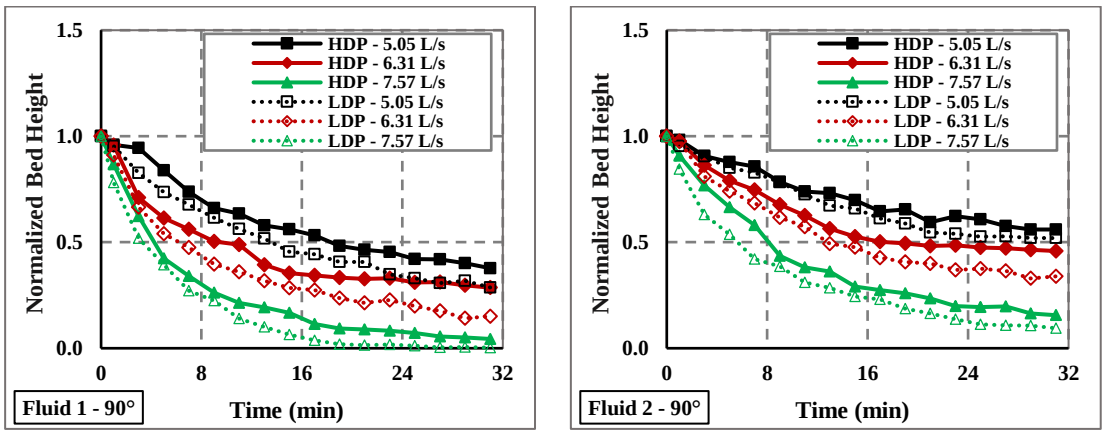
4.6.2 Results – Bed Erosion Curves

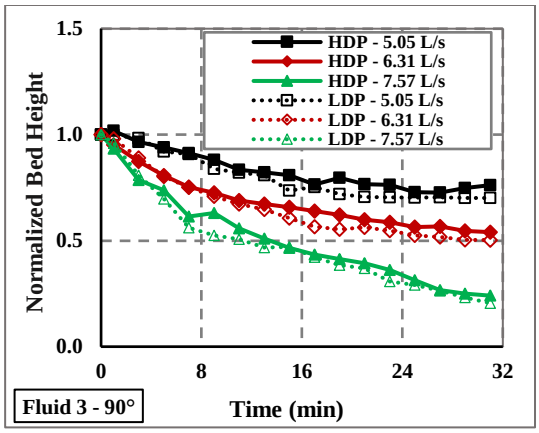
Obtaining a considerably accurate bed height reading is only possible when the bed is stable. Stable bed formation was evident in inclination angles over 60°. Hence, bed erosion curves are only obtained for inclination angles greater than 60°. Fig 4.7 represents the bed erosion curves for cleanout tests conducted to erode bed with different solid densities (HDP and LDP). The cleanout process was conducted at various flow rates using different fluids and varying the inclination of the test section (60°, 75°, and 90°).

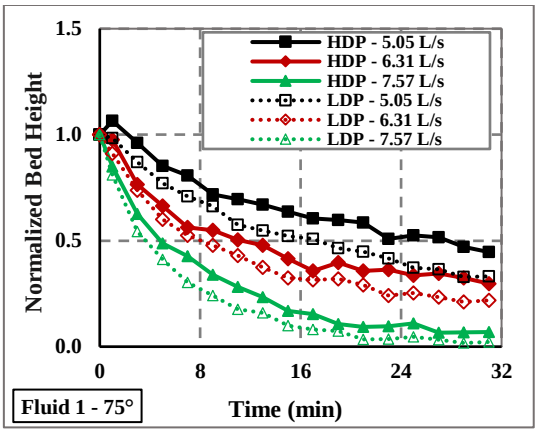
Fluid efficiency in bed erosion process at varying inclination is influenced by various factors such as solid density, fluid viscosity, and flow rate. Hole cleanout was enhanced with flow rate at all inclinations. This is due to the significant increase in bed shear stress and the intensification of hydrodynamic drag and lift forces caused by the increase in local fluid velocity near the bed. The density of solids directly impacts the minimum lifting force required to lift the flow

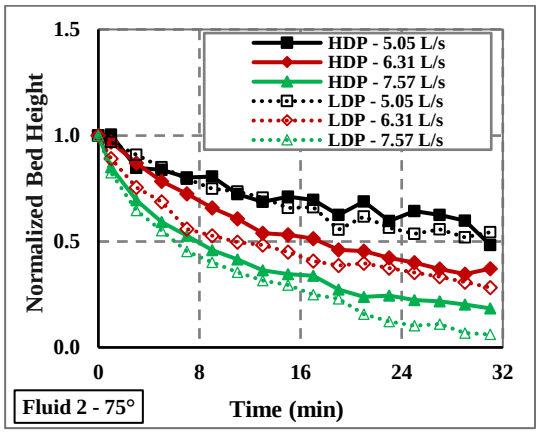
protruding bed particle. The transport mechanisms (rolling or lifting) of solids particles are governed by hydrodynamic forces and also dependent on the difference between solid and fluid density. As anticipated, a particle with a higher density is more challenging in terms of bed erosion. Increase in the density of particle results in a higher gravitational force acting on particle; therefore, the collective effect of buoyancy and hydrodynamic forces provided by cleanout fluid must be sufficiently large to overcome the effect of the particle weight in order to achieve efficient bed erosion. Hence, hole cleaning was more efficient with solids having a reduced density (LDP in this case) for all cleanout fluids employed.

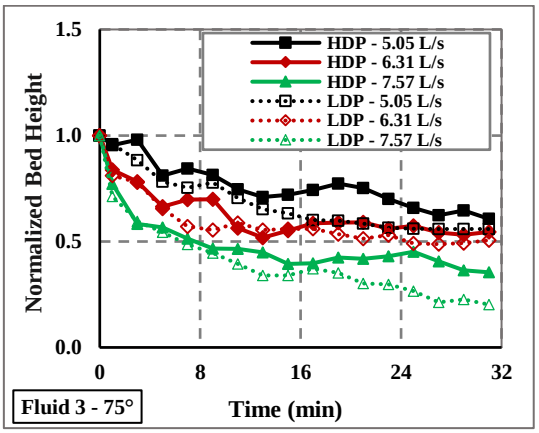
Fluid 2 and 3 exhibited diverse bed geometries as compared to Fluid 1. This variation in bed profiles attributed to the average fluctuations in bed height measurement as seen in Fig. 4.8. This resulted in a smoother decay of bed erosion curves for Fluid 1. Fluctuations in bed height also intensified with the reduction in inclination angle. This is attributed to prominent bed irregularity at lower inclinations resulting from the generation of dunes and ripples. The structure of these irregularities in normal flow pattern is a factor of bed height, solids properties, fluid properties, flow parameters (fluid velocity, flow regime) and inclination. The occurrence of dunes and ripples is distinct as the bed approaches a steady state.

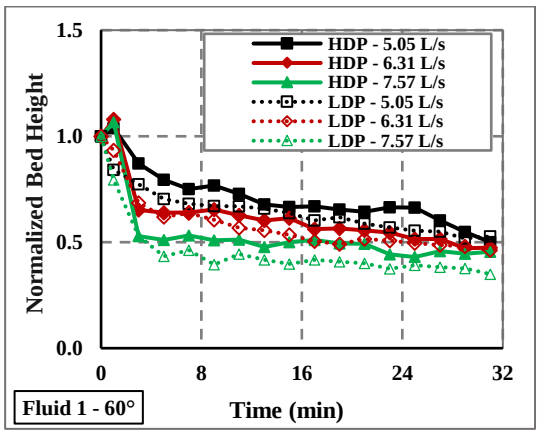


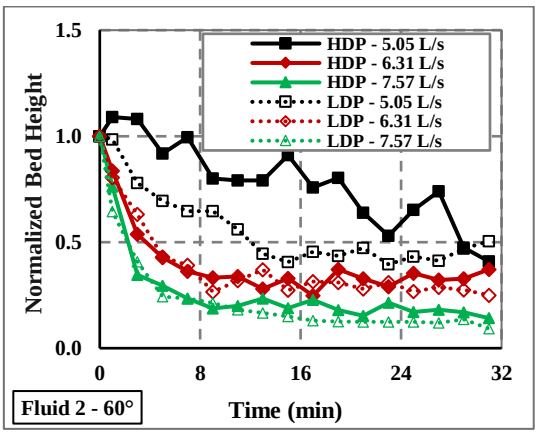

HDP - 5.05 L/s
HDP - 6.31 L/s
HDP - 7.57 L/s
LDP - 5.05 L/s
LDP - 6.31 L/s
LDP - 7.57 L/s
Normalized Bed Height
1.5
1.0
0.5
0.0
0
8
16
24
32
Time (min)
Fluid 3 - 90°


HDP - 5.05 L/s
HDP - 6.31 L/s
HDP - 7.57 L/s
LDP - 5.05 L/s
LDP - 6.31 L/s
LDP - 7.57 L/s
Normalized Bed Height
1.5
1.0
0.5
0.0
0
8
16
24
32
Time (min)
Fluid 1 - 75°


HDP - 5.05 L/s
HDP - 6.31 L/s
HDP - 7.57 L/s
LDP - 5.05 L/s
LDP - 6.31 L/s
LDP - 7.57 L/s
Normalized Bed Height
1.5
1.0
0.5
0.0
0
8
16
24
32
Time (min)
Fluid 2 - 75°


HDP - 5.05 L/s
HDP - 6.31 L/s
HDP - 7.57 L/s
LDP - 5.05 L/s
LDP - 6.31 L/s
LDP - 7.57 L/s
Normalized Bed Height
1.5
1.0
0.5
0.0
0
8
16
24
32
Time (min)
Fluid 3 - 75°


HDP - 5.05 L/s
HDP - 6.31 L/s
HDP - 7.57 L/s
LDP - 5.05 L/s
LDP - 6.31 L/s
LDP - 7.57 L/s
Normalized Bed Height
1.5
1.0
0.5
0.0
0
8
16
24
32
Time (min)
Fluid 1 - 60°


HDP - 5.05 L/s
HDP - 6.31 L/s
HDP - 7.57 L/s
LDP - 5.05 L/s
LDP - 6.31 L/s
LDP - 7.57 L/s
Normalized Bed Height
1.5
1.0
0.5
0.0
0
8
16
24
32
Time (min)
Fluid 2 - 60°

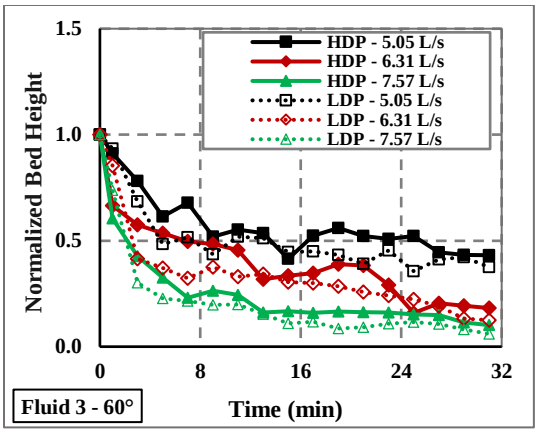
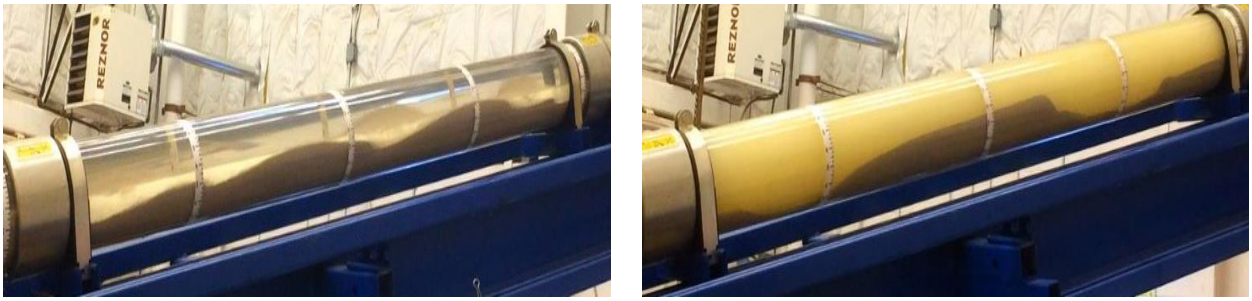


Fig. 4.7: Bed erosion curves for different particle densities, cleanout fluids, and inclination angles. (Pandya et al., 2019)



(a) (b)

Fig. 4.8: Bed profiles in inclined test section with different fluids: a) Fluid 1; and b) Fluid 3 (Pandya et al., 2019)

4.6.3 Results – Cleanout Efficiencies

Cleanout efficiency plots are effective in presenting results of all inclinations. Fig. 4.9 provides a comparison of cleanout efficiencies for different fluids used to erode bed formed with different densities. Fluid 1 demonstrated better cleanout at higher inclinations whereas Fluids 2 and 3 had a reverse trend and were more efficient in bed erosion at low inclinations. This observation is justified by analyzing particle transport mechanism in vertical and inclined wellbores. In the vertical section of the well, hydrodynamic drag is the main force affecting solids transport. Hence, fluids having larger viscosity have extraordinary wellbore cleanout performance in

vertical wells as they generate strong drag force to counteract gravitational force/effective weight of the solids and prevent sedimentation.

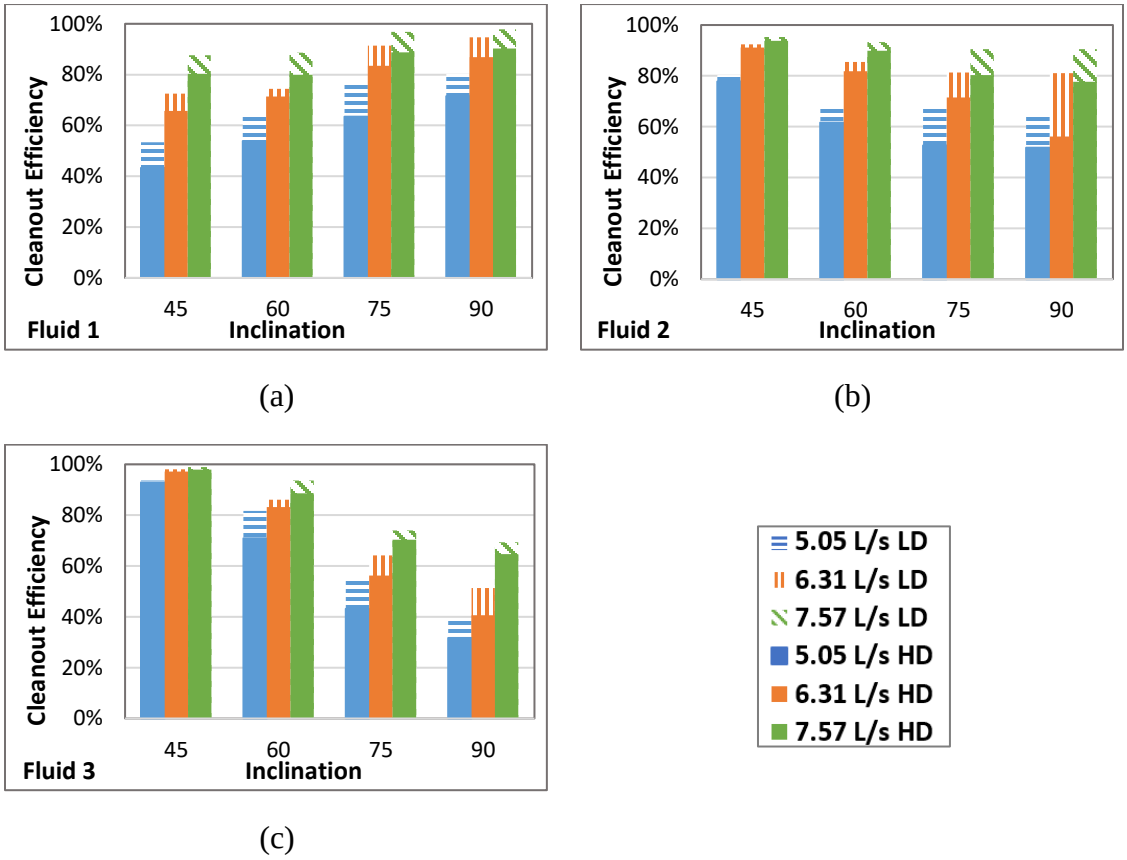


Fig. 4.9: Cleanout efficiencies of a) Fluid 1, b) Fluid 2, and c) Fluid 3 at various inclinations for high and low-density proppants at different flow rates (Pandya et al., 2019).

Unlike highly viscous fluids, low-viscosity fluid like water (Fluid 1) generates a very weak force which is not sufficient to overcome the weight of the particle and therefore, unable to prevent settling of solids. Subsequently, fluids with low-viscosity tend to allow particles to accumulate in the wellbore which increases the in-situ concentration of solids. In deviated sections, solids transport behavior is more complex due to lateral settling of particles, decreased settling in the axial direction, and generation of stable bed. At intermediate inclinations (between 45° and 60°), fluids with higher viscosity avert the development of consolidated bed by delaying the lateral

particle settling. Due to this, two-layer flow is developed in annular section and this flow comprises of high-velocity dispersed and low-velocity concentrated layer that can move upward or downward depending on the inclination, mean flow velocity, fluid and solids properties (Fig. 4.10).

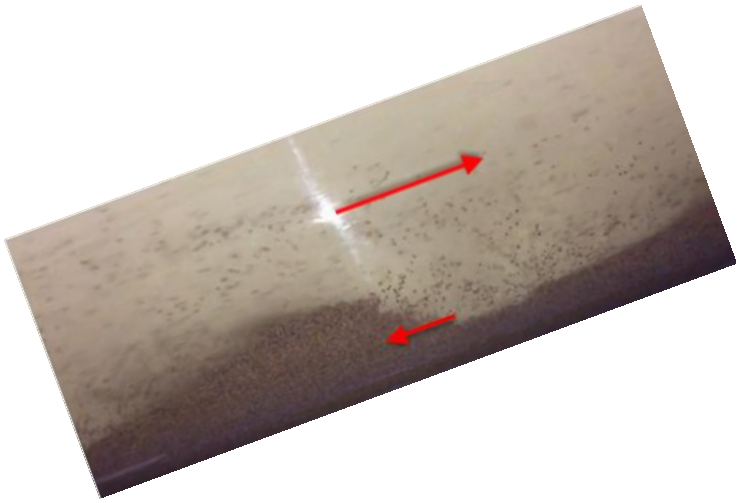


Fig. 4.10: Secondary flow pattern observed during erosion of HDP with Fluid 2 and at 60° inclination (Pandya et al., 2019).

Quantity for solids eroded from the bed by a unit volume of fluid is a strong function of rheological properties of that fluid. Fluids with higher viscosity are a better medium for suspension of solids but poor in eroding the solids from the bed. Although low-viscosity fluids exhibit better erosion, they cannot carry the particles in the flow stream for a longer duration. The lack of viscosity can be compensated to a certain extent by a marginal increase in flow rate in order to improve cleanout efficiency of low-viscosity fluids. However, the circulation of fluids in CT is restricted to certain allowable maximum flow rate depending on the friction pressures generated and technical specifications of the tubing.

The effect of solids density on cleanout efficiency was found to be only moderate (up to 35% reduction) in comparison with other influencing parameters such as well inclination, flow rate

and rheology of fluid. It was more pronounced in near-horizontal inclinations. This is reflected by a significant improvement in cleanout efficiencies between HDP and LDP with an increase in inclination. The buoyant force acts to counter the gravitational force in all inclinations, but the vertical component of the drag force acting against gravity is maximum in vertical wells and decreases as the inclination increases. Hence, with limited flow velocity, stationary bed often deposits on the low-side of a horizontal wellbore, even for the case of low-density solids.

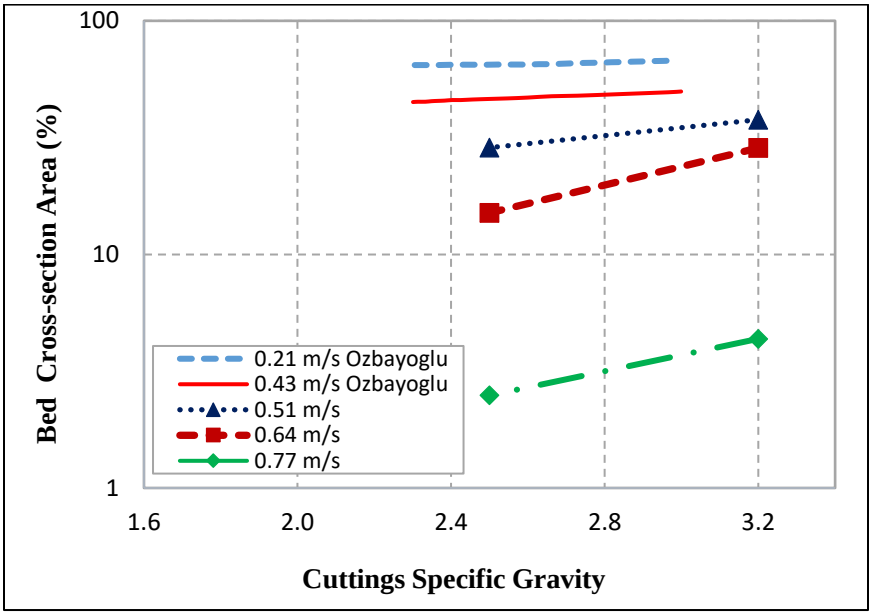


Fig. 4.11: Comparison of the current measurements with model predictions of Ozbayoglu et al. (2004)

For comparative purpose, approximate bed height values of Fluid 1 in a horizontal well profile are considered. Although these readings were obtained as hole-cleaning approached steady-state condition, they can be prevalently used for evaluating the effect of density on the equilibrium bed height. The observation-based on solids density from this research is compared (Fig. 4.11) with published model predictions (Ozbayoglu et al. 2004). Fig. 4.11 presents model predictions (4.73 and 9.46 L/s) along with measurements (5.05, 6.31 and 7.57 L/s) obtained in a horizontal

configuration. The flow rates have been changed to average flow velocity for more correct representation as both studies involve different annular cross-sectional area available for flow. The cross-sectional area on annulus occupied by bed increases prominently with the increase in solids density at higher velocities. As the velocity reduces, this effect becomes less significant. At very low fluid velocities (lesser than 0.43 m/s), cleanout fluid tends to become ineffective in solids removal irrespective of the density of the solids.

4.6.4 Critical Inclination Angle

Critical angle of inclination is defined at which the cleanout efficiencies of all fluids at a constant flow rate are approximately equal. Fluids with low viscosity perform better at inclinations higher than critical and high viscosity fluids exhibit better cleanout performance at lower inclinations. Efficiency ratio plots were generated in order to study the critical inclination. The efficiency ratio is defined as the ratio of cleanout efficiency of test fluid over cleanout efficiency of reference fluid at an inclination.

$$Efficiency\ Ratio = \frac{[Cleanout\ efficiency\ (Test\ Fluid)]}{[Cleanout\ efficiency\ (Reference\ Fluid)]} \tag{4.6}$$

Or

$$Efficiency\ Ratio = \frac{\left[\frac{m_{30}}{m_{30}+m_{flush}}(Test\ Fluid)\right]}{\left[\frac{m_{30}}{m_{30}+m_{flush}}(Reference\ Fluid)\right]} \tag{4.7}$$

For the scope of this research, Fluids 2 and 3 are considered as test fluids and Fluid 1 is used as reference fluid. By definition, critical point exists when cleanout efficiencies of both fluids are the same, or the ratio is equal to one (Fig. 4.12). Results show that irrespective of flow rate, the

critical angle of inclination for HDP and LDP exists between 64° – 67° and at approximately 69°, respectively.

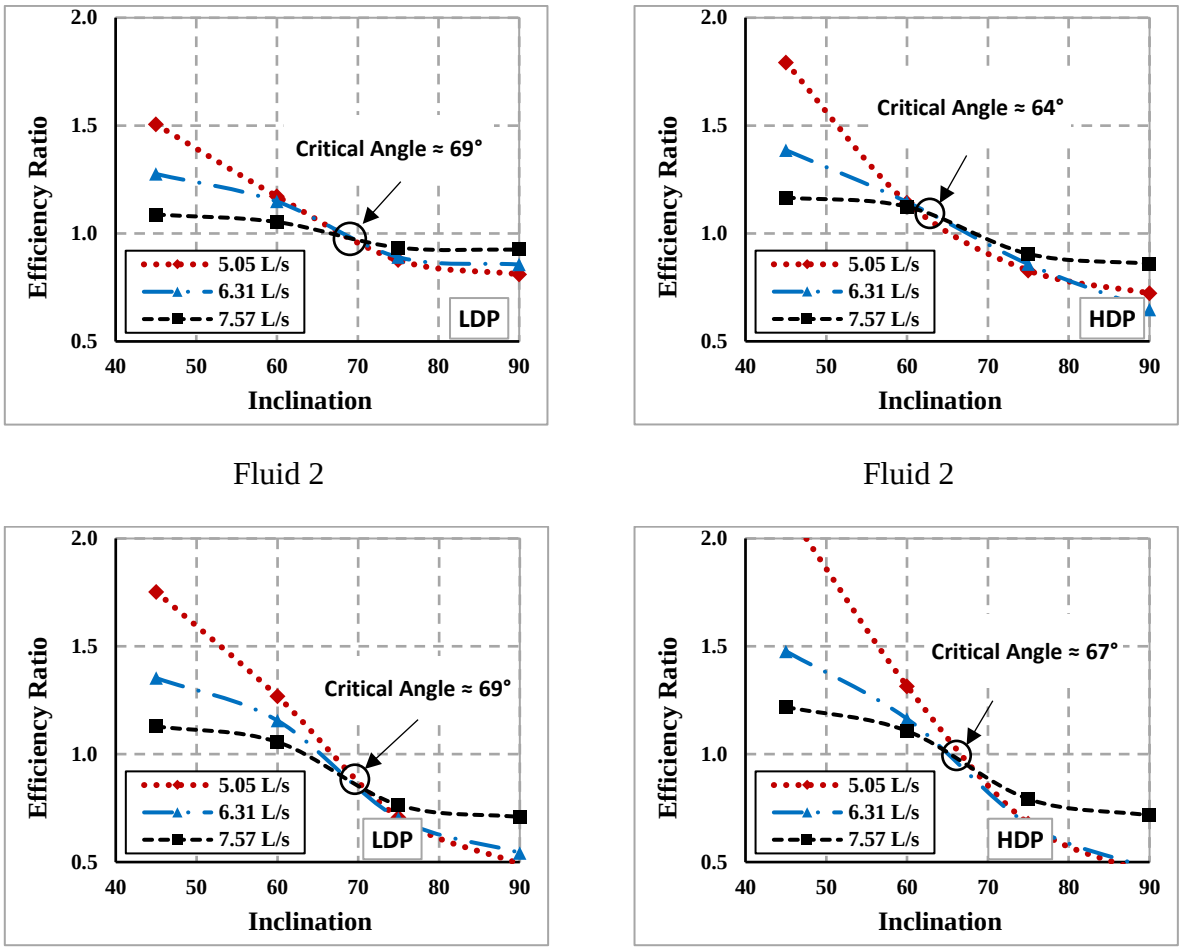


Fig. 4.12: Cleanout efficiency ratio versus inclination angle (Pandya et al., 2019)

CHAPTER 5

DIMENSIONAL ANALYSIS

Several mechanistic and empirical correlations have been formulated to assess cleanout efficiency as a function of different influencing parameters. An empirical correlation was initially developed by Adari et al. (2000) to predict the average bed height as a function of mud circulation time when other contributing factors are known. A major drawback of such empirical models is that since they are developed solely using non-linear regression techniques, they are mostly restricted to the experimental conditions and hence cannot be up-scaled to model the field case scenarios. Dimensional analysis is an established fluid mechanics method used for developing a generalized relationship between output and input parameters. Dimensionless parameters ensure the consistency of the model with the similitude theory. The similitude theory states that an engineering concept obtained through a model is valid to a real-life application if both share geometric, dynamic and kinematic similarities. The geometric similarity is met when the model has the same shape as that of the application. In most cases, models are a geometrically scaled-down version of field application. While it is convenient to achieve geometric similarity by simple scaling, other parameters like velocity and fluid rheology may not be directly scaled down. Kinematic and dynamic similarities establish the fulfillment of these conditions. Kinematic similarity compels the model to account for similar fluid streamlines and rate of change in particle position as that in the application. Dynamic similarity states that the ratio of forces acting on all phases and phase interface is constant across various scales. An agreement in dynamic similarity automatically demonstrates the existence of geometric and kinematic similarity. The three similarities can be achieved using the following steps:

- Properly identification of all variables affecting a physical process to be studied within the application system.
- Defining a set of dimensionless parameters and using these parameters to develop a model using dimensional analysis technique.
- Defining a range of these dimensionless parameters that encapsulate the value of these parameters for all scales of model or application.

This chapter describes the dimensionless relationship (correlation) that is developed for the purpose of the upscaling of cleanout model for field applications. The model is validated for the accuracy of predictions using two techniques. Initially, training dataset (80% of total data) and testing dataset (remaining 20%) are sorted out by randomly selecting the experiments from the previously defined test matrix. Train data is utilized to develop the model and the test data is used to validate the model. Subsequently, the model is validated using published experimental measurements (Adari et al. 2000) obtained from a geometrically different flow loop.

5.1 Buckingham Pi Theorem (Dimensionless Parameters)

Dimensional analysis is frequently applied to define a simple function that relates the target variable (bed height) to independent parameters (flow parameters, fluid and solids properties, flow geometry). This procedure requires determining the number of fundamental dimensions that can define all the parameters and variables involved in dimensionless groups. Buckingham Pi method (Buckingham, 1914) is used in conjugation with experimental data obtained to develop dimensionless parameters and a subsequent correlation that defines the wellbore clean-out process.

In this problem, $mass\ [M], length\ [L] and\ time\ [T]$ are three fundamental units ($m = 3$) that can sufficiently describe all variables that affect the wellbore clean-out process. Using the Buckingham Pi theorem, the dimensionless normalized bed height (h_n) can be expressed in terms of influential parameters – mean velocity (U in m/s), fluid density (ρ_f in kg/m^3), particle density (ρ_s in kg/m^3), apparent viscosity (μ_a in Pa.s), solids diameter (d_s in m), hydraulic diameter (d_h in m), circulation time (t in seconds), lateral/section length (l in m) and angle of inclination (θ in radian).

5.2 Model Development

Hole-cleaning is empirically found to be affected by ten variables ($k + l = 10$). The variables are $h_n, \mu_a, \mathrm{g}, \mathrm{t}, \rho_s, d_p, \theta, U, \rho_f$ and d_h. Considering this, the process variables can be described using three fundamental units ($m = 3$), Buckingham Pi theorem stated that $k + l - m = 10 - 3 = 7$ dimensionless parameters can be defined. Repeating variables considered in the development of the system of dimensionless parameters are d_h, ρ_f and U. The derivation of different Pi groups is included in Appendix A. Table 5.1 recapitulates the final dimensionless parameters and specifies their range of validity for the accuracy of predicted results.

Table 5.1: Π-Groups as formulated using Buckingham Pi method

Pi-Group	Definition	Description	Range
Π_1	h_n	Dimensionless bed height	0 to 1
Π_2	$(\rho_f U d_h)/\mu_a$	Reynolds number	1,250 to 87,800
Π_3	gt^2/d_h	Dimensionless time	3.43E+5 to 4.03E+8
Π_4	ρ_s/ρ_f	Density ratio	2.5 to 3.2
Π_5	$l^2/d_s d_h$	Length to diameter ratio	1.74E+6 to 2.20E+6
Π_6	$\mathrm{U}/\sqrt{g \cdot sin(\theta) d_h}$	Froude number	0.58 to 1.23

The application of non-linear regression technique on the data suggested that the normalized dimensionless bed height (Π_1) is logarithmically dependent on other $\Pi-$groups (Eq. 5.3). Although, both logarithmic and polynomial functions can be applied to this dependency, the logarithmic decay describes the relationship more accurately since it does not reduce the bed height to zero at any time. Therefore, non-linear regression analysis with logarithmic dependency on contributing factors is considered. The constant parameters (A to E) used in Eq. 5.3 are tabulated in Table 5.2. Apparent viscosity (μ_a) is defined as: $\mu_a = K_v \left(\frac{8U}{d_h}\right)^{n-1}$.

$$\Pi_1 = \mathrm{A} + \left(\frac{\mathrm{B}\log_{10}\Pi_2}{\kappa}\right) + \left(\frac{\mathrm{C}\log_{10}\Pi_3}{\kappa}\right) + \left(\frac{\mathrm{D}\log_{10}\Pi_4}{\kappa}\right) \tag{5.3}$$

where,

$$\kappa = 10^{\frac{\log_{10}\Pi_6}{(\log_{10}\Pi_5 + E)}}$$

Table 5.2: Values of constants (A to E) as used in Eq. (5.3)

π_1 Range	A	B	C	D	E
0.0 to 0.4	1.98	-0.04924	-0.24567	0.768	-8.47
0.4 to 1.0	2.15				

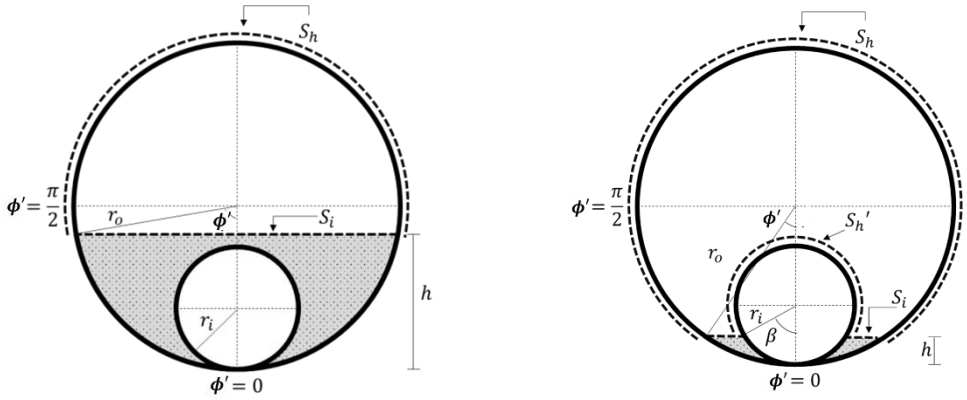
Eq. 5.3 is practically valid if all three similarities (i.e. geometric, kinematic and dynamic similarity) are achieved. Therefore, the pipe to hole diameter ratio (wellbore diameter ration) and particle to hole diameter ratio should approximately match that of this study. Other mandatory requirements (range of Π-groups) to fulfill the concept of similarity are specified in Table 5.1.

Hydraulic diameter (d_h) calculations are very critical in the case of eccentric annuli. Due to the asymmetric geometry, hydraulic diameter calculation requires a number of preceding calculations including a central angle with respect to outer pipe (ϕ') and inner pipe (β). If the annular section is completely empty, then the maximum cross-sectional area of the flow (A_a), the

circumference of the inner pipe (S_b) and circumference of the outer pipe (S_a) can be calculated as:

$A_a = \pi(r_o^2 - r_i^2)$;

$S_a = 2\pi r_o$; $S_b = 2\pi r_i$



(a) (b)

Fig. 5.1: a) inner pipe completely covered; b) inner pipe partially covered (Pandya et al., 2019)

The two most common bed configurations exist during cleanout operation are schematically presented in Fig 5.1. The cross-sectional flow area (A) and wetted perimeter (S) when the inner pipe is completely buried in the bed (Fig 5.1a) can be calculated using the following relations.

Pipe completely covered: $\boldsymbol{h \geq d_i}$

- $Flow\ area\ (A) = A_a - A_{bed} = r_o^2\left(\pi - \phi' + \frac{sin\phi'}{2}\right)$ (5.4a)
- $Wetted\ Perimeter\ (S) = S_i + S_h$ (5.4b)
- $S_i = 2r_o sin\phi'$ (5.4c)
- $S_h = 2r_o(\pi - \phi')$ (5.4d)

Similarly, Fig 5.1b represents a scenario in which the inner pipe is only partially submerged in bed. For this scenario, the flow area and wetted perimeter can be calculated using the following equations:

Pipe partially covered: $\boldsymbol{h < d_i}$

- $A = A_a - A_{bed} = r_o^2\left(\pi - \phi' + \frac{sin2\phi'}{2}\right) - r_i^2\left(\pi - \beta + \frac{sin2\beta}{2}\right)$ (5.5a)
- $Wetted\ Perimeter\ (S) = S_i + S_h + S_h{}'$ (5.5b)
- $S_i = 2(r_o sin\phi' - r_i sin\beta)$ (5.5c)
- $S_h = 2r_o(\pi - \phi')$ (5.5d)
- $S_h' = 2r_i(\pi - \beta)$ (5.5e)
- $\beta = \pi - \cos^{-1}\left[\frac{r_o(1-cos\phi')-r_i}{r_i}\right]$ (5.5f)

Hydraulic diameter (d_h) is mathematically defined as the four times the flow area divided by the total wetted perimeter. Using the above relations, hydraulic diameter (d_h) for either scenario can be calculated as, $d_h = 4 * \frac{A}{S}$.

5.3 Model Validation

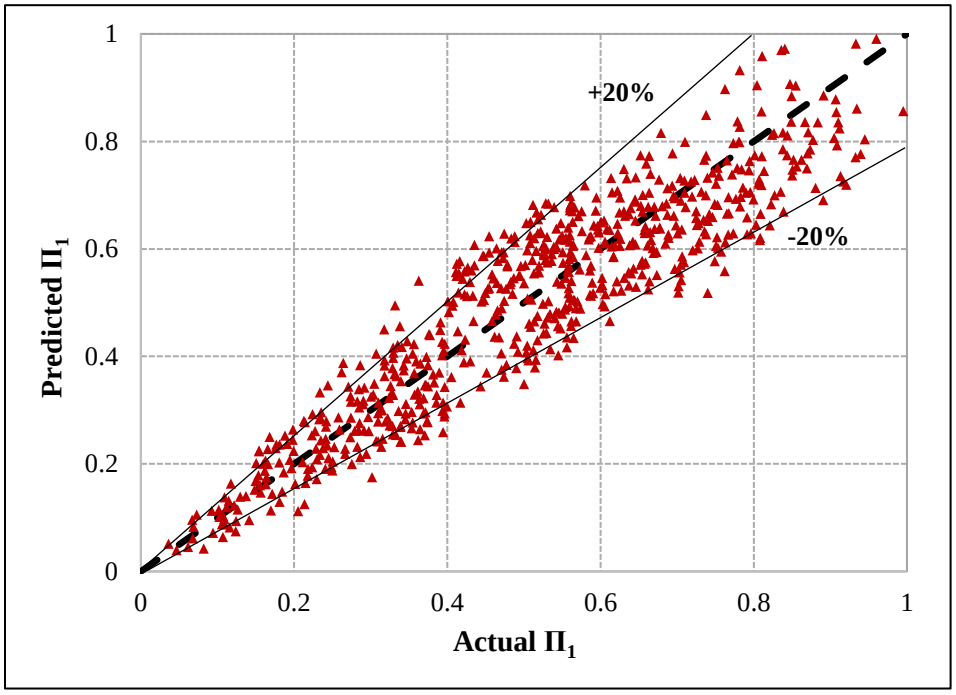
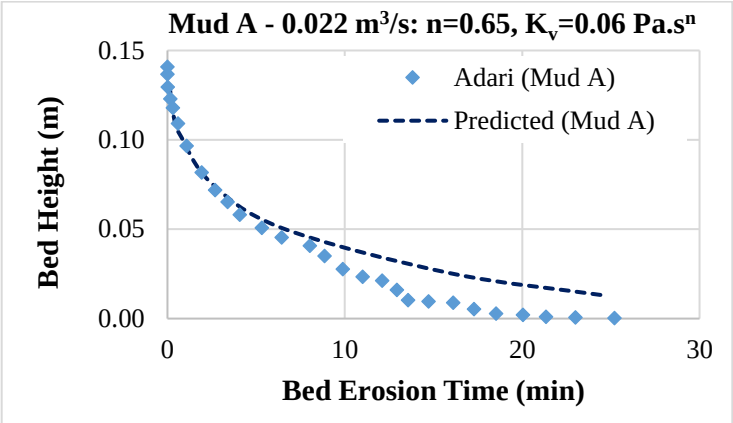


Fig. 5.2: Cross plot for modeled prediction and experimental results of bed height. (Pandya et al., 2019)

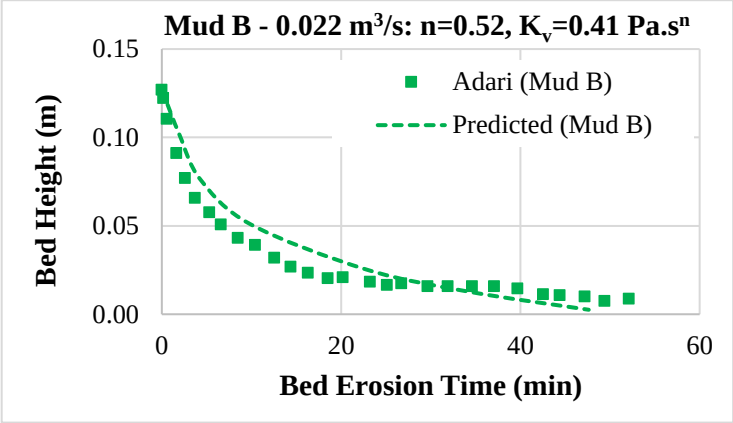
The results obtained from the model have been validated against 'test' dataset as mentioned previously. Accuracy and precision of the model are shown in Fig. 5.2. Average error observed between experimental data and model prediction is 16%. Formation of dunes and ripples develop bed irregularities when normalized bed height is less than 0.4. A correction factor (parameter A is as presented in Table 5.2) is therefore required at lower bed heights to predict the bed height more accurately.

In the second step, model validation is performed by predicting the results for experiments conducted by Adari et al. (2000). Although the experiments conducted by Adari et al. involved drilling mud as a cleanout fluid, the study provided the power-law model parameters for tests fluid. The developed model uses the power-law parameters for predictions. The comparison is presented in Fig 5.3. Three fluids with different rheology/viscosity are assessed in terms of cleanout capability under the turbulent flow regime. Adari et al. conducted experiments in a 24.5-m long annular test section with an outer pipe of 200 mm ID and inner pipe of 110 m OD. Although these dimensions are different from the one used in this study, the ratios of the dimensions in both studies are comparable. However, some of the properties of test solids utilized these two studies were substantially different. Adari et al. used drilled cuttings (with an average diameter of 3 mm) as solids medium whereas ceramic proppant with size ranging from 0.63 to 0.78 mm were used in this study. Despite this difference in solid properties, the predictions obtained using new correlation show reasonable agreement with the published experimental measurements. Inconsistency is observed between measured and predicted values, which tends to increase at low bed heights (less than 30 mm). The error in predictions at lower bed heights occurs as the defined dimensionless parameters tend to fall out of the range of applicability of correlation.

(a)



(b)



(c)

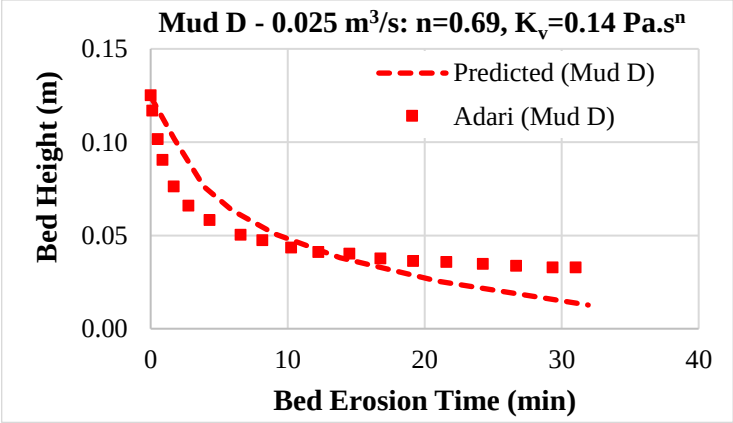


Fig. 5.3: Bed-erosion curves from experimental data (Adari et al.) and predicted curves (from correlation) for 87° inclination.

5.4 Sensitivity Analysis

Correlation matrix analysis was conducted to examine the effect of individual parameters influencing the normalized bed height (Π_1) calculation (Table 5.3). The absolute coefficient value obtained through this method is a direct measure of the degree of the influence of the corresponding variable on the output. Therefore, a parameter with a corresponding coefficient of – 1 or + 1 will have a very strong but inverse or direct effect, respectively, on the response or normalized bed height and that with a coefficient value of 0 will have no effect. This also infers that ambiguity in any parameter with a larger coefficient will result in larger inaccuracy in the calculation of desired response. A negative value of the coefficient suggests an inverse relationship between the variable and the output. For instance, the flow velocity has a coefficient of −0.87. This depicts that an increase in flow velocity has the maximum influence on the reduction of normalized bed height when compared to other variables.

Table 5.3: Correlation matrix – Effects of various parameters on Π_1.

Input Parameters	Coefficient Relating to Effect on Output (Π_1)
Solid's Diameter - d_s	-0.04
Solid's Density - ρ_s	0.09
Fluid Density - ρ_f	-0.26
Average Flow Velocity - U	-0.87
Flow Behavior Index - n	0.04
Fluid Consistency Index - K_v	0.01
Hydraulic Diameter - d_h	0.31
Length of Well Section - l	0.08

The effect of these parameters based on the model developed was further studies by plots relating the change in a variable and calculated normalized bed height. Table 5.4 lists the values of each parameter that were kept constant for the case when anyone variable was varied. The specific set of parameters with corresponding values in Table 5.4 (except the variable parameter for each case) was considered as the baseline set. Fig. 5.4 represents the trend and magnitude of all the variables listed in Table 5.3. These plots essentially represent normalized bed height that can be attained with the corresponding value of an independent parameter (x-axis) given that other factors are kept constant at their respective values as shown in Table 5.4. A normalized bed height (Π_1) value of 1 represents the initial bed height or a bed height before initiating circulation of fluid to erode the bed. Value of the same corresponding to 0.4 refers to a condition that 40% of the initial bed height remains in the section (60% eroded). Therefore, achieving a lower value of Π_1 is beneficial.

Table 5.4: Baseline values for sensitivity analysis

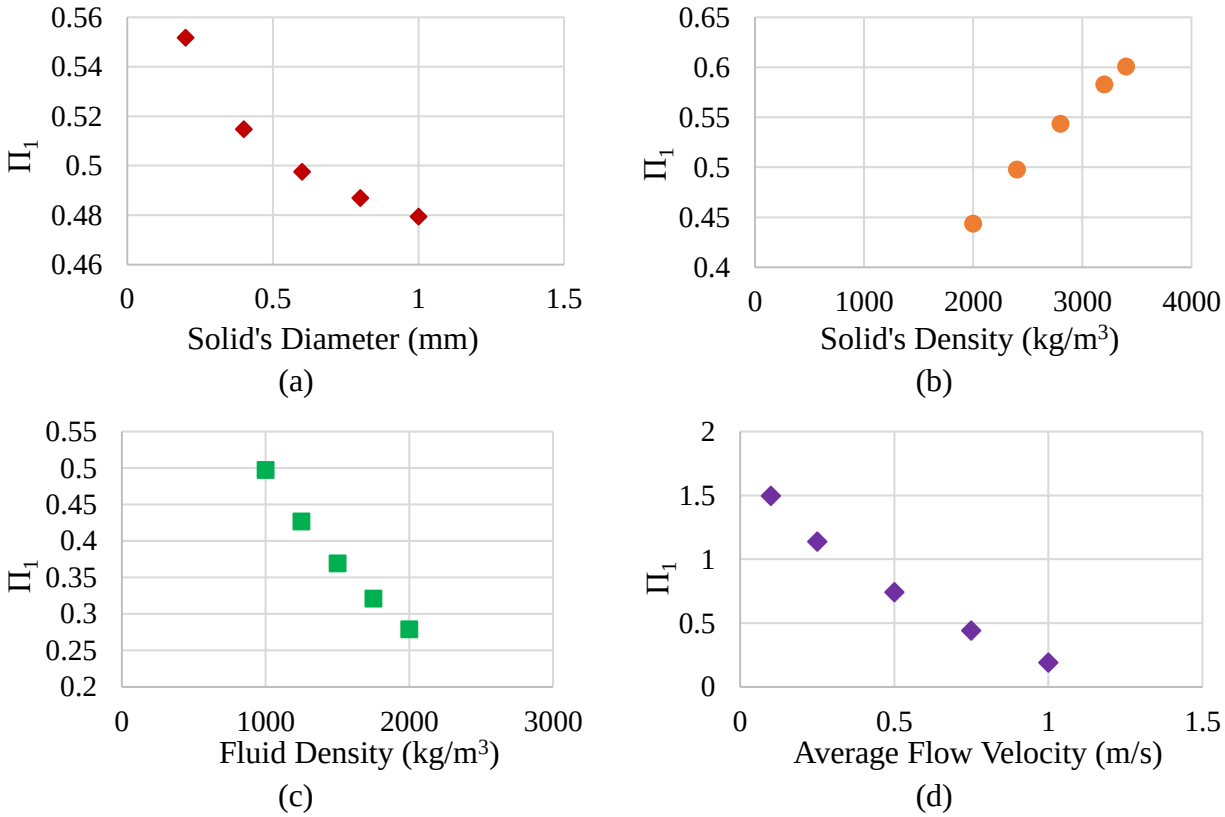
Input Parameters	Baseline constant value
Solid's Diameter - d_s	0.6 mm
Solid's Density - ρ_s	2400 kg/m^3
Inclination Angle - θ	1.571 rad (90°)
Fluid Density - ρ_f	1000 kg/m^3
Average Flow Velocity - U	0.7 m/s
Acceleration due to Gravity - g	9.8 m/s
Flow Behavior Index - n	0.6
Circulation Time - t	900 s (15 min)
Fluid Consistency Index - K_v	0.04 Pa.s^n
Hydraulic Diameter - d_h	83.5 mm
Length of Well Section - l	10 m

It can be observed from Fig 5.4a that increase in the size of the solids forming up the bed reduces the bed height that can be achieved when other parameters remain constant. This is due to a larger area of the protruding particle that is projected to the flow of the fluid near the wall. Hence, the higher velocity imparted near the wall is applied to a larger area of the particle making it easier to lift. Moreover, small particles form a more compact stationary bed thereby preventing erosion of the particles from the bed. This observation was also reported by previous researchers such as Larsen (1990) for the case of horizontal well profile. In general, an increase in particle size reduces the achievable normalized bed height following a power-law function.

Fig 5.4b represents the effect of an increase in particle density on the achievable reduction in bed height. As observed during the experimental part of this research, reduction in density has a moderate effect on the rate of erosion. The logarithmic reduction in attainable bed height suggests that the all the solids in the test section can be removed if the density of solids is equal to fluid's density, thereby, making the particles neutrally buoyant. Similarly, increasing the fluid density (Fig 5.4c) reduces the difference between the densities of both media. This increases the buoyant force acting on the particle making it easier to prevent particle settling. However, from a field application perspective, increasing fluid density may not be feasible as it results in an increase in static ECD that may exceed fracture pressure of the formation.

Increase in the average fluid velocity results in an exponential reduction in the bed height (Fig. 5.4d). This observation has been reiterated many times during this study as all the approach undertaken suggest the same. The correlation matrix developed also suggests that the average fluid velocity is the most dominant factor and influences the rate of bed height reduction significantly with the increase of the average velocity. An important aspect to be considered is

that with the reduction in bed height, the hydraulic diameter of the flow increases. Therefore, the impact of an increase in hydraulic diameter results in increased bed height for a given circulation time (Fig. 5.4e). Although the effect of average velocity and hydraulic diameter are independently studied here, the effects of these parameters are coupled in practical aspects as the increase in hydraulic diameter reduces the average velocity for a constant flow rate. Therefore, both these factors are inter-related and display an inverse relationship with each other. It was also observed that the length of the well section required to be cleaned linearly affects the rate of reduction in bed height for a constant circulation time (Fig. 5.4f).



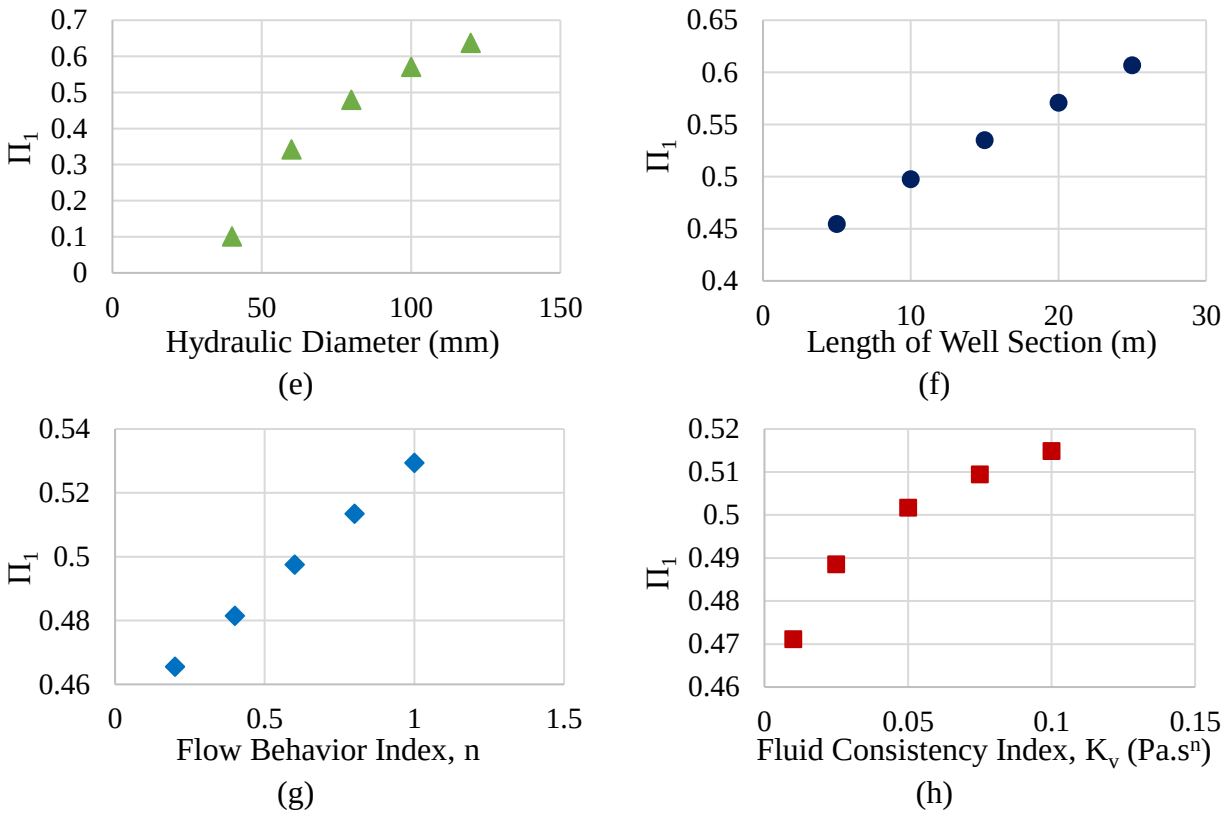


Fig. 5.4: Effect of various parameters on calculated bed height through model.

The effect of apparent viscosity or the measure of thickness of fluid on achievability of reduction in bed height can be distinctly measured in terms of power-law rheological parameters. It was observed that fluid behavior index had a linear effect on ability of fluid to erode the bed in horizontal well profile. Reduction in flow behavior index reduces the apparent viscosity of the fluid logarithmically as represented in Fig 5.5a. This allows the fluid with lower viscosity to generate a very thin hydrodynamic layer and imparts higher local velocity of the particle protruding from the bed. Hence, reduction in flow behavior index allows better erosional capability of cleanout fluid. Similar conclusion are obtained for fluid consistency index of fluid that linearly impacts the apparent viscosity of fluids (Fig. 5.5b). Reduction in fluid consistency index makes the fluid much thinner thereby eroding the bed efficiently.

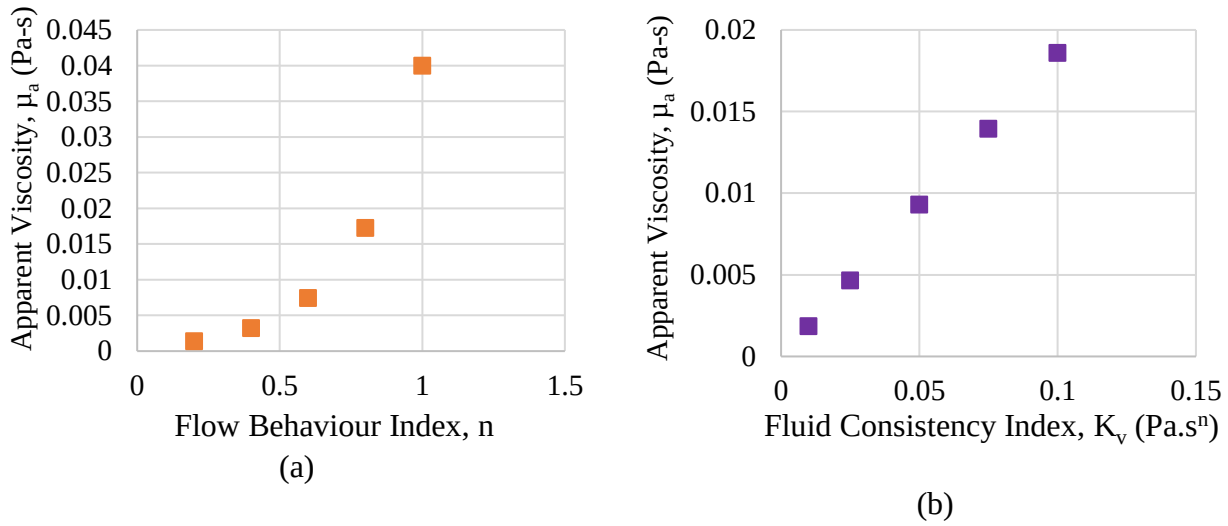


Fig. 5.5: Effect of power-law rheological parameters on apparent viscosity of the fluid.

5.5 Model Implementation

This section describes the implementation of the new correlation to predict optimal values for various parameters affecting cleanout operations. One variable at a time is considered using various circumstances for this purpose. Other influencing parameters are kept constant during each of these scenarios. These cases demonstrate the likelihood of upscaling of correlation to field application within valid ranges of dimensionless parameters (Table 5.1).

Example Problem (Pandya et al., 2019):

A hydraulic fracturing stimulation job was conducted in 60° inclined section of a well that was constructed with 5-in. ID outer casing. Fracturing schedule involved pumping of slurry with 20/40 US Mesh ceramic proppant. The mean particle diameter of the proppant was 600 microns and its specific gravity was 3.2. The fracturing job screened off before the tail flush stage could be completely pumped in the formation. This resulted in the formation of 2.5-in. proppant bed in the wellbore. It is required to clean a 34 ft well section down to at least 0.75-in (0.01905 m)

before any further operation can be carried out in the well. A 2.375-in CT is deployed to perform cleanout operation using a 10 lbm/Mgal Guar (n = 0.6594, K_v = 0.000812 lbf.s^n/ft^2) fluid that has an apparent viscosity of 5.31 cP at 511 s^{-1} shear-rate. The inner pipe is expected to lay eccentrically in this section of the well during the cleanout operation. If the fluid is circulated at the flow rate of 100 gpm, what would be the predicted circulation time required the achieve the objective?

Solution:

Following are the data given (in SI units):

- Casing ID = 5-in. or 0.127 m.
- Tubing OD = 2.375-in. or 0.06 m.
- Particle diameter = 600 μm.
- Solids density = 3000 kg/m^3
- Fluid density = 1000 kg/m^3
- Initial bed height = 2.5-in. or 0.0635 m.
- Apparent viscosity = 5.31 cP or 0.00531 Pa-s.
- Fluid consistency index = 0.000812 lbf.s^n/ft^2 or 0.0389 Pa.s^n.
- Flow rate = 100 gpm or 0.00631 m^3/s.
- The angle of inclination = 60° or 1.0472 rad.
- Gravitational acceleration = 9.8 m/s^2.

The first step involves calculating the hydraulic diameter when the final bed height is attained. Central angle with respect to outer pipe (ϕ') can then be calculated using Eqs (4.2) and (4.4) with reference to Fig 4.6. Here, final bed height (h) = 0.01905 m. Therefore,

$$\phi' = \cos^{-1}\left(\frac{r_o - h}{r_o}\right) = \cos^{-1}\left(\frac{0.0635 - 0.01905}{0.0635}\right) = \cos^{-1}(0.7) = 0.795 \text{ rad} \quad (5.6)$$

Similarly, the central angle with respect to the inner tubing (β) is calculated using Eq. (5.5f).

$$\beta = \pi - \cos^{-1}\left[\frac{r_o(1-\cos\phi') - r_i}{r_i}\right] = 1.193 \text{ rad} \quad (5.7)$$

With known values of central angles, the flow area and wetted perimeter in contact with fluid can be calculated using Eq. (5.5).

$$A = A_a - A_{bed} = r_o^2\left(\pi - \phi' + \frac{\sin 2\phi'}{2}\right) - r_i^2\left(\pi - \beta + \frac{\sin 2\beta}{2}\right) = 0.00939\ m^2 \quad (5.8)$$

$$S_i = 2(r_o \sin\phi' - r_i \sin\beta) = 0.0346\ m$$

$$S_h = 2r_o(\pi - \phi') = 2 * 0.0635(\pi - 0.795) = 0.2980\ m$$

$$S_h' = 2r_i(\pi - \beta) = 2 * 0.030163(\pi - 1.193) = 0.1175\ m$$

$$S = S_i + S_h + S_h' = 0.4501\ m \quad (5.9)$$

Substituting these values in the definition of hydraulic diameter, we get:

$$d_h = \frac{4A}{S} = \frac{4*0.00939}{0.4501} = 0.0835\ m \quad (5.10)$$

The average flow velocity can then be calculated using given flow rate and calculated flow area.

$$U = \frac{Q}{A} = \frac{0.00631}{0.00939} = 0.6718\ m/s \quad (5.11)$$

It is given from the problem that the fluid available for cleanout can be characterized using power-law rheological model. Hence, its effective/apparent viscosity can be calculated as,

$$\mu_a = K_v\left(\frac{8U}{d_h}\right)^{n-1} = (0.0389)\left(\frac{8*0.6718}{0.0835}\right)^{0.6584-1} = 0.00942\ Pas \quad (5.12)$$

Obtaining the values of these parameters allows for the calculation of all Pi-groups. These are calculated as follows:

$$\Pi_1 = h_n = \frac{h_t}{h_i} = \frac{0.75}{2.5} = 0.3 \quad (5.13a)$$

$$\Pi_2 = \frac{\rho_f U d_h}{\mu_a} = \frac{(1000)(0.6718)(0.0835)}{(0.00942)} = 5956 \qquad \log\Pi_2 = 3.775 \quad (5.13b)$$

$$\Pi_4 = 3.2 \qquad \log\Pi_4 = 0.5052 \quad (5.13c)$$

$$\Pi_5 = \frac{l^2}{d_s d_h} = \frac{(10.3632)^2}{(0.0006)(0.0835)} = 2143631.023 \qquad \log\Pi_5 = 6.33 \quad (5.13d)$$

$$\Pi_6 = \frac{U}{\sqrt{g.\sin\theta.d_h}} = \frac{0.6718}{\sqrt{(9.8)(\sin(1.0472))(0.0835)}} = 0.798 \quad \log\Pi_6 = -0.098 \quad (5.13e)$$

Using the values of these Pi groups, Π_3 can be calculated from Eq. (5.3).

$$\Pi_1 = A + \left(\frac{B \log_{10} \Pi_2}{\kappa}\right) + \left(\frac{C \log_{10} \Pi_3}{\kappa}\right) + \left(\frac{D \log_{10} \Pi_4}{\kappa}\right)$$

$$\kappa = 10^{\frac{\log_{10} \Pi_6}{(\log_{10} \Pi_5 + E)}} = 1.111$$

$$\therefore 0.3 = (1.98) + \frac{-0.04924 * 3.775}{1.111} + \frac{-0.24567 * \log_{10} \Pi_3}{1.111} + \frac{0.768 * 0.50515}{1.111}$$

$$\log_{10} \Pi_3 = 8.419 \rightarrow \Pi_3 = 10^{8.419} = 2.63\ \text{E08}$$

$$\therefore gt^2/d_h = 2.63\ \text{E08} \text{ or, } t^2 = 2236150$$

Hence, $t = 1495$ seconds or 25 mins.

Experimental results obtained under similar conditions indicate that 29% or original bed height (Π_1) remains after the period of 25 mins. Hence, the model developed performs well with negligible errors.

The fluid implemented in the previous problem is equivalent to Fluid 2 used in the experimental study. Considering a case in which Fluid 3 was used as a cleanout fluid instead of Fluid 2, a similar procedure leads to a conclusive result that 70% bed reduction (30% of original bed height remains) is attained after 29 minutes of fluid circulation.

In the third case, a hypothetical fluid (with rheological parameters between Fluid 2 and Fluid 3) is considered as a cleanout medium. The rheological parameters of this fluid are assumed to be: $K_v = 0.1147\ \text{Pa.s}^n$ and $n = 0.6215$. Incorporating these values in the model results in a prediction that shows the same level of bed height (30%) can be achieved within 27 minutes of fluid circulation. Hence, this hypothetical fluid would require longer duration than Fluid 2 but less time than Fluid 3 to attain required cleanout.

The variation of well section length is expected to increase the time required for hole cleaning. Consider a case in which the well length to be cleaned is 79 ft. (24 m). The value of κ for this

case is equal to 1.17. Using these values, the model predicts 41 minutes of fluid circulation to achieve similar cleanout conditions. The results from these different scenarios are consistent with the anticipated trend and illustrate the functionality of the model in field application that will allow field engineers to perform quick calculations towards efficient cleanout operations. A minor limitation of the model is that a good estimation of initial bed height is required for the application of the model. In general, the model can be directly implemented in field applications within the specified range of Pi-groups.

CHAPTER 6

COMPUTATIONAL FLUID DYNAMICS (CFD) FOR PARTIALLY BLOCKED ANNULUS

Several studies (Jain et al., 2004, Singhal et al., 2005, Pereira et al., 2007 and Farber, 2008, Tu et al., 2008; Gopal et al., 2016, Heydari et al., 2017) have implemented CFD techniques to investigate flow hydrodynamic in pipe flow. Some studies (Bicalho et al., 2016, Tang et al., 2016) verified the ability of CFD techniques to solve flow problems in complex geometries such as partially blocked annulus. The accuracy of the results was confirmed with experimental data. Nevertheless, Roache (1998) described simulated flow problems solutions to be more empirical in nature than theoretical/mechanistic. This was attributed to the input values required by turbulent CFD models that are majorly based on the experimental conditions to be simulated since results obtained from CFD simulations are specific to the input provided to the model.

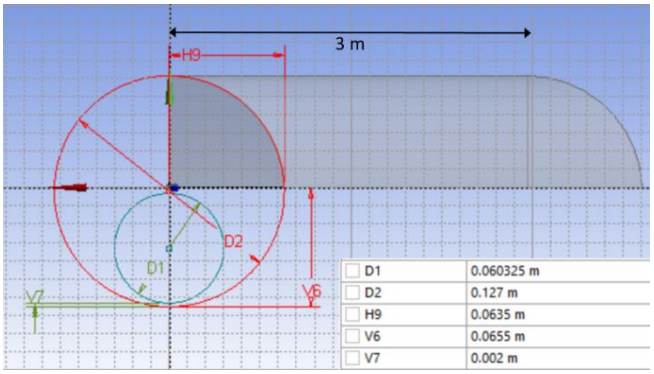
The aim of the CFD study is to understand and explain the flow phenomena occurring at bed interface during bed erosion process. A widely used commercial CFD software (ANSYS version 19.2) is utilized in this study. The software allows the generation of structured or unstructured mesh for complex flow problems and solves the associated flow equations. The software module comprises of different components including pre-processors to generate a flow geometry, meshing component for generation of an efficient mesh structure, solvers and post-processing component for flow visualization and other graphical user interfaces. Following sections describes the model details including generation of geometry, meshing, solver specifications, boundary conditions and simulation results for non-Newtonian power-law fluid flow within eccentric annuli.

6.1 CFD Model Description

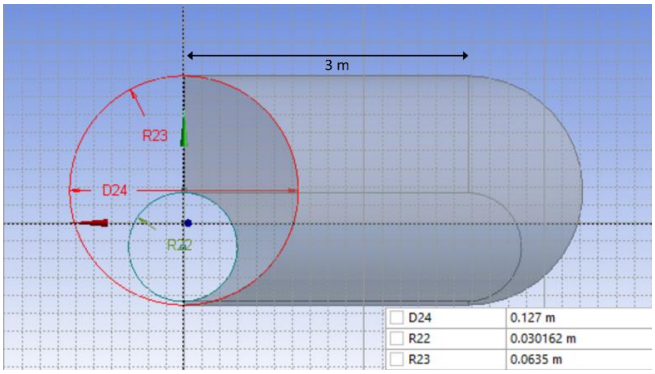
6.1.1 Geometry

Constructing an accurate flow model is the most critical step towards flow simulation process. The ANSYS DesignModeler application has been used to edit the flow geometry for different bed heights. Four different flow geometries were constructed for this study. These geometries differ from each other in terms of the stationary bed height. A case in which eccentrically ($\varepsilon = 94\%$) placed inner pipe is fully submerged is referred to as a 100% bed height scenario. The four scenarios simulated were 100%, 75%, 50% and 25% bed height (Fig. 6.1).

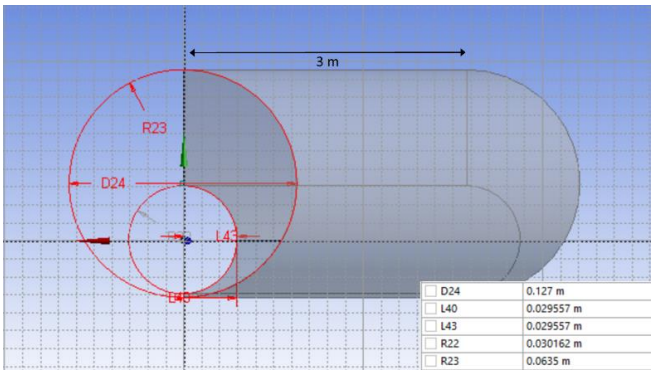
(a) 100% bed height -



(b) 75% bed height -



(c) 50% bed height -



(d) 25% bed height -

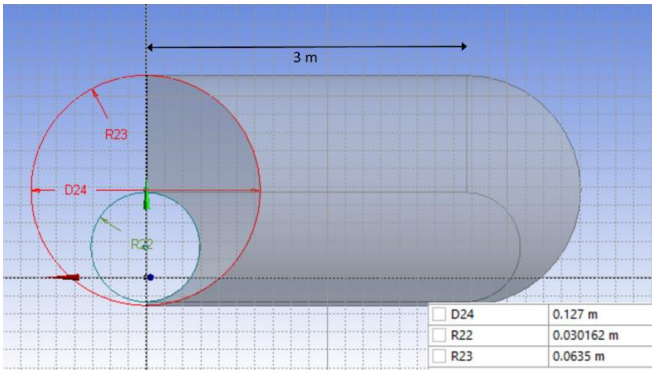


Fig. 6.1: Flow geometries as generated in DesignModeler for four scenarios simulated.

It is essential to consider a long annulus in which a fully developed flow is attained. The minimum geometry or annular length required to achieve fully developed flow related to the entrance length (L_e) as presented in Fig. 6.2. The total pipe length can be considered for flow calculations and entrance effect can be ignored only if the pipe length exceeds the entrance length. Entrance length can be estimated if the Reynolds number and hydraulic diameter of the pipe are known.

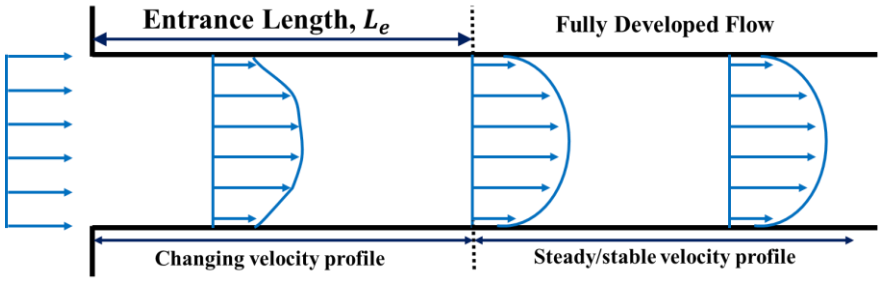


Fig. 6.2: Schematic of entrance length in pipe flow.

Two distinct equations are developed to calculate entrance length based on the fluid flow regime.

Laminar Flow - $\frac{L_e}{D_h} = 0.06\, Re$ (6.1a)

Turbulent Flow - $\frac{L_e}{D_h} = 4.4\, Re^{\frac{1}{6}}$ (6.1b)

The simulations conducted in this study are for turbulent fluid flows. Hence, Eq. (6.1b) can be used to calculate entrance length. It is evident that highly turbulent flow requires a longer length to fully develop. Hence, the longest entrance length is required for a case with the low fluid viscosity and high fluid velocity. This corresponds to a scenario with an inner pipe completely submerged (100% bed height) and water as a cleanout fluid at a flow rate of 9.46 L/s. The entrance length for this particular case is 2.6 m. Owing to this, 3-m long annulus is used for all CFD simulation cases. Sensitivity analysis pertaining to the effect of length on velocity and pressure gradient suggested that these values plateau out after 2 m and entrance effects become negligible (Fig 6.3).

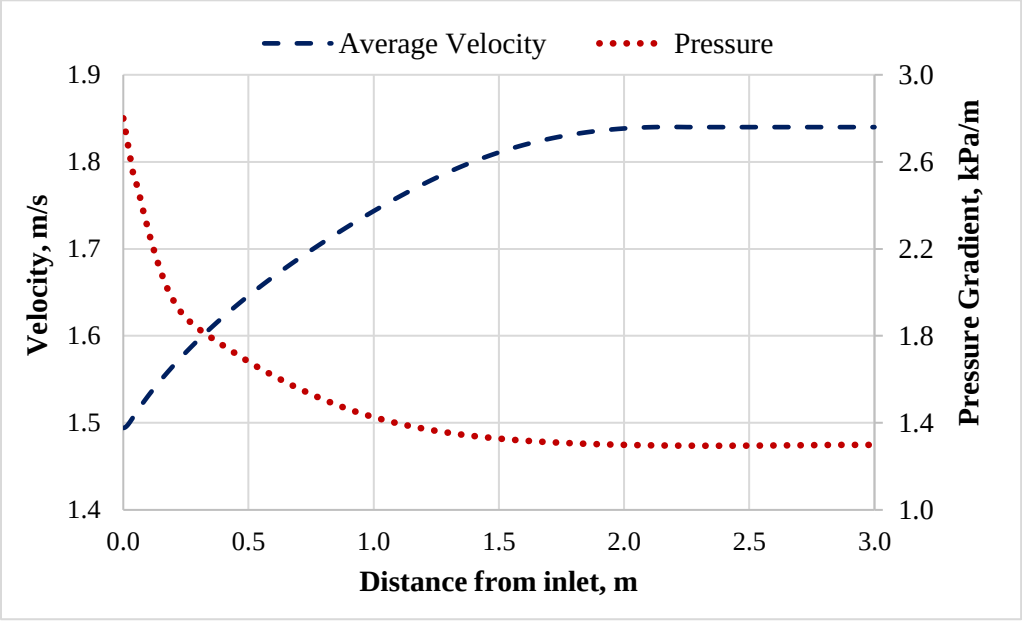
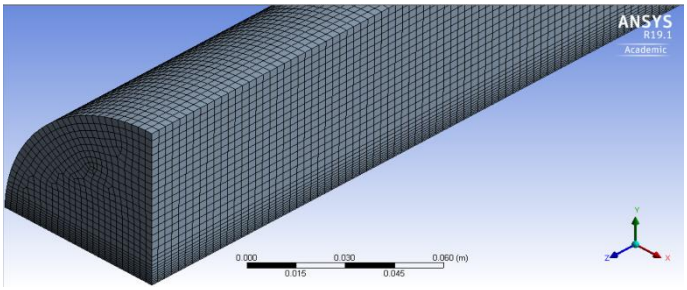


Fig. 6.3: Velocity profile and pressure gradient along the length of CFD model

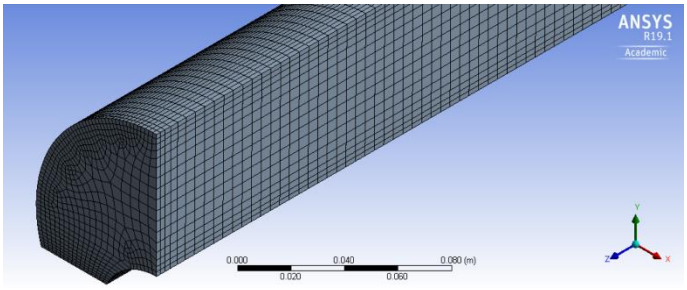
6.1.2 Meshing / Grid Generation

ANSYS Fluent provides a robust method for meshing of the flow geometry through a grid generation program capable of handling hexahedral, tetrahedral, cutcell and unstructured cells. Although most of these structures can handle the current flow problem, a hexahedral unstructured mesh structure was used for the scope of this geometry. A hexahedral unstructured grid system allows for manual grid inflation at wall and interface boundaries. Subsequently, the grids generated close to the walls are very fine and hence near-wall effects can be captured accurately. Additionally, hexahedral cells have a tendency to align grid system parallel to the direction of the flow as well as pipe walls making it a very reliable option for discretization. Although this was the general grid system implemented in all case scenarios, the exact mesh was each system differed due to the change in flow geometry with the reduction in bed height (Fig. 6.4). Despite the change in geometry, it was ensured that flow behavior at the bed interface was accurately captured in all cases by use of grid and layer inflation at the bed.

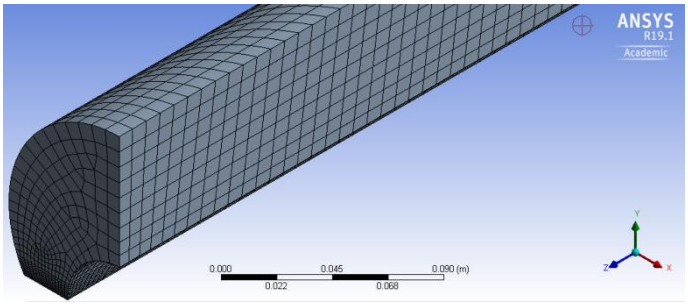
(a) 100% bed height -



(b) 75% bed height -



(c) 50% bed height -



(d) 25% bed height -

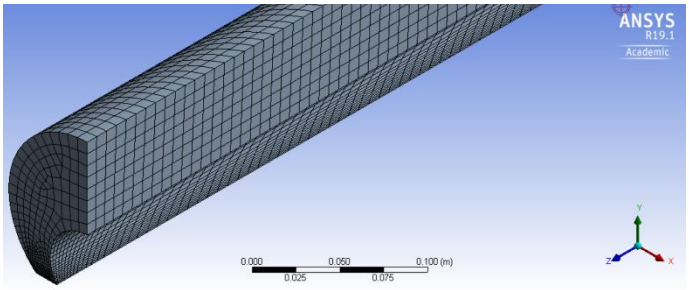


Fig. 6.4: Meshing structures for four scenarios simulated.

There was a variation in a number of cells and grids in each mesh generated due to the difference in geometry of all four cases. Table 6.1 summarizes statistics for each mesh. The number of cells considered in the mesh reduces with a decrease in bed height. This was done to reduce the computational time required to simulate cases with lesser bed height as a lower bed height scenario results in relatively higher flow area. Maintaining the maximum cell size for these cases will results in a grid with a larger number of cells that would increase computational time tremendously. Near bed flow effect is the key target aspect of these simulations. Hence, it was essential to create a finer grid near the interface of solids bed and flow domain. Therefore, some compromise was made in the core of the flow domain by allowing a coarser grid system. This resulted in an overall decrease in the number of cells generated with a decrease in bed height. Although there were some compromises made on meshing system to account for computational time, it can be observed from Table 6.1 that the mesh quality was good as average skewness and cell quality have the recommended values.

Table 6.1: Mesh statistics

Mesh for	100% bed height	75% bed height	50% bed height	25% bed height
Number of cells	631368	369026	127344	120901
Number of nodes	2670320	1578588	551008	527463
Maximum cell size	0.003 m	0.005 m	0.008 m	0.008 m
Average skewness	0.055	0.151	0.286	0.149
Average cell quality	0.77	0.61	0.57	0.86

Sensitivity of the results from the generated grids has been analyzed for partially blocked annulus geometry of all bed heights. Adequacy of mesh refinement and utilization of proper element size for the generation of grids were studied in terms of stable results of pressure gradient and consistency of the same. Fig. 6.5 represents the resultant pressure gradient from CFD models with element size utilized to generate the respective grid. The simulations were carried out for water at 5 m/s to ensure highly turbulent flow regime. Lower element size results in higher number of nodes and elements through which solutions are obtained. It was observed that element size less than 0.01m results in consistent results. To capture the wall effects in all cases, the maximum element size was restricted to 0.005m for all cases.

Reliability of mesh structure can be determined by analyzing mesh quality in each case. Mesh quality guarantees the satisfactory results for the problem, decreases the amount of additional analysis while consequently improving the predictive ability of the model. The primary measure of determining mesh quality considered in this study is skewness distribution of all cells for each scenario as presented in Fig 6.6.

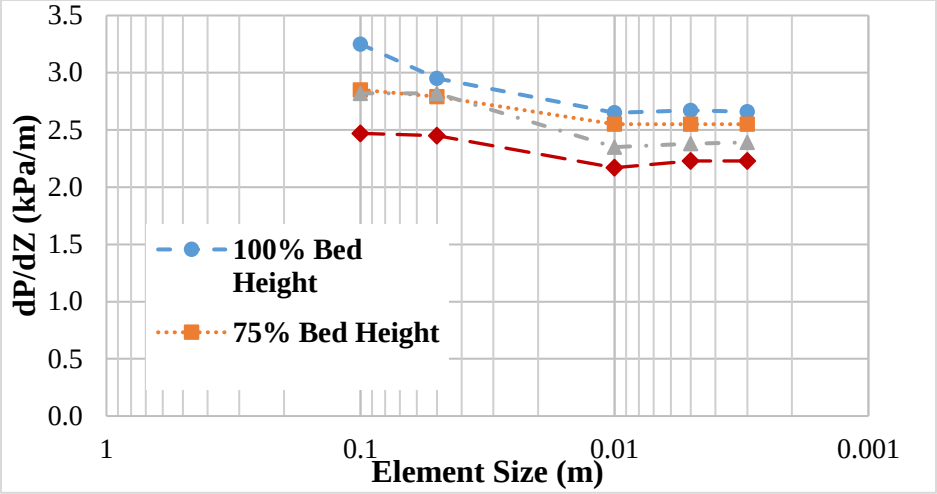


Fig. 6.5: Pressure gradient vs element size of grids generated for bed heights.

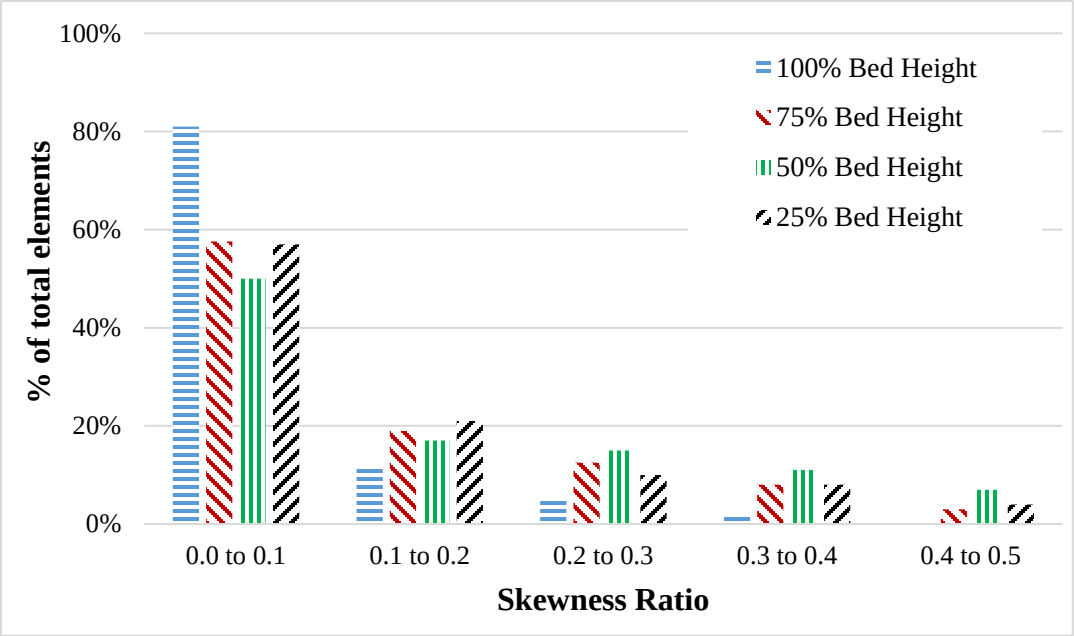


Fig. 6.6: Skewness ratio distribution for each mesh case

Skewness is a primary and most commonly used factor to determine mesh reliability. It is essentially a measure of equilateral nature of a cell. In a volume derived method, the skewness ratio is defined as,

$$Skewness\ Ratio = 1 - \frac{Actual\ Cell\ Size}{Ideal\ Cell\ Size} \tag{6.2}$$

Based on this definition, a skewness ratio of 0 is representative of an ideal or equilateral cell whereas the skewness ratio of 1 represents a degenerate cell. Table 6.2 provides a relationship between skewness and cell quality. Based on the definition and its corresponding cell quality, cells with higher skewness ratio should be avoided as they result in erroneous results. Maximum skewness of 0.4 is assumed to be the threshold for good quality mesh. It is observed from Fig. 6.6 that volumetric cells generated during mesh design for each case have a maximum skewness of 0.5. Less than 10% of cells are of poor quality (> 0.4 skewness ratio) and the majority of cells have a skewness ratio between 0 and 0.1. Each mesh can be considered a good quality 3D mesh as most cells have a good or better skewness measure.

Table 6.2: Skewness ratio range and corresponding cell quality (ANSYS® Meshing User's Guide)

Skewness	Cell Quality
1.00	Degenerate
0.90-1.00	Bad
0.75-0.90	Poor
0.50-0.75	Fair
0.25-0.50	Good
0.00-0.25	Excellent
0.00	Perfect

Numerical verification of results from CFD data were conducted by comparison of pressure gradient obtained through simulations and those predicted using hydraulic model for all bed heights, fluids and flow rates as illustrated in Fig. 6.7. The simulated pressure gradient data is in good agreement with analytical solution developed for turbulent flow of non-Newtonian fluids with errors less than 20% as demonstrated in the cross-plot.

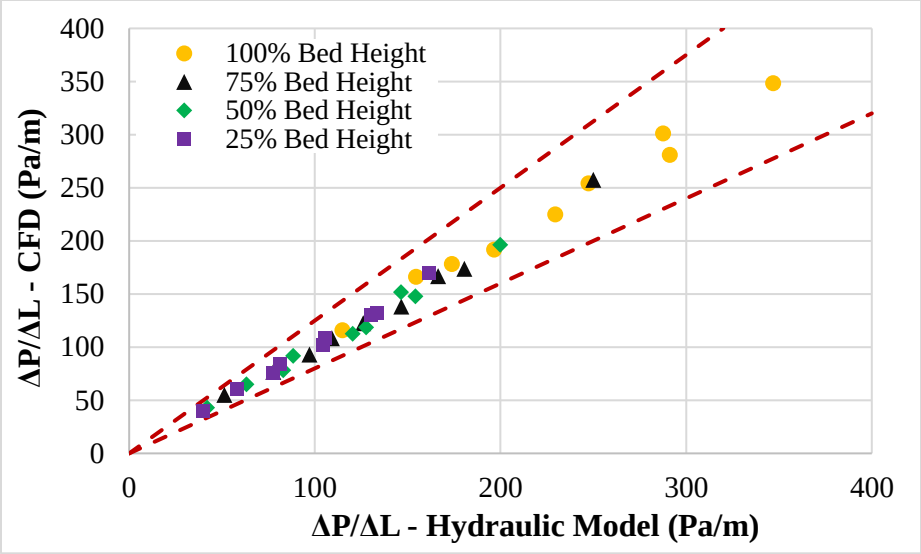


Fig. 6.7: Comparison of pressure gradient from CFD simulation and analytical model.

6.1.3 Governing Equations and Model Selection

The governing equations to be solved form are the cornerstone of CFD modeling. The governing equations are – continuity equation and momentum equation. This is only true with systems involving incompressible flow such as that in this study. Additionally, the energy equation is required to solve flow systems with compressible fluids.

Continuity equation (conservation of mass) is useful in describing accumulation of a fluid volume. It states that rate of mass accumulation of fluid in a finite volume element is equal to the rate at which fluid mass enters the element minus rate at which it exits the element, or $rate\ of\ mass_{accumulate} = rate\ of\ mass_{in} - rate\ of\ mass_{out}$.

Mathematically, this can be represented in differential form as,

$$\frac{\partial \rho}{\partial t} + \nabla.(\rho \vec{u}) = 0 \qquad (6.3)$$

Momentum is defined as the product of object mass and its velocity. Conservation of momentum states that momentum is constant within a finite volume element – it is neither created nor

destroyed, but only altered when any force acts on it. Since momentum is conserved in all coordinates at the same time, it can be represented as,

$$\rho\left(\frac{\partial\vec{u}}{\partial t}+\vec{u}.\nabla\vec{u}\right)=-\nabla p+\nabla.\vec{\tau}+\rho\vec{g} \tag{6.4}$$

For a flow existing only in the x-direction, this equation can be represented as,

$$\rho\left(\frac{\partial u}{\partial t}+u\frac{\partial u}{\partial x}+v\frac{\partial u}{\partial y}+w\frac{\partial u}{\partial z}\right)=-\frac{\partial \mathrm{p}}{\partial \mathrm{x}}-\left(\frac{\partial \tau_{\mathrm{xx}}}{\partial x}+\frac{\partial \tau_{\mathrm{yx}}}{\partial y}+\frac{\partial \tau_{\mathrm{zx}}}{\partial z}\right)+\rho g_x$$

Solving these equations require some assumptions as follows. Few other applicable to specific geometries will be discussed later in this chapter.

1. Fluid flow is homogenous, flowing in a purely turbulent or laminar flow regime and is of isothermal nature.
2. Fluids incorporated as cleanout fluids are incompressible.
3. Inner CT is non-rotating and stationary.
4. Simulations are only conducted for the case of horizontal flow. Hence, gravity is not considered in the analysis.
5. Flow velocity at inlet is constant for each of the geometry and it is calculated using flow rate and flow area.
6. The no-slip boundary is assumed to exist at the bed interface.
7. The flow is considered to be a fully developed and steady
8. The effect of solids on the hydrodynamics is neglected
9. The bed is considered stable, uniform, and consolidated
10. Bed particles have a uniform size distribution
11. The walls of the inner pipe and casing/hole are considered smooth
12. The flow properties of the fluid follow the power-law fluid model

These set of equation form the well-known Navier-Stokes (NS) equations that are solved using ANSYS Fluent. Fluent comprises of two types of solvers – pressure-based solver and density-based solver. Ideally, pressure-based solvers are used for incompressible flow and density-based approach is used to solve compressible fluid flows at higher velocity. Since the fluids considered in this study are incompressible, a pressure-based approach is selected for flow simulations. The pressure-based solver is based on an algorithm known as the projection method. Within this algorithm, the mass conservation equation is solved by solving a pressure equation. This pressure equation is obtained from the momentum and the continuity equations such that resultant velocity satisfies the condition of continuity. The resulting set of equations are coupled and non-linear. Hence, the solution procedure requires iterations until the criteria of convergence are attained.

Most of the simulations carried out involve fluid flow in highly turbulent flow regime. The presence of turbulence causes an unsteady and a periodic motion (fluctuations in space and with time) of mass and momentum. Therefore, the fluid properties are not constant and velocity varies randomly. Many turbulent specific models are available in ANSYS but there is no single model that can predict turbulent nature with practical reliability and accuracy. Reynolds-Averaged Navier-Stokes (RANS) model is widely used to simulate industrial flow systems. The model solves the time-averaged NS equations and hence, less expensive in terms of computational requirement. Due to time averaging, RANS modeling results in an additional unknown called Reynolds stress. The Reynolds stress is obtained from an additional closure equation called Boussinesq hypothesis which allows Reynolds stresses to be modeled using a term called turbulent viscosity, μ_T. This viscosity can be obtained from a dimensionless length scale and dimensionless time scale.

In this study, a two-equation viscous realizable $k-\epsilon$ model is used to calculate turbulent viscosity and subsequently solve the flow problem. Here, k is the turbulent kinetic energy and ϵ is the turbulent dissipation rate. This model was used as it performs superiorly for flows involving boundary layers at higher pressure gradients and due to its faster computation time. A major drawback of any $k-\epsilon$ model is that it is unable to calculate the turbulent dissipation rate (ϵ) near the wall. To work around this, standard wall function is used in addition to the model selected. This function implements a log-law correlation for turbulent boundary layers to obtain required boundary conditions. Standard wall function uses coarse grid system near the wall when compared to enhance wall treatment option that uses a refined grid near the wall. Despite this, the former results in reliable solutions with lesser computational power.

6.2 Simulation Details

6.2.1 Setup and Post-Processing

Simulations were conducted using multiple solvers in parallel to reduce the computational time and to utilize maximum available computational power. Due to the disparate nature of length scales in geometry (l/d ratio), a double-precision model was selected within the solvers. This also aided in improving the accuracy of the calculations at bed interface and the wall where pressure differences driving the flow are relatively small. Generic problem settings related to mesh and solver were using a default pressure-based solver as described earlier, absolute velocity formulation and a steady flow. Absolute velocity formulation was selected because the flow domain is assumed to be stationary. The gravitational acceleration term was disabled in all simulations since only the horizontal flow profile is simulated. Models task page lists options for different models that can be selected for flow simulations. The viscous model was modified for

all simulations. Other flow models were turned off for all cases. A realizable $k-\epsilon$ model with standard wall functions was selected for turbulent flow simulations as described earlier.

Three fluid materials (Fluid 1, Fluid 2 and Fluid 3) were selected for the simulations. As mentioned earlier, Fluid 1 corresponds to plain water, Fluid 2 corresponds to 1.2 g/L guar fluid and Fluid 3 represents a 2.4 g/L guar fluid. Properties of these fluids are listed in Table 6.3. Turbulent flow concerning non-Newtonian type fluids, as in this study, requires enabling of non-Newtonian options for fluid viscosity. This can be achieved by entering following command in ANSYS Fluent console – "*define/models/ viscous/turbulence-expert/turb-non-newtonian?-Y*".

Table 6.3: Properties of fluids used in the simulations

Fluid Name	Density (kg/m^3)	Fluid Type	Rheology Type	Viscosity (kg-m/s)	Consistency Index, K ($kg\text{-}s^{n-2}/m$)	Power Law Index, n
Fluid 1	1000	Newtonian	Constant	0.001	-	-
Fluid 2	1000	Non-Newtonian Power Law	Shear rate dependent	-	0.0389	0.6584
Fluid 3	1000	Non-Newtonian Power Law	Shear rate dependent	-	0.1904	0.5846

- Options pertaining to Cell Zones Conditions allows the user to set cell zone condition parameters for each zone. Simulations involved in this study comprise of only one zone or flow domain. This task page allows the user to enter one of the previously defined fluids to be simulated within the flow domain. For all cases, the operating pressure for flow simulations was fixed at standard pressure (101325 Pa). The Boundary Conditions option allows the user to set properties for various boundaries in the flow geometry.

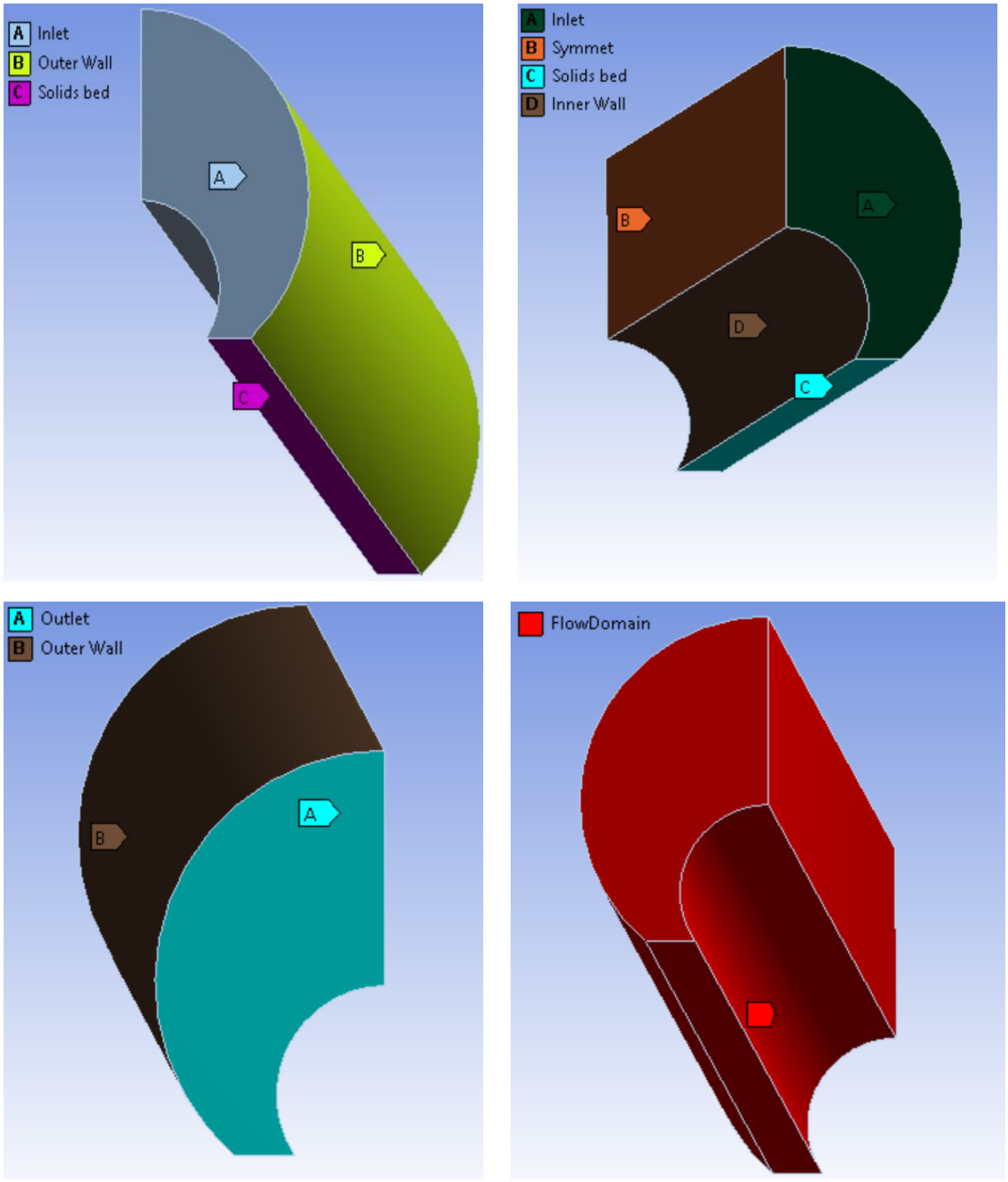


Fig. 6.8: Different flow boundaries defined in all flow geometries

These boundaries are represented in Fig. 6.8. The different boundaries defined in these simulations are –

- 'Inlet' and 'Outlet' of the flow domain.
- 'Outer Wall' representing flow boundary due to the outer smooth pipe.

- ‘Inner Wall’ representing flow boundary due to the inner smooth pipe. Flow geometry for 100% bed height does not involve inner wall boundary because the inner pipe is completely submerged in solids bed.
- ‘Solids bed’ representing rough bed interface between flow domain and solids bed.
- ‘Symmet’ representing the plane of symmetry that allows replication of results on either side of it. Due to the symmetric nature of the flow, simulating half of the actual flow domain insufficient in all cases.

Flow Domain is the volumetric area in which fluid flow occurs. The zones of each named selection can be selected from the Boundary Conditions tab. Description and details of boundary condition allotted to each boundary have been described in Table 6.4. For the inlet boundary, momentum parameters can be input using velocity inlet dialog box. Velocity specification field can be used to set the process used to describe inlet velocity. The magnitude of inlet velocity is computed from the absolute flow rate and average flow area. Turbulence intensity (I), also known as turbulence level, is mathematically defined as the ratio of root-mean-square of velocity fluctuations (u') and mean velocity (U). For the case of $k-\epsilon$ models and $k-\omega$ models, this turbulent intensity can also be defined in terms of turbulent kinetic energy (k) as represented in Eq. 6.5. The geometry of all flow models was designed to attain a fully developed flow in the annulus. For a fully developed flow, intensity can also be expressed in terms of Reynolds number calculated using hydraulic diameter (empirical relation).

$$I = \frac{u'}{U} = \sqrt{\frac{2}{3}k} = 0.16\, Re_{dh}^{-1/8} \tag{6.5}$$

For annular flow, turbulence intensity at the inlet boundary governed by upstream history of the flow. A low turbulent intensity can be used if the upstream flow is under-developed and vice

versa for the case of fully developed flow. The calculated turbulent intensity for Reynolds number of 50,000 using this correlation is approximately 4%.

Table 6.4: Details of all boundaries defined in all flow models

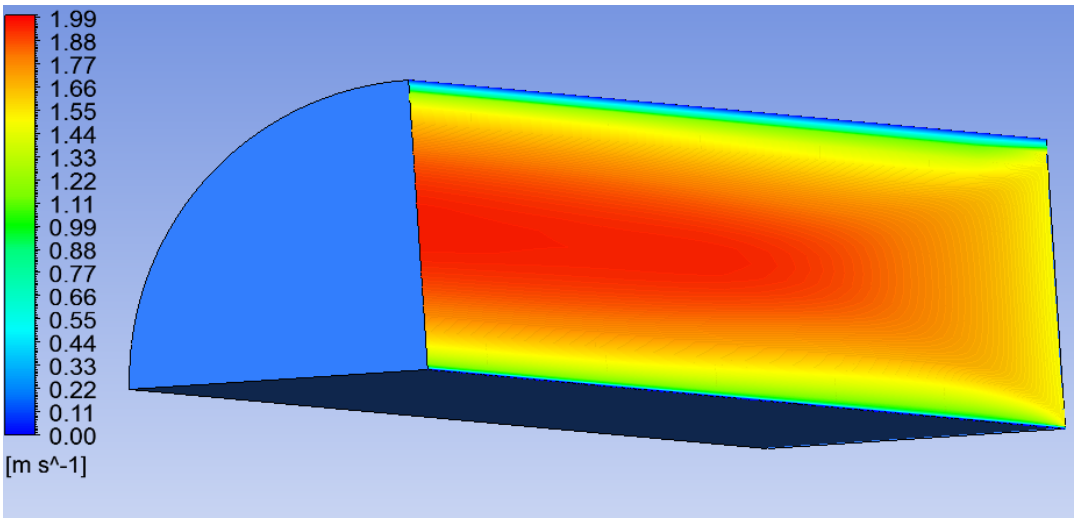
Boundary Name	Type	Details
Inlet	Velocity inlet	Reference frame – Absolute Velocity specification – Normal to the boundary
Outlet	Pressure outlet	Reference frame – Absolute Gauge pressure – 0 Pa
Inner Wall	Wall	Wall motion – Stationary wall Shear condition – No slip Roughness height – 0 m
Outer Wall		
Solids Bed	Wall	Wall motion – Stationary wall Shear condition – No slip Roughness height – 0.0006 m Roughness constant – 0.5
Symmet	Symmetry	
Flow Domain	Interior	

Simulations are intended to model the flow over stationary bed height generated using spherical proppant. To simulate the effect of protruding particles, the bed roughness was maintained constant at 0.006 m (average proppant size). Wall roughness is simulated in fully developed wall-bounded turbulent flow through Standard Law of the Wall. Simulations in this study have been performed mostly for turbulent flow cases (with only a couple of scenarios under laminar flow regime) using Semi-Implicit Pressure Linked Equations (SIMPLE) pressure-velocity coupling scheme. This scheme is selected because of its ability to accurately simulate incompressible flow. The second-order method was selected for the discretization of pressure, momentum, turbulent kinetic energy and turbulent dissipation rate.

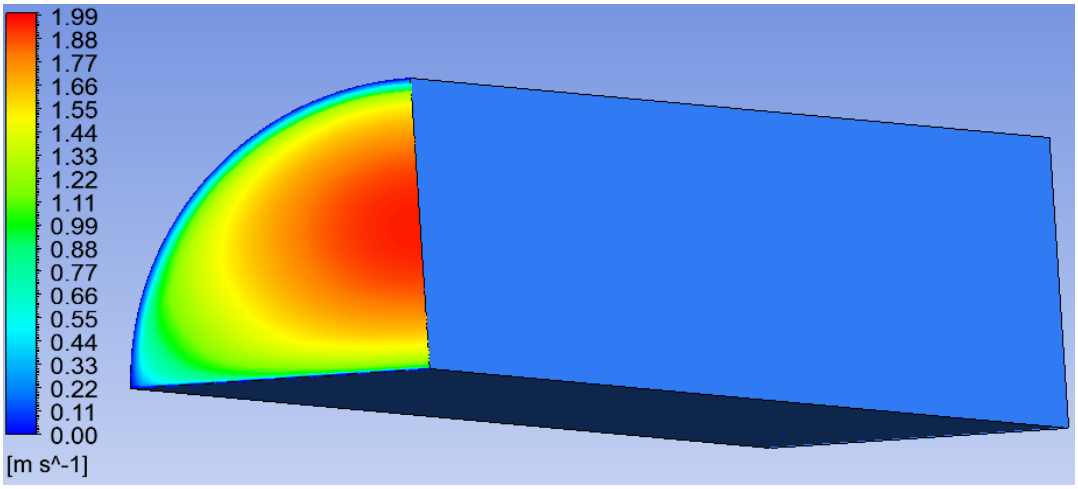
Convergence conditions can be specified to define stop conditions for solvers. Residuals related to continuity, x-velocity, y-velocity, z-velocity, turbulent kinetic energy, and turbulent dissipation rate were monitored and checked for convergence. The absolute criteria of convergence for these residuals were set at 10^{-8} and upper iteration limit was set at 5000 iterations. These conditions ensured absolute convergence of residuals and accuracy in obtained solutions.

ANSYS CFD-Post is the commonly used post-processing tool for simulations involving fluid dynamics. This is a powerful tool that allows users to visualize and analyze the results obtained by CFD solver. Velocity, shear, and pressure distribution were analyzed using flow visualization techniques such as contour and cartesian plots.

Figs. 6.9a and 6.9b present velocity contour plots at the outlet (3 m from inlet) and axially across the flow domain, respectively. Contour plot shown in Fig 6.9b along with a plot of axial flow velocity against axial length (Fig. 6.3) can be used to confirm attainment of fully developed flow. It can be observed that average velocity increases initially to a certain extent before it starts to flatten out. Average velocity is nearly constant at a distance of 3 m from the inlet and hence, the flow is fully developed by this length. Due to this reason, average velocity, cross-sectional velocity profile, pressure distribution, and average bed shear are obtained at 3 m from the inlet.



(a)



(b)

Fig. 6.9: Velocity contour plot a) across the axial length and b) at the outlet

Fig. 6.10 is a velocity contour plot across cross-sectional flow area at the outlet (3 m from inlet). The contour plot is developed by applying instance transform of half simulated flow area across the plane of symmetry to represent the entire flow area. Fig. 6.11 is a plot of velocity profile across the plane of symmetry from top of solids bed (0 m) to the outer pipe wall (0.0635 m).

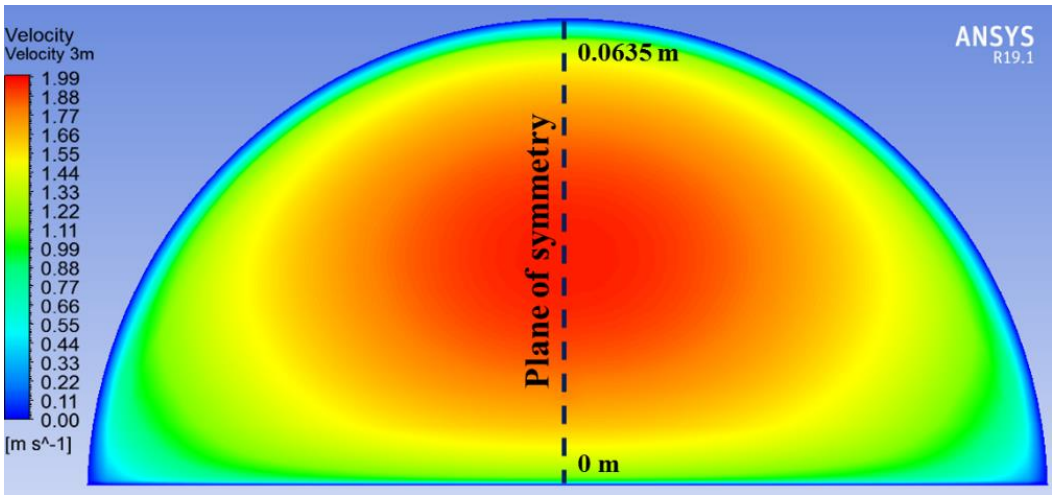


Fig. 6.10: Flow velocity contour for the entire cross-sectional area of flow

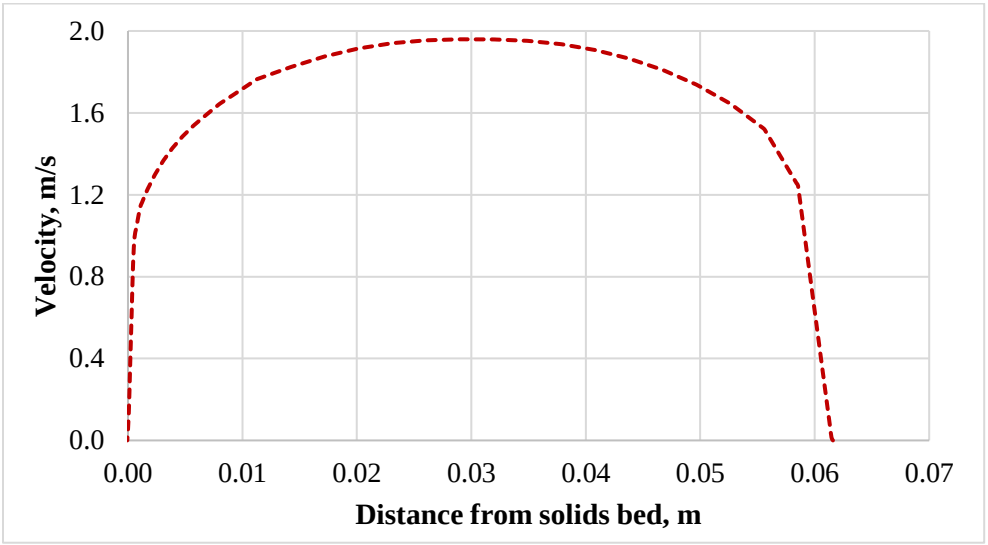


Fig. 6.11: Flow velocity contour for the entire cross-sectional area of flow

Fig. 6.12 represents the bed shear profile at the surface of solids bed from one end of the flow to another end of it in the lateral direction with the center being at the center of the outer pipe. The area under this curve was integrated to calculate the average bed shear across the solids bed at the outlet. Earlier visualizations are presented for only a single case – 100% bed height at a single flow rate with one type of fluid. This set of analysis was conducted for each simulation as described in the simulation matrix.

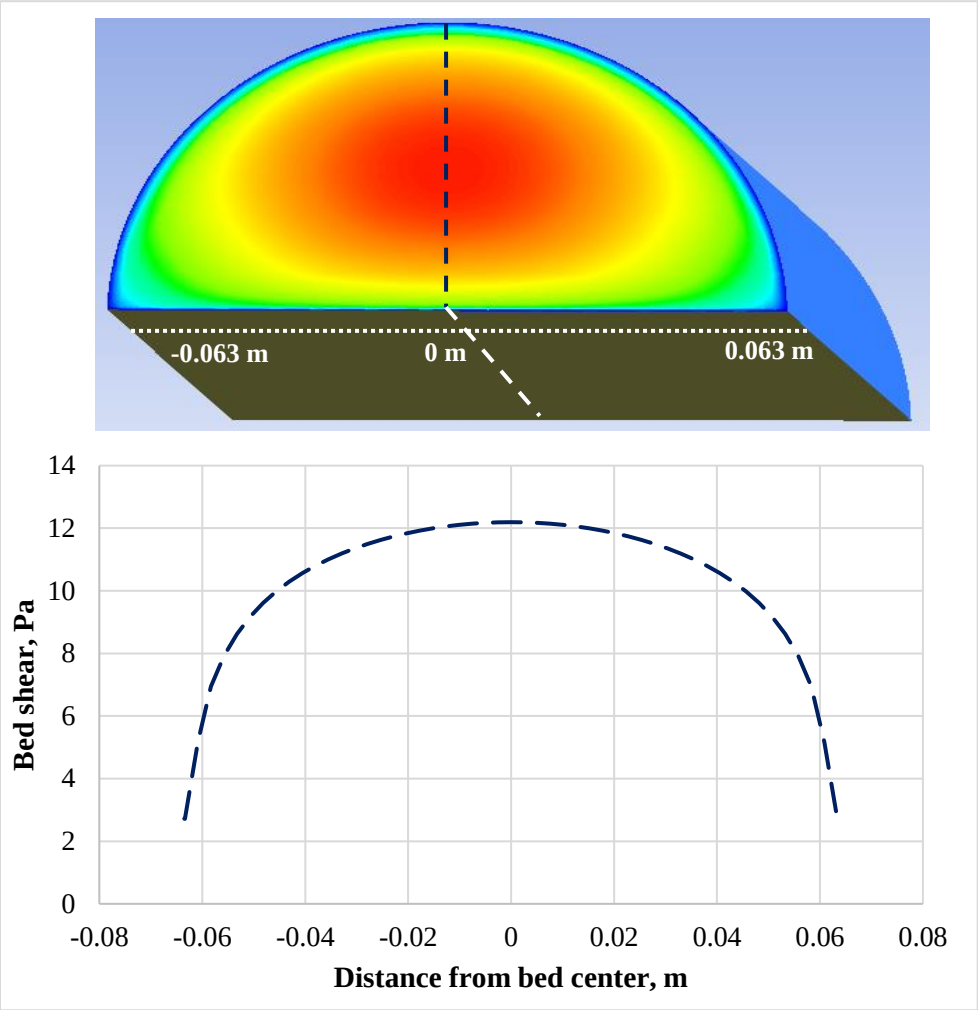


Fig. 6.12: Bed shear profile at the solid-fluid interface.

6.2.2 Simulation Matrix

A total of 48 simulations were conducted with varying bed heights, flow rates, and fluid rheology. Bed heights considered were 100% bed height (inner pipe completely buried under solids bed), 75% bed height, 50% bed height, and 25% bed height. Selection of these bed heights was sufficient to study the steady-state behavior as well as a combined transient behavior related to the reduction of bed height with time. Flow rates considered were the same as that in the experimental investigation – 5.05 L/s, 6.31 L/s, and 7.57 L/s. Additionally, a higher flow rate of

9.46 L/s was included for the purpose of these simulations as field applications involve pumping fluids within a higher range of flow rate. For the purpose of input values in the CFD model, these flow rates were converted to average velocity by use of cross-sectional flow area obtained using hydraulic diameter. The hydraulic diameter was calculated using the previously mentioned methodology. Simulations were conducted using three cleanout fluids – Fluid 1, Fluid 2 and Fluid 3. Definition and detailed description of these fluids have been provided earlier in this manuscript. All simulations were conducted on a machine with Intel® Xeon® CPU E5-2697 v4 2.30 GHz dual processor with 24 GB RAM and 64-bit operating system. Due to the difference in geometry, the number of cells generated during the meshing process varied. However, in general, the average time taken to complete a single simulation was 4 to 5 hours.

CHAPTER 7

ANALYSIS AND MODELING

The results from experimental and simulation studies can be inter-related to establish a relationship between bed shear and rate of bed erosion that can aid in accurate prediction of wellbore cleanout and allow for quicker optimization of the process. Results pertaining to experimental studies will only be described as required since they have already been discussed previously in Section 4.5. CFD simulations were carried out for distinct values of various combination of input variables as listed in Table 7.1. The targeted parameters in simulation study involve velocity profile as a function of distance from the solids bed (across line XY in Fig. 7.1) and shear stress at bed interface (across line AB in Fig. 7.1). These parameters were obtained at the outlet (a distance of 3 m from inlet) where the flow is considered fully developed for all bed heights.

Table 7.1: Input variables used in CFD Simulations

Bed height	0.0655 m (100%) 0.0491 m (75%) 0.03275 m (50%) 0.016375 m (25%)
Fluids	Fluid 1 (μ=0.001 kg-m/s) Fluid 2 (K=0.0389 kg-s^{n-2}/m, n=0.66) Fluid 3 (K=0.1904 kg-s^{n-2}/m, n=0.59)
Average flow rates	0.005047 m^3/s 0.006309 m^3/s 0.007571 m^3/s 0.009464 m^3/s
Annular flow area	0.006334 m^2 (100% bed height) 0.008061 m^2 (75% bed height) 0.008964 m^2 (50% bed height) 0.009520 m^2 (25% bed height)

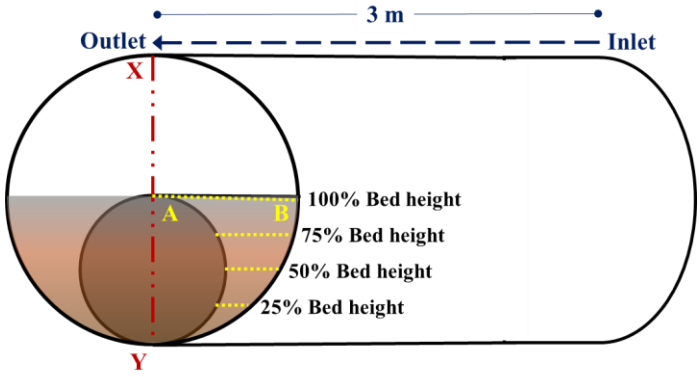


Fig. 7.1: Location within geometry used to obtain flow parameters

7.1 Velocity Profiles

Simulations were also conducted in the absence of solids bed (Fig. 7.2). The inner pipe was considered eccentric with very narrow clearance at the bottom (0.002 m) for this case and average velocity of 2 m/s was considered. This case was simulated as a pilot case to compare the local velocities of different fluids. It can be observed that low viscosity fluid such as Fluid 1 results in a significantly higher velocity in the narrow section. This allows for better erosion of solids from the bed.

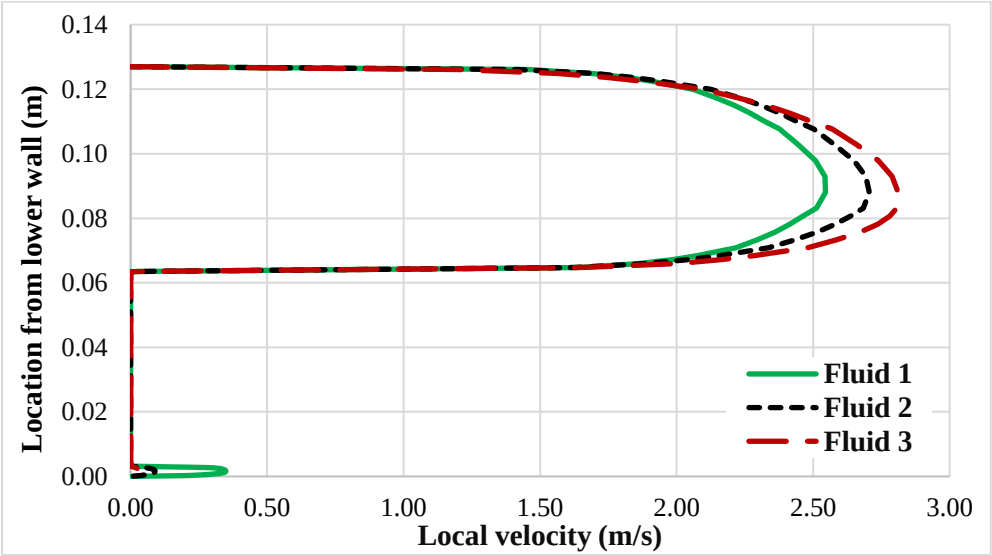


Fig. 7.2: Cross-sectional velocity profile in the absence of bed

A specific case of 50% bed height and flow rate of 5.05 L/s was considered to study the near-bed velocity profile (Fig. 7.3). In the near-wall region, low viscosity fluids (Fluid 1) exhibit greater local velocity as compared to highly viscous fluids. Consequently, the former generates relatively stronger hydrodynamic forces; thereby easily initiating rolling and lifting mechanism of particles. Once particles are lifted in the flow stream and enter the core flow region, thin fluids fail to maintain particle suspension and hence, cannot transport solid particles in the axial direction for an extended period. However, in the core of the flow, high viscosity fluids exhibit high velocity and have a better suspension capacity.

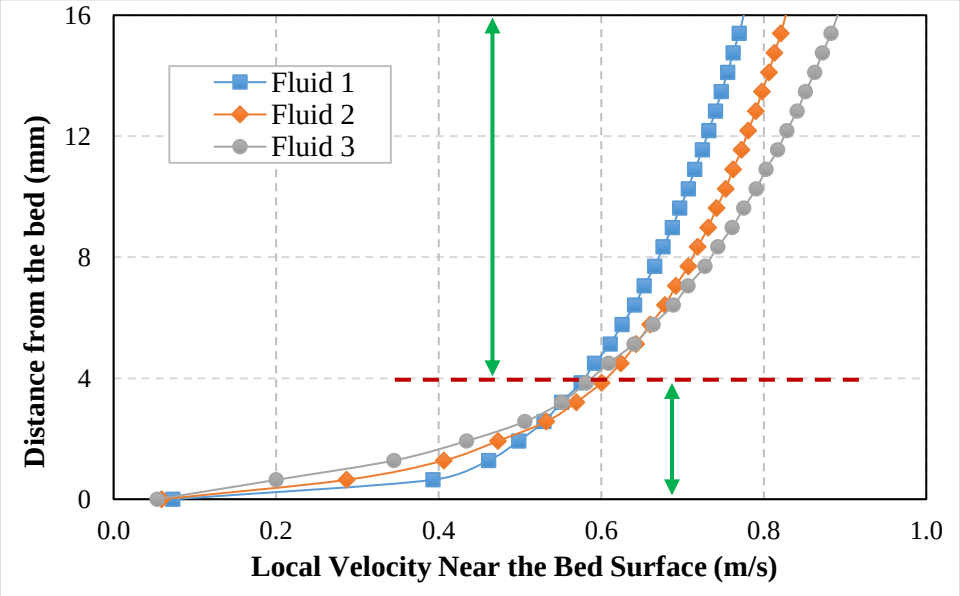


Fig. 7.3: CFD simulation of near-bed velocity profiles of different fluids at 5.05 L/s and 50% bed height (Pandya et al. 2019)

Fig. 7.4 presents velocity profiles of Fluid 1 at 5.05 L/s for various bed heights. 100% bed height, in this case, corresponds to half (50%) of the linear cross-sectional area. It can be observed that the increase in bed height or reduction in flow area increases the average flow velocity as well as maximum flow velocity. An in-built assumption of no-slip at bed and wall results in a thin stationary layer of fluid adjacent to the wall. With the reduction in bed height,

the maximum local flow velocity in core and average bulk velocity both decrease and hence, the rate of erosion also decreases. A similar trend can be observed for all fluids and at all flow rates as presented by velocity profile plots in Appendix B. An interesting observation made from these plots is that the peak of the velocity profile is slightly shifted towards the outer wall of the inner pipe. For typical pipe flow in absence of bed and inner pipe, this peak velocity is ideally located in the center.

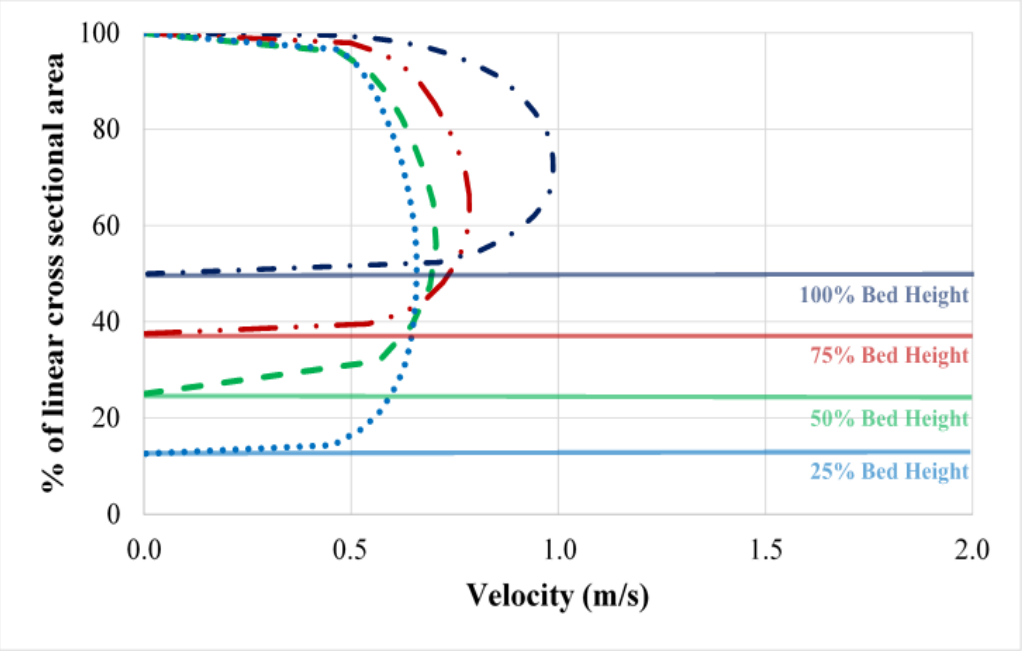


Fig. 7.4: Velocity profile for various bed heights using Fluid 1 at a flow rate of 5.05 L/s

Fig. 7.5 reiterates these conclusions through visual observations of velocity contour plots. The plots represented are for flow of Fluid 1 at increasing flow rates (from left to right) and with the reduction in bed height (from top to bottom). It can be observed that the velocity closest to the wall of outer and inner pipe as well as the bed interface is nearly zero in all cases, thereby satisfying the no-slip condition. With the reduction in bed height, the flow is more evenly distributed with a lesser difference in local velocities at core flux and narrower section. However,

lower bed heights generate a larger area of near-stagnant flow zones when compared to a case with greater bed height. Similar velocity contours for Fluids 2 and 3 are included in Appendix C.

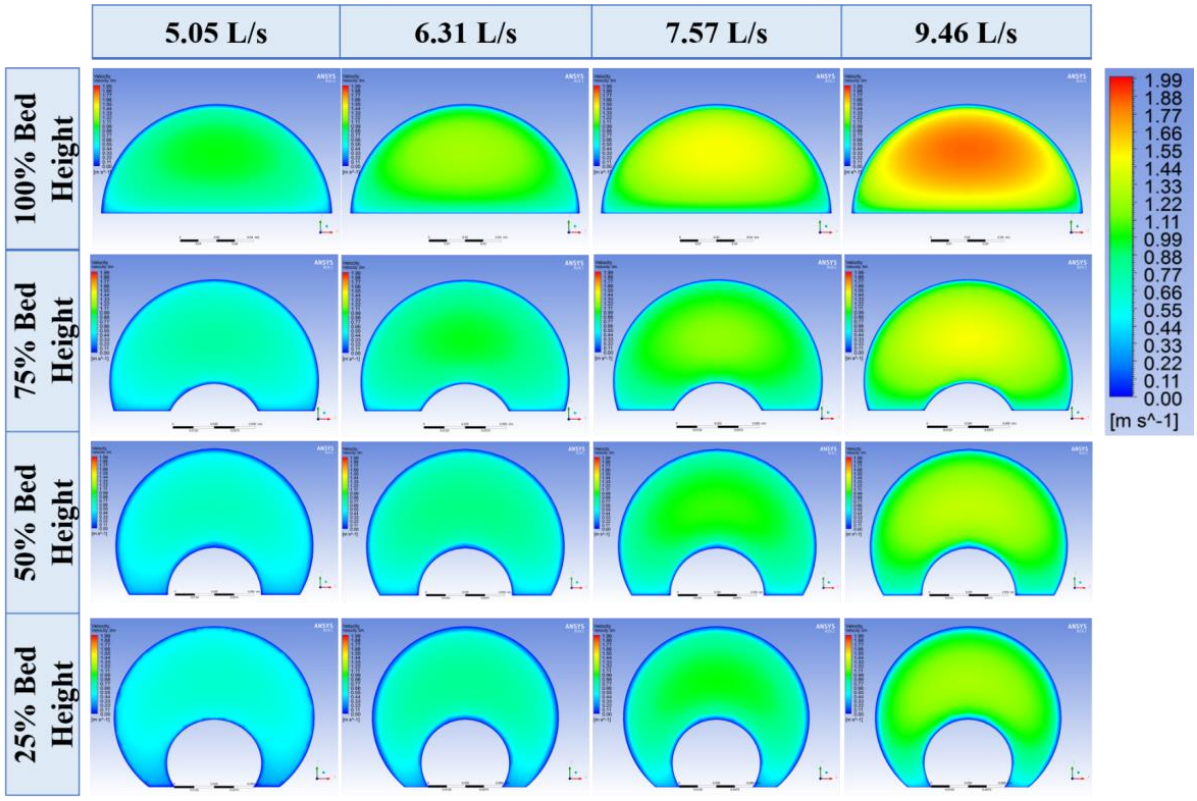


Fig. 7.5: Velocity contours for Fluid 1 varying flow velocity and bed height

Fig. 7.6 exhibits the trends in velocity profiles for change in bed height for different fluids. The viscosity of cleanout fluid increases from left to right (Fluid 1 being least viscous). At all bed heights, the local velocity of the core region increases with an increase in viscosity. On the contrary, increasing viscosity reduces the local velocity near the boundaries. Hence, viscous fluids are poor in eroding the bed but better at transporting the solids once particle the enters the core region. Similar plots for other flow rates are included in Appendix D.

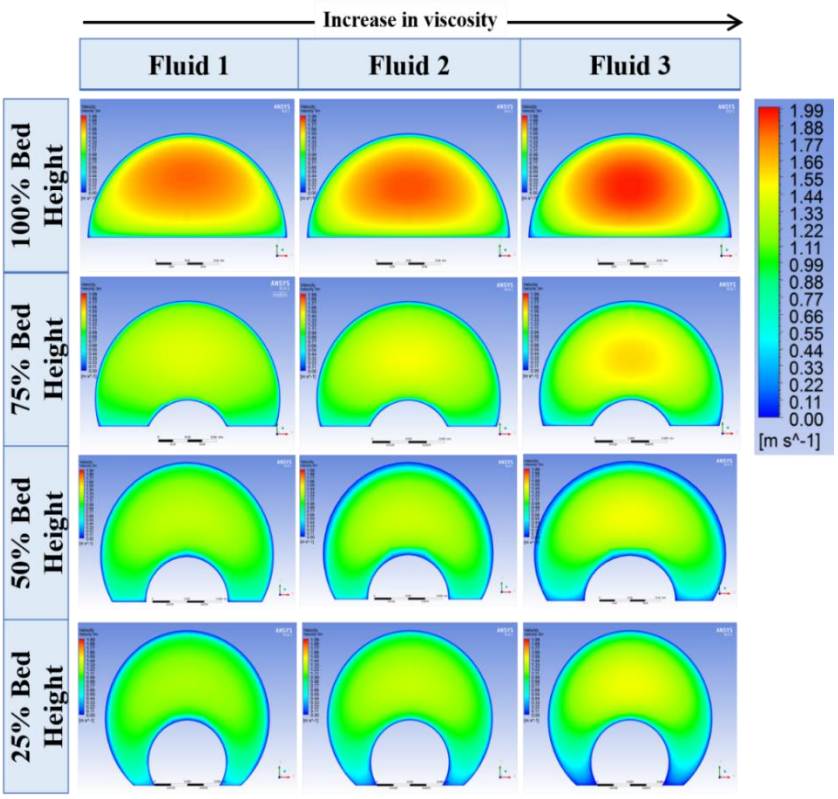


Fig. 7.6: Velocity contour plots for different fluids with various bed height at 9.46 L/s

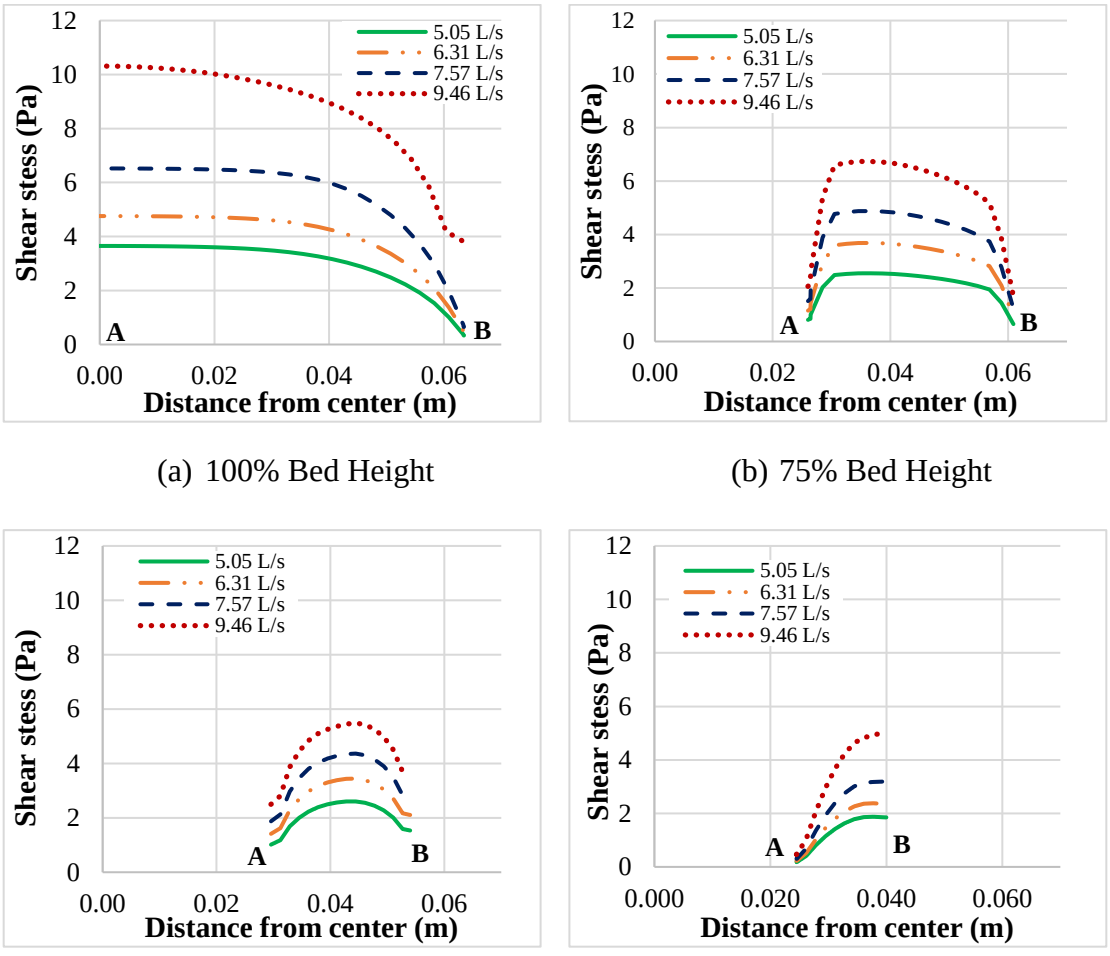
Overall, in an eccentric annulus with solids bed, the velocity profile can vary considerably as flow behavior can be significantly impacted by the shear rate distribution. A higher velocity region exists in the core region of the flow whereas stagnant zones can be developed in very narrow clearance regions. Therefore, local turbulent and local laminar flow regime can simultaneously exist in annular flows.

7.2 Shear Stress at Bed Interface

As mentioned earlier bed shear stress was also obtained along line AB for all bed heights as shown in Fig. 7.1. Erosion of bed is highly dependent on the bed shear stress acting on the bed. In eccentric annuli, bed shear stress distribution is not uniform due to the variation in the annular cross-sectional area. The presence of solids bed makes it more complex to predict the non-

uniformity of shear stress. However, the average shear stress acting on the solids bed can be predicted and used to study the erosion of solids.

Fig. 7.7 presents bed shear distribution (line AB in reference to Fig. 7.1) of Fluid 3 at different bed heights. For all cases, it is evident that increasing the flow velocity increases the overall bed shear. However, there exists a shift in the point of maximum bed shear from the outer wall of the inner pipe (point A) to the inner wall of the outer pipe (point B) with the reduction in bed height. This was observed for all fluids and at all flow rates. The plots pertaining to other cases are included in Appendix E.



(a) 100% Bed Height

(b) 75% Bed Height

(c) 50% Bed Height

(d) 25% Bed Height

Fig. 7.7: Bed shear stress profiles for Fluid 3 at various bed heights and flow rates

The area under the curve of each bed shear stress plot as represented in Fig. 7.7 was divided by the lateral length of the bed (distance from point A to point B) to obtain average bed shear ($\bar{\tau}_{bed}$) stress value.

$$\bar{\tau}_{bed} = \frac{Area\ under\ curve}{X_{AB}} \tag{7.1}$$

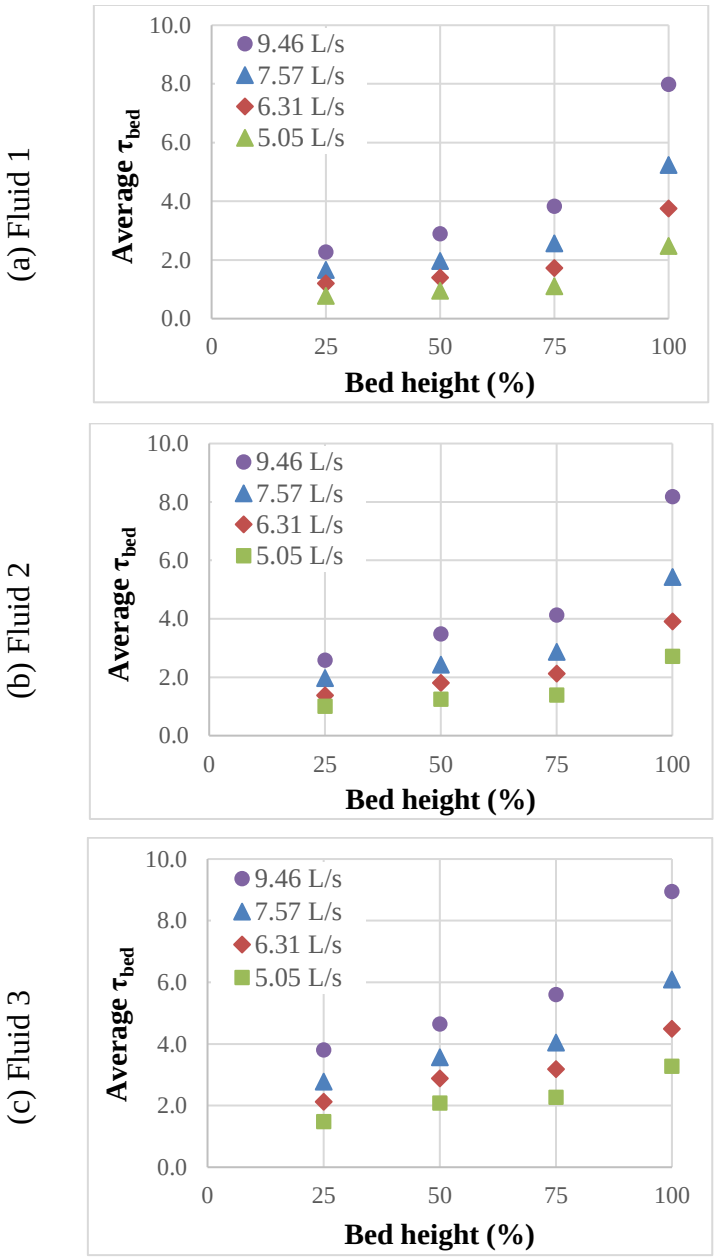


Fig. 7.8: Average bed shear exhibited by various fluids at different bed heights and mentioned flow rate.

The average bed shear plots are shown in Fig. 7.8. The plots describe the relationship between average bed shear stress, bed height and flow rate for the three distinct fluids investigated this study. It is observed that the decrease in average bed shear stress is extremely sharp with a reduction in bed height from 100% to 75% in all cases.

To further evaluate the contribution of bed shear stress on the bed erosion, reduction of bed height with time (transient process) was compared with variation of bed shear with time. The latter relationship was obtained through combined results of all steady-state CFD simulations. The transient nature of bed shear stress was developed by using bed height as a common variable between circulation time and bed shear. For instance, CFD data is initially obtained for bed shear stress at particular bed height. Experimental results are available for circulation time required to attain this bed height for a combination of flow rate and fluid type. Hence, the shear stress acting on the bed after this circulation time can be obtained by a combination of CFD and experimental results.

Fig. 7.9 presents the bed height and the corresponding bed shear stress a function of time. Data points and connecting lines in red represent the normalized bed height with time. Data points are shown for five distinct cases – 100%, 75%, 50%, 25% and final bed height, for which the CFD simulation results were obtained. The final bed height corresponds to the bed height obtained during experimental investigation. It should be noted that bed height was not reduced down to 25% for many cases. Bed shear stress is represented in a normalized form to compare all cases with similar initial conditions. It is observed that the reduction in shear stress at bed interface follows a similar transient behavior as that of reduction on normalized bed height. The bed

height and bed shear attain a steady-state condition for a few cases (high viscosity fluids and lower flow rates).

Increasing the fluid viscosity and/or reducing the flow rate tend to generate conditions that can lead to the development of near steady-state before 25% bed height. Near the steady-state bed, height is defined as the condition at which the rate of reduction of shear stress and bed height is negligible. While there exists a general dependency between bed shear stress and the rate of erosion, it is difficult to quantify this effect in terms of a correlation that can predict the rate of erosion as a function of other parameters including bed shear stress, and circulation time.

For the purpose of predicting pressure loss during erosion, the average bed shear is predicted at all other bed heights ranging from 100 % to 0 % (approximately). In order to do this, the available data of average bed shear is used to develop a modified version of an existing model (Kozicki et al., 1966). The model is developed based on a correlation derived from Haggen-Poiseuille equation that could be used to predict pressure loss in an arbitrarily shaped duct. The model uses two geometric parameters, a and b, to account for the shape factor of an arbitrary cross-section of the duct.

Fanning friction factor (f) is a dimensionless parameter widely used in continuum fluid flow and is defined as the ratio of shear stress ($\bar{\tau}_{bed}$) and flow kinetic energy density ($\rho U^2/2$). By this definition, the bed shear can be expressed as,

$$\bar{\tau}_{bed} = f\frac{\rho U^2}{2} \tag{7.2}$$

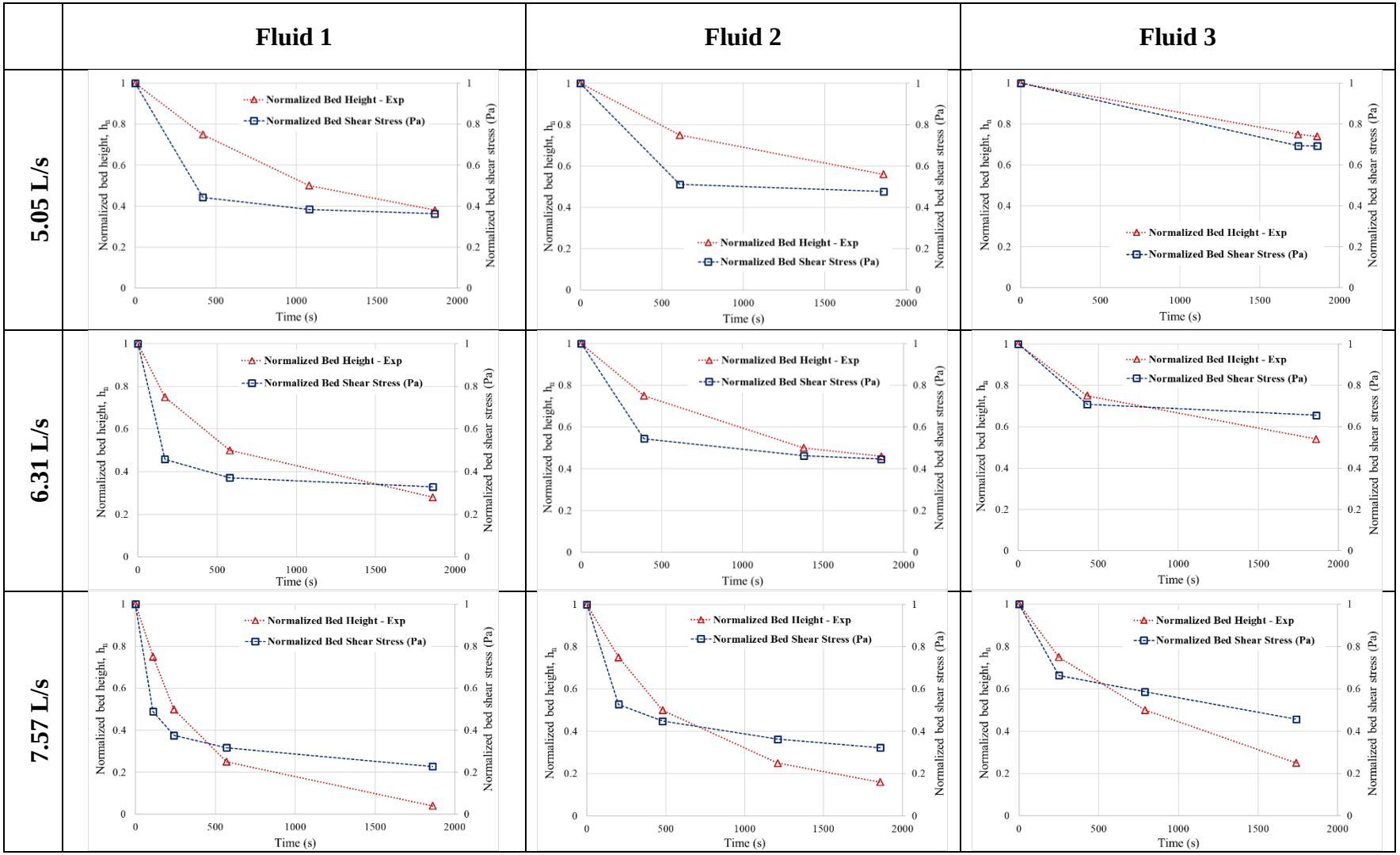


Fig. 7.9: Rate of normalized bed height & normalized bed shear.

Fanning friction factor correlation used to predict shear stress in turbulent flow at different bed height considers flow over the rough wall (roughness equivalent to grain size) and power-law fluid model incorporated into it. This relationship was derived by Reed and Pilehvari (1993) and is a combined model using Dodge-Metzner (1959) equation and Colebrook (1937) equation.

$$\frac{1}{\sqrt{f}} = -4\log_{10}\left\{\frac{0.27\epsilon}{D_h} + \frac{1.26^{(n)^{-1.2}}}{[Re.f^{1-0.5n}]^{n^{-0.75}}}\right\} \tag{7.3}$$

Eq.7.3 is only valid for uniform shape and cannot be directly used to calculate bed shear in the partially blocked annulus. Kozicki et al. (1966) included additional term with shape factors a corrective term.

$$\frac{1}{\sqrt{f}} = -4\log_{10}\left\{\frac{0.27\epsilon}{D_h} + \frac{1.26^{(n)^{-1.2}}}{\left[Re.f^{1-0.5n}.\left(\frac{4(a+bn)}{1+3n}\right)^{n}\right]^{n^{-0.75}}}\right\} \tag{7.4}$$

Roughness factor (ϵ) indicates the value of average roughness over bed and walls that the flow is exposed to. It can be calculated using the following relationship where S_i and S_h are bed perimeter and total wetted perimeter in reference to Fig. 5.1 and Eq. 5.4/5.5.

$$\epsilon = \frac{[\epsilon_{bed}S_i + \epsilon_{wall}(S_h - S_i)]}{S_h} \tag{7.5}$$

For the scope of this study, the wall roughness (ϵ_{wall}), that is the roughness of inner and outer pipe was omitted as the pipes were considered smooth. Therefore,

$$\epsilon = \frac{\epsilon_{bed}S_i}{S_h} = (6 * 10^{-4})\left(\frac{S_i}{S_h}\right) \tag{7.6}$$

Aworunse (2012) proposed a numerical model for shape factors a and b based on curvilinear coordinate transformation and expressed as a function of diameter ratio of pipes, eccentricity,

bed height and flow behavior index. The model was derived using a methodology suggested by Ahmed et al. (2006). The shape factors suggested by Aworunse (2012) were only applicable for 80% eccentric annuli. Rojas et al. (2017) extended this model using regression analysis to predict shape factors for partially blocked annular at various bed height as a function of normalized bed height and diameter ratio. The dimensionless shape factor parameters are correlated to bed height as,

$a = \alpha_1 h_n^3 + \alpha_2 h_n^2 + \alpha_3 h_n + \alpha_4$ and,

$$b = \beta_1 h_n^3 + \beta_2 h_n^2 + \beta_3 h_n + \beta_4 \tag{7.7}$$

where α_x and β_x are a function of diameter ratio (κ) as listed in Table 7.2. The diameter ratio is defined as,

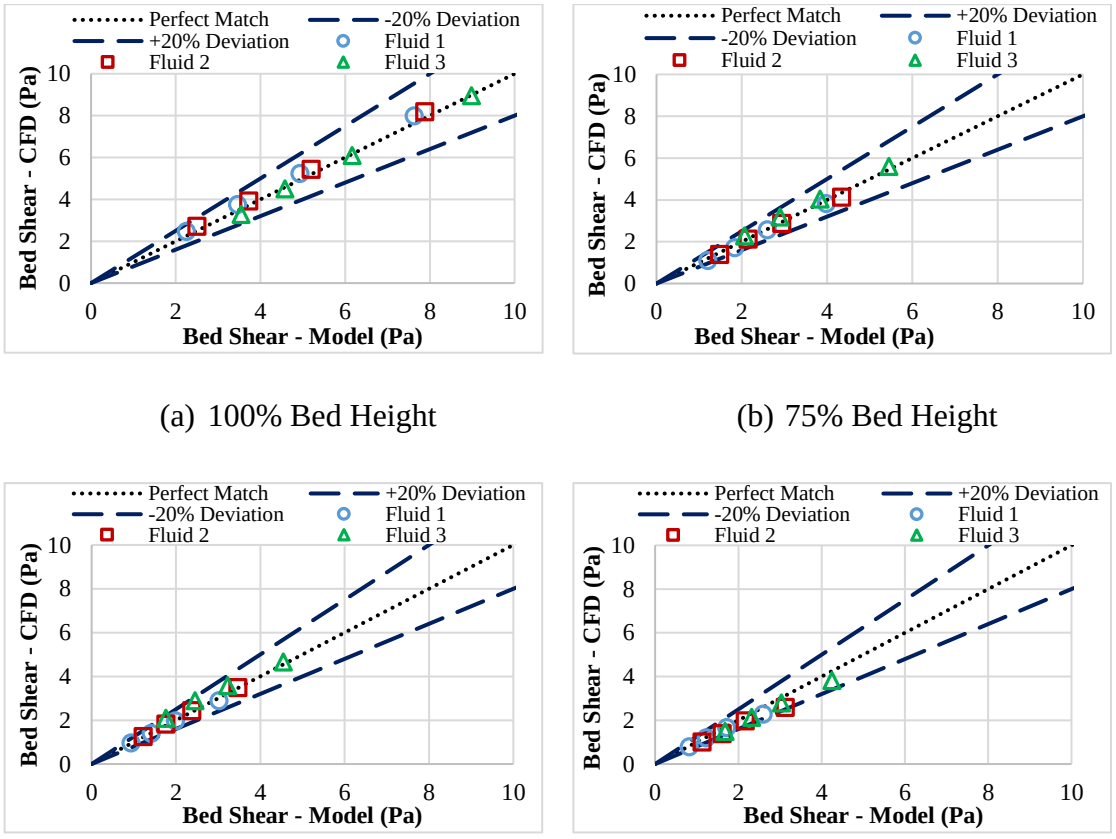
$$\kappa = \frac{d_i}{d_o} \tag{7.8}$$

Table 7.2: Correlations for regression coefficients α_x and β_x.

$\alpha_1 = -6.233\kappa^2 + 4.200\kappa - 0.845$	$\beta_1 = -0.964\kappa^2 + 5.425\kappa - 1.322$
$\alpha_2 = 9.152\kappa^2 - 6.780\kappa + 1.110$	$\beta_2 = 0.179\kappa^2 - 8.176\kappa + 2.088$
$\alpha_3 = -3.236\kappa^2 + 2.778\kappa - 0.088$	$\beta_3 = 0.836\kappa^2 + 3.412\kappa - 0.932$
$\alpha_4 = 0.284\kappa^2 - 0.427\kappa + 0.067$	$\beta_4 = 0.246\kappa^2 - 0.293\kappa + 0.876$

This correlation is able to accurately predict the bed shear and the maximum absolute error between values predicted by the model and that obtained by CFD software was 20% with an

average absolute error of 4.6%. Cross plots between these values for all bed heights simulated are presented in Fig. 7.10.



(a) 100% Bed Height

(b) 75% Bed Height

(c) 50% Bed Height

(d) 25% Bed Height

Fig. 7.10: Cross-plots between CFD bed shear and Kozicki's model

CHAPTER 8

CONCLUSIONS AND RECOMMENDATIONS

Several conclusions are derived from the experimental and computational modeling techniques during this study. Solids bed erosion tests were carried out using three cleanout fluids and varying flow rate, inclinations, and solids density. A dimensionless relationship is developed to allow the upscaling of the experimental results. A number of recommendations have been proposed for future research in hole cleanout. These conclusions and recommendations have been outlined in this chapter.

8.1 Conclusions

1. Hole cleanout is strongly impacted by fluid rheology. High viscosity fluids are more effective cleanout media for solids transport than low viscosity fluids in vertical and near-vertical inclination. However, high viscosity fluids are ineffective in horizontal and highly inclination configurations. This is attributed to the development of a thin hydrodynamic boundary layer at the bed interface that aids the lifting of the bed particles with low-viscosity fluid.

2. The mode of solids transport is substantially diverse at different well inclinations. Saltation and particle rolling governs the particle transport mechanism in highly inclined well sections.

3. A critical inclination angle exists in the wellbore trajectory at which various cleanout fluids exhibit similar efficiency. The critical inclination exists between 62° and 67° in the case of high-density proppant and between 69° and 71° for low-density proppant.

4. Overall, the density of solids has a moderate impact on the efficiency of hole-cleaning (maximum of 30% reduction in bed height due to the difference in density of solids). The lower density of solids results in a more efficient wellbore cleanout at a constant flow rate, especially in higher inclinations. Data obtained suggest that the implication of proppant density is very negligible at lower flow velocities (< 0.43 m/s).

5. A dimensionless relationship was obtained to upscale the lab-scale model and to predict the efficiency of bed erosion process for various circumstances. The model was validated with data obtained in other studies with good accuracy.

8.2 Recommendations

1. A quantitative analysis of dunes and ripple formation should be undertaken to understand particle dynamics within different fluid flow regimes.

2. Bed erosion process in the turbulent flow should be studied using Particle Imaging Velocimetry (PIV) technique to analyze the trajectory of solids particle.

3. A relationship between bed height and other influencing factors, including bed shear stress should be obtained using data from different CFD simulations in order to increase the predictability as well as the use of the model in field scenarios.

4. A discrete phase modeling technique should be utilized to study solids bed movement in turbulent and laminar flow during hole cleaning process at various inclinations using CFD techniques.

NOMENCLATURE

A	–	cross-sectional area of the flow domain.
A_a	–	maximum cross-sectional area for flow.
A_H	–	Hamaker constant.
A_p	–	the projected area of the particle over a mean bed surface.
a	–	circumferential reading from the top of the pipe.
a_p	–	the instantaneous acceleration experienced by the solids particle.
b	–	circumferential reading from the bottom of the pipe.
c	–	average volumetric solid's concentration.
C_D	–	drag coefficient.
C_L	–	lift coefficient.
D_b	–	the diameter of viscometer bob.
D_c	–	diameter of viscometer cup.
dA	–	differential area.
d_h/D_h	–	hydraulic diameter.
d_s	–	the diameter of the solid particle.
e	–	distance between centers of the inner pipe and outer pipe.
E_r	–	rate of solids erosion.
f	–	fanning friction factor.
$F_{buoyant}$	–	force due to buoyancy.
F_{drag}	–	drag force.
$F_{gravity}$	–	force due to gravity.

F_{lift} – lift force.

F_{van} – Van der Waals force / plastic force.

$F_{\Delta P}$ – force due to the pressure gradient in the flow.

g – acceleration due to gravity.

h_n – normalized bed height.

$h(t)$ – transient bed height.

h_i – initial bed height.

I – turbulence intensity.

K – fluid consistency index.

K_v – viscometer-based fluid consistency index.

k – turbulent kinetic energy.

l – lateral length.

L_e – entrance length.

m – the mass of the solid particle.

m_{30} – the dry weight of solids removed after 30 mins of erosion test.

m_{flush} – the dry weight of solids removed after flushing of test section.

n – flow behavior index.

P_e – pressure gradient in eccentric profile.

P_c – pressure gradient in concentric profile.

Re – Reynolds number.

S – wetted perimeter.

S_a – circumference of the outer pipe.

S_b – circumference of inner pipe.

r – radial distance.

r_o – radius of outer pipe.

r_i – radius of inner pipe.

s – distance between surface of two spherically shaped particles.

t – time / circulation time.

u – local fluid velocity.

u^* – frictional velocity.

u' – velocity fluctuations (in axial direction).

u_δ – velocity at interface of sublayer and buffer layer.

$\langle u \rangle$ – mean velocity.

u_{lift} – minimum velocity required for lifting of particle.

u_{roll} – minimum velocity required for rolling of particle.

U – average or bulk velocity of fluid.

U_{max} – maximum velocity.

v – particle settling velocity.

v' – velocity fluctuation in direction normal to flow.

V_s – volume of particle.

GREEK LETTERS

β	–	viscometer bob to cup ratio / central angle with respect to inner pipe.
Γ_{rolling}	–	torque required to initiate rolling motion.
$\delta_{sublayer}$	–	thickness of viscous sublayer.
ϵ	–	turbulent dissipation rate / roughness height.
ϵ_{wall}	–	wall roughness.
ϵ_{bed}	–	bed roughness.
ε	–	eccentricity, %.
ε_t	–	entrainment function .
θ	–	angle of inclination.
μ	–	dynamic viscosity of fluid.
μ_a	–	apparent viscosity.
μ_t	–	eddy viscosity of fluid.
Π	–	dimensionless parameter.
ρ_f	–	absolute density of fluid.
ρ_s	–	absolute density of solids particle.
τ_{bed}	–	shear stress at bed interface.

τ_{lam} – laminar shear stress.

τ_{total} – total shear stress.

τ_{turb} – turbulent shear stress.

τ_w – wall shear stress.

ϕ – complementary angle to bed's angle of repose.

ϕ' – central bed angle.

ϕ_p – bed porosity.

ABBREVIATIONS

CDV	–	Critical Deposition Velocity
CFD	–	Computational Fluid Dynamics
CFR	–	Critical Flow Rate
CRV	–	Critical Re-suspension Velocity
CT	–	Coiled Tubing
CTV	–	Critical Transport Velocity
DNS	–	Direct Numerical Simulation
ECD	–	Equivalent Circulating Density
HDP	–	High-Density Proppant
HEC	–	Hydroxy-Ethyl-Cellulose
ID	–	Inner Diameter
LDP	–	Low-Density Proppant
LES	–	Large Eddy Simulation
LSRV	–	Low Shear Rate Viscosity
MTV	–	Minimum Transport Velocity
NS	–	Navier-Stokes
OBM	–	Oil Based Mud

OD	–	Outer Diameter
PL	–	Power Law
RANS	–	Reynolds Averaged Navier-Stokes
ROP	–	Rate Of Penetration
RPM	–	Rotations/Revolutions Per Minute
SG	–	Specific Gravity
SIMPLE	–	Semi-Implicit Pressure Linked Equations
VFD	–	Variable Frequency Drive
WBM	–	Water Based Mud
WOB	–	Weight On Bit
YPL	–	Yield Power Law

REFERENCES

Adari, R. B. Development of Correlations Relating Bed Erosion to Flowing Time for Near Horizontal Wells. MSc. Thesis. The University of Tulsa. 1999.

Adari, R. B., Miska, S., Kuru, E., Bern, P., & Saasen, A. Selecting Drilling Fluid Properties and Flow Rates For Effective Hole Cleaning in High-Angle and Horizontal Wells. SPE-63050-MS. 2000.

Ahmed, R., Saasen, A., & Skalle, P. Application of the Minimum Transport Velocity Model for Drag-Reducing Polymers. Journal of Petroleum Science and Engineering, 44(3-4), 303-316. 2004.

Ahmed, R., Skalle, P., Johansen, S.T., Svein, J., Saasen A., Mechanistic Model for Cuttings Removal from Solid Bed in Inclined Channels, Journal of Petroleum Science and Engineering, Volume 30, Issues 3–4, pp. 129-141. 2001.

Akrong, J.A. Effect of Pipe Eccentricity on Hole Cleaning and Wellbore Hydraulics. MSc. Thesis, African University of Science and Technology. 2010.

ANSYS® Meshing User's Guide, Release 15.0, Help System, ANSYS, Inc., pg 137, 2013.

Arnipally, S.K., Hirpa, M.M., Bizhani, M., Kuru, E. Effect of Particle Size on the Near Wall Turbulence Characteristics and the Critical Velocity Required for the Particle Removal from the Sand Bed Deposited in Horizontal pipelines. BHR Group Multiphase pp. 443-458. 2018.

Aworunse, O.A. Modeling of Power-Law Fluid Flow in Annulus with Cutting Bed Buildup. MS Thesis, the University of Oklahoma, Norman, OK. 2012.

Azar, J. J. and Sanchez, R. A. Important Issues in Cuttings Transport for Drilling Directional Wells. Latin American and Caribbean Petroleum Engineering Conference and Exhibition, Rio de Janeiro, SPE-39020-MS, 1997.

Bagchi, P., & Balachandar, S. Effect of Turbulence on the Drag and Lift of a Particle. Physics of Fluids. 2003.

Bagnold, R. A. Experiments on a Gravity-Free Dispersion of Large Solid Spheres in a Newtonian Fluid under Shear. Proceedings of the Royal Society A: Mathematical, Physical and Engineering Sciences. 1954.

Becker, T. E., & Azar, J. J. Mud-Weight and Hole-Geometry Effects on Cuttings Transport While Drilling Directionally. SPE-14711-MS. 1985.

Bern, P. A., Hosie, D., Bansal, R. K., Stewart, D., & Bradley, L. A New Downhole Tool for ECD Reduction. SPE-81642-MS. 2003.

Best, J., Bennett, S., Bridge, J., & Leeder, M. Turbulence Modulation and Particle Velocities Over Flat Sand Beds at Low Transport Rates. Journal of Hydraulic Engineering, 123(12), 1118-1129. 1997.

Bicalho, I. C., dos Santos, D.B.L., Ataíde, C.H., Duarte, C.R., Fluid-Dynamic Behavior of Flow in Partially Obstructed Concentric and Eccentric Annuli with Orbital Motion, Journal of Petroleum Science and Engineering, Volume 137, pp. 202-213. 2016.

Bilgesu, H. I., Ali, M. W., Aminian, K., & Ameri, S. Computational Fluid Dynamics (CFD) as a Tool to Study Cutting Transport in Wellbores. SPE-78716-MS. 2002.

Bizhani M, Kuru E. Effect of Sand Bed Deposits on the Characteristics of Turbulent Flow of Water in Horizontal Annuli. ASME. J. Fluids Eng. 141(5):051102-051102-14. 2018.Boycott, A.E. 1920. Sedimentation of Blood Corpuscles. Nature, January 22.

Brown, N. P., Bern, P. A., & Weaver, A. Cleaning Deviated Holes: New Experimental and Theoretical Studies. SPE-18636-MS, 1989.

Buckingham, E. On Physically Similar Systems; Illustrations of the Use of Dimensional Equations. Physical Review. 4 (4): pp. 345–376. 1914.

Cano, V., Cardona, W. G., Murphy, C., & de Araujo, M. Improved CT Well Cleanout and Milling Procedures Utilizing Only Non-Viscous Cleanout Fluids. SPE-179070-MS. 2016.

Capecelatro, J., Desjardins, O. Eulerian-Langrangian Modeling of Turbulent Liquid-Solid Slurries in Horizontal Pipes. International Journal of Multiphase Flow 55 pp. 64-79, 2013.

Carbonneau, P. E., Bergeron, N. E., The Effect of Bedload Transport on Mean and Turbulent Flow Properties, Geomorphology, Volume 35, Issues 3–4, pp. 267-278. 2000.

Clark, R. K., & Bickham, K. L. A Mechanistic Model for Cuttings Transport. SPE-28306-MS. 1994.

Colebrook, C.F., White C.M. Experiments with Fluid Friction in Roughened Pipes. Proc. Roy. Soc. Ser. A Math. Phys. Sci. 161(906), 367-381. 1937.

Csuka, Z., Olšiak, R. The Profile of Shear Stress in the Liquid at Turbulent Flow. AIP Conference Proceedings 1768, 020032. 2016.

Diplas, P., Dancey, C., Celik, A., Valyrakis, M., Greer, K., & Akar, T. The Role of Impulse on the Initiation of Particle Movement under Turbulent Flow Conditions. Science, 322(5902), pp. 717-720. 2008.

Dodge, D. W. and Metzner, A. B. Turbulent Flow of Non-Newtonian Systems. AIChE J., 5: 189-204. 1959.

Doron, P., & Barnea, D. Flow Pattern Maps for Solid-Liquid Flow in Pipes. International Journal of Multiphase Flow, 22(2), 273–283. 1996.

Duan, M., Miska, S. Z., Yu, M., Takach, N. E., Ahmed, R. M., & Zettner, C. M. Transport of Small Cuttings in Extended-Reach Drilling. SPE-104192-PA. 2008.

Duan, M., Miska, S. Z., Yu, M., Takach, N. E., Ahmed, R. M., & Zettner, C. M. Critical Conditions for Effective Sand-Sized Solids Transport in Horizontal and High-Angle Wells. SPE-106707-PA. 2009.

Einstein, A., & Fürth, R. Investigations on the theory of Brownian movement. New York, N.Y: Dover Publications. 1906.

Engelund, F. Transport of Bed Load at High Shear Stress. Institute of Hydrodynamics and Hydraulic Engineering, ISVA, Technical University Denmark, Lyngby, Progress Rep. 53, 1981.

Engineering ToolBox, (2010). Lift and Drag. [online] Available at: https://www.engineeringtoolbox.com/lift-drag-fluid-flow-d_1657.html [Accessed August 2nd 2019].

Escudier, M.P., Oliveira, P.J., Pinho, F.T., & Smith, S.R. Fully Developed Laminar Flow of Non-Newtonian Liquids Through Annuli: Comparison of Numerical Calculations with Experiments. Experiments in Fluids, 33, 101-111. 2002.

Espinosa-Paredes, G., & Cazarez-Candia, G. Two-Region Average Model for Cuttings Transport in Horizontal Wellbores I: Transport Equations, Petroleum Science and Technology, 29:13, 1366-1376. 2011.

Farber, S. Pressure Loss Modeling of Non-Symmetric gas Turbine Exhaust Ducts using CFD. MSc Thesis, Concordia University, Montreal, Quebec, Canada. 2008

Ford, J. T., Peden, J. M., Oyeneyin, M. B., Gao, E., & Zarrough, R. Experimental Investigation of Drilled Cuttings Transport in Inclined Boreholes. SPE-20421-MS. 1990.

Ford, J. T., Goo, E., Oyeneyin, M. B., Peden, J. M., Larrucia, M. B., & Parker, D. A New MTV Computer Package for Hole-Cleaning Design and Analysis. SPE-26217-PA. 1996.

Gavignet, A. A., & Sobey, I. J. Model Aids Cuttings Transport Prediction. SPE-15417-PA. 1989.

Gavrilov, A.A., Rudyak, V.Y. Reynolds-Averaged Modeling of Turbulent Flows of power-Law Fluids. Journal of Non-Newtonian Fluid Mechanics 227 pp. 45-55, 2016.

Gnambode, P.S., Orlandi, P., Rouiss, M.O., Nicolas, X. Large-Eddy Simulation of Turbulent Pipe Flow of Power-Law Fluids. International Journal of Heat and Fluid Flow 54 pp. 196-210, 2015.

Gopaliya, M.K., Kaushal, D.R. Modeling of Sand-Water Slurry Flow Through Horizontal Pipe Using CFD. J. Hydrol. Hydromech. 64, 3, pp. 261-272, 2016.

Gore, R.A., Crowe, C.T., Effect of Particle Size on Modulating Turbulent Intensity, International Journal of Multiphase Flow, Volume 15, Issue 2, pp. 279-285. 1989.

Guo, X., Wang, Z., Long, Z. Study on Three-Layer Unsteady Model of Cuttings Transport for Extended-Reach Well, Journal of Petroleum Science and Engineering, Volume 73, Issues 1–2, pp. 171-180. 2010.

Hartnett, J.P., Kostic, M. Turbulent Friction Factor Correlations for Power Law Fluids in Circular and Non-Circular Channels. Int. Comm. Heat Mass Transfer. Vol. 17, pp. 59-65, 1990.

Heydari, O., Sahraei, E., Skalle, P. Investigating the Impact of Drillpipe's Rotation and Eccentricity on Cuttings Transport Phenomenon in Various Horizontal Annuluses Using

Computational Fluid Dynamics (CFD). Journal of Petroleum Science and Engineering 156, pp. 801-813, 2017.

Heyman, J., Mettra, F., Ma, H. B., and Ancey, C. Statistics of Bedload Transport Over Steep Slopes: Separation of Time Scales and Collective Motion, Geophys. Res. Lett. 40, pp. 128– 133, 2013.

Hughes, W. F., & Brighton, J. A. Schaum's outline of theory and problems of fluid dynamics. New York: McGraw Hill. 1999.

Iyoho, W., Schlumberger, D., Azar, J. J. Transport in Directional Wells. The University of Tulsa. 1986.

Jain, S., Singhal, N., & Shah, S. N. Effect of Coiled Tubing Curvature on Friction Pressure Loss of Newtonian and Non-Newtonian Fluids - Experimental and Simulation Study. SPE-90558-MS. 2004.

Jalukar, L. S. A Study of Hole Size Effect on Critical and Subcritical Drilling Fluid Velocities in Cuttings Transport for Inclined Wellbores. MSc. Thesis, The University of Tulsa. 1993.

Kelessidis, V. C., & Mpandelis, G. E. Flow Patterns and Minimum Suspension Velocity for Efficient Cuttings Transport in Horizontal and Deviated Wells in Coiled-Tubing Drilling. SPE-81746-MS. 2004

Kelessidis, V. C., & Bandelis, G. E. (2004, December 1). Flow Patterns and Minimum Suspension Velocity for Efficient Cuttings Transport in Horizontal and Deviated Wells in Coiled-Tubing Drilling. Society of Petroleum Engineers. doi:10.2118/81746-PA

King, I., Trenty, L., & Vit, C. How the 3D Modeling Could Help Hole-Cleaning Optimization. SPE-63276-MS. 2000.

Kozicki, W., Chou C. H., Tiu C. Non-Newtonian Flow in Ducts of Arbitrary Cross-Sectional Shape, Chemical Engineering Science, Vol. 21–8, pp. 665-679, 1966.

Kudela, H. Turbulent flow. 2010 - http://www.itcmp.pwr.wroc.pl/~znmp/dydaktyka/fundam_FM/Lecture_no3_Turbulent_flow_Modelling.pdf

Larsen, T. I. A Study of the Critical Fluid Velocity in Cuttings Transport for Inclined Wellbores. MSc. Thesis. The University of Tulsa. 1990.

Larsen, T. I., Pilehvari, A. A., & Azar, J. J. Development of a New Cuttings-Transport Model for High-Angle Wellbores Including Horizontal Wells. SPE-25872-PA. 1997.

Li, J., & Luft, B. Overview of Solids Transport Studies and Applications in Oil and Gas Industry - Experimental Work. SPE-171285-MS. 2014.

Li, J., & Walker, S. Sensitivity Analysis of Hole Cleaning Parameters in Directional Wells. SPE/ICoTA Coiled Tubing Roundtable. SPE-54498-MS.1999.

Li, J., & Wilde, G. Effect of Particle Density and Size on Solids Transport and Hole Cleaning With Coiled Tubing. Proceedings of SPE/ICoTA Coiled Tubing Conference and Exhibition, 1–9. SPE-94187-MS. 2005.

Luo, Y., & Peden, J. M. Flow of Drilling Fluids Through Eccentric Annuli. In Proceedings - SPE ATCE (Vol. Delta, pp. 389-396). 1987.

Martins, A. L., & Santana, C. C. Evaluation of Cuttings Transport in Horizontal and Near Horizontal Wells – A Dimensionless Approach. SPE-23643-MS, 1992.

Masuda, Y., Doan, Q., Oguztoreli, M., Naganawa, S., Yonezawa, T., Kbayashi, A., & Kamp, A. Critical Cuttings Transport Velocity in Inclined Annulus: Experimental Studies and Numerical Simulation. SPE-65502-MS. 2010.

Meyer-Peter, E. and Müller, R. Formulas for Bed Load Transport. Proceedings of 2nd Meeting, IAHSR, Stockholm, pp. 39-64, 1948.

Naganawa, S., & Nomura, T. Simulating Transient Behavior of Cuttings Transport over Whole Trajectory of Extended Reach Well. SPE-103923-MS. 2006.

Nazari, T., Hareland, G., & Azar, J. J. Review of Cuttings Transport in Directional Well Drilling: Systematic Approach. SPE-132372-MS, 2010.

Nouri JM, Whitelaw JH. Flow of Newtonian and Non-Newtonian Fluids in a Concentric Annulus With Rotation of the Inner Cylinder. ASME. J. Fluids Eng.116(4):821-827. 1994.

Okrajni, S., & Azar, J. J. The Effects of Mud Rheology on Annular Hole Cleaning in Directional Wells. SPE-14178-PA. 1986.

Ozbayoglu, M. E., Miska, S. Z., Reed, T., & Takach, N. Analysis of the Effects of Major Drilling Parameters on Cuttings Transport Efficiency for High-Angle Wells in Coiled Tubing Drilling Operations. SPE-89334-MS. 2004.

Ozbayoglu, M. E., Saasen, A., Sorgun, M., & Svanes, K. Effect of Pipe Rotation on Hole Cleaning for Water-Based Drilling Fluids in Horizontal and Deviated Wells. SPE-114965-MS. 2008.

Pandya, S., Ahmed, R., Shah, S., Experimental Study on Wellbore Cleanout in Horizontal Wells, Journal of Petroleum Science and Engineering, Volume 177, Pages 466-478, 2019.

Pandya, S. Experimental Study of Proppant Transport in Horizontal and Directional Wells. MSc Thesis, University of Oklahoma. 2016.

Pandya, S., Goyal, S., & Pandey, Y. Optimizing the Fracturing Treatments by Intersecting Production Data and Fracture Diagnostics. SPE-178101-MS. 2015.

Pandya, S., Ahmed, R., & Shah, S. Effects of Particle Density on Hole Cleanout Operation in Horizontal and Inclined Wellbores. SPE-194240-MS. 2019.

Pandya, S., Ahmed, R., & Shah, S. Wellbore Cleanout in Inclined and Horizontal Wellbores – The Effects of Flow Rate, Fluid Rheology, and Solids Density. SPE-194240-PA. 2019.

Pereira, F. A. R., Barrozo, M. A. S., & Ataíde, C. H. CFD Predictions of Drilling Fluid Velocity and Pressure Profiles in Laminar Helical Flow. Brazilian Journal of Chemical Engineering, 24(4), 587-595. 2007.

Pratap Singh, A., & Samuel, R. Effect of Eccentricity and Rotation on Annular Frictional Pressure Losses With Standoff Devices. SPE-124190-MS. 2009.

Reed, T. D., & Pilehvari, A. A. A New Model for Laminar, Transitional, and Turbulent Flow of Drilling Muds. SPE-25456-MS. 1993.

Roache, P. J., Verification and Validation in Computational Science and Engineering. SIAM Review 44(1): pp. 162-163. 1998.

Rojas, S., Ahmed, R., Elgaddafi, R., George, M., Flow of Power-Law Fluid in a Partially Blocked Eccentric Annulus, Journal of Petroleum Science and Engineering, Volume 157, pp. 617-630. 2017.

Rolovic, R., Weng, X., Hill, S., Robinson, G., Zemlak, K., & Najafov, J. An Integrated System Approach to Wellbore Cleanouts with Coiled Tubing. SPE-89333-MS, 2004.

Salem, S. K. E., & El-Din, M. A. N. Drillpipe Eccentricity Prediction During Drilling Directional Wells. Petroleum Society of Canada. 2006.

Sanchez, R. A., Azar, J. J., Bassal, A. A., & Martins, A. L. Effect of Drillpipe Rotation on Hole Cleaning During Directional-Well Drilling. SPE-56406-PA. 1999.

Santana, M., Martins, A. L., & Sales, A. Advances in the Modeling of the Stratified Flow of Drilled Cuttings in High Horizontal Wells. SPE-39890-MS. 1998.

Sayindla, S., Lund, B., Ytrehus, J. D., Saasen, A., Hole-Cleaning Performance Comparison of Oil-Based and Water-Based Drilling Fluids, Journal of Petroleum Science and Engineering, Vol. 159 pp. 49-57, 2017.

Shah, S., Patel, H., Pandya, S. Motion of Fracturing Fluid and Associated Environmental Impact. 2015.

Sifferman, T. R., & Becker, T. E. Hole Cleaning in Full-Scale Inclined Wellbores. SPE-20422-PA. 1992.

Singhal, N., Shah, S. N., & Jain, S. Friction Pressure Correlations for Newtonian and Non-Newtonian Fluids in Concentric Annuli. SPE-94280-MS. 2005.

Szilas, A.P. Production and Transport of Oil and Gas, Part A: Flow Mechanics and Production. United States. 1985.

Tang, M., Ahmed, R., He, S., Modeling of Yield-Power-Law Fluid Flow in a Partially Blocked Concentric Annulus, Journal of Natural Gas Science and Engineering, Volume 35, Part A, pp. 555-566. 2016.

Thomas, R.P., Azar, J.J., and Becker, T.E., Drillpipe Eccentricity Effect on Drilled Cuttings Behavior in Vertical Wellbores, J. Petrol. Technol. pp. 1929-1937, 1982.

Tomren, P. H., Iyoho, A. W., & Azar, J. J. Experimental Study of Cuttings Transport in Directional Wells. SPE-12123-PA. 1986.

Tu, J.; Yeoh, G.H.; Liu, C. Computational Fluid Dynamics: A Practical Approach, 2nd Edition. Burlington: 577 Butterworth-Heinemann, 456 p. ISBN-13: 978-0080982434. 2008.

Walker, S., & Li, J. The Effects of Particle Size, Fluid Rheology, and Pipe Eccentricity on Cuttings Transport. SPE-60755-MS. 2000.

Wang, Z., Guo, X., Li, M. Effect of Drillpipe Rotation on Borehole Cleaning for Extended Reach Well. Journal of Hydrodynamics. Vol. 21, Issue 3, pp. 366-372. 2009.

Wiberg, P. L., and Rubin, D. M. Bed Roughness Produced by Saltating Sediment, J. Geophys. Res., 94 (C4), 5011– 5016. 1989.

Wilson, K.C. Bed-Load Transport at High Shear Stress. Proc. ASCE Journal of Hydrodynamics. Div. 113 (1) pp. 97-103. 1987.

Zamora, M., & Hanson, P. Selected Studies in High-Angle Hole Cleaning. Paper IPA 90-228 presented at the 19th Annual Conv., Indonesian Petroleum Association. 1990.

APPENDIX A

DERIVATION OF PI GROUPS

DIMENSIONLESS VARIABLE, π_1

$\pi_1 = (h_n)(d_h)^a(\rho_f)^b(U)^c$

Substituting the basic dimensions of each variable,

$\rightarrow M^0L^0T^0 = [-][L]^a[ML^{-3}]^b[LT^{-1}]^c$

$\rightarrow M^0L^0T^0 = [M]^b[L]^{a-3b+c}[T]^{-c}$

Comparing the terms of M, L and T on both sides,

$b = 0; \quad a - 3b + c = 0; \quad -c = 0$

Solving these equations result in,

$a = 0; \quad b = 0; \quad c = 0$

Therefore,

$$\boldsymbol{\pi_1 = h_n} \qquad \textbf{(A1)}$$

DIMENSIONLESS VARIABLE, π_2

$\pi_2 = (\mu_a)(d_h)^a(\rho_f)^b(U)^c$

Substituting the basic dimensions of each variable,

$\rightarrow M^0L^0T^0 = [ML^{-1}T^{-1}][L]^a[ML^{-3}]^b[LT^{-1}]^c$

$\rightarrow M^0L^0T^0 = [M]^{1+b}[L]^{-1+a-3b+c}[T]^{-1-c}$

Comparing the terms of M, L and T on both sides,

$1 + b = 0; -1 + a - 3b + c = 0; -1 - c = 0$

Solving these equations result in,

$a = -1; \quad b = -1; \quad c = -1$

Therefore,

$$\boldsymbol{\pi_2 = \mu_a/(d_h \rho_f U)} \qquad \textbf{(A2)}$$

DIMENSIONLESS VARIABLE, π_3

$\pi_3 = (g)(d_h)^a(\rho_f)^b(U)^c$

Substituting the basic dimensions of each variable,

$\rightarrow M^0L^0T^0 = [LT^{-2}][L]^a[ML^{-3}]^b[LT^{-1}]^c$

$\rightarrow M^0L^0T^0 = [M]^b[L]^{1+a-3b+c}[T]^{-2-c}$

Comparing the terms of M, L and T on both sides,

$b = 0; \quad 1 + a - 3b + c = 0; \quad -2 - c = 0$

Solving these equations result in,

$a = 1; \quad b = 0; \quad c = -2$

Therefore,

$$\boldsymbol{\pi_3 = g d_h/U^2} \qquad \textbf{(A3)}$$

DIMENSIONLESS VARIABLE, π_4

$\pi_4 = (t)(d_h)^a(\rho_f)^b(U)^c$

Substituting the basic dimensions of each variable,

$\rightarrow M^0L^0T^0 = [T][L]^a[ML^{-3}]^b[LT^{-1}]^c$

$\rightarrow M^0L^0T^0 = [M]^b[L]^{a-3b+c}[T]^{1-c}$

Comparing the terms of M, L and T on both sides,

$b = 0; \quad a - 3b + c = 0; \quad 1 - c = 0$

Solving these equations result in,

$a = -1; \quad b = 0; \quad c = 1$

Therefore,

$$\boldsymbol{\pi_4 = Ut/d_h} \qquad \textbf{(A4)}$$

DIMENSIONLESS VARIABLE, π_5

$\pi_5 = (\rho_s)(d_h)^a(\rho_f)^b(U)^c$

Substituting the basic dimensions of each variable,

$\rightarrow M^0L^0T^0 = [ML^{-3}][L]^a[ML^{-3}]^b[LT^{-1}]^c$

$\rightarrow M^0L^0T^0 = [M]^{1+b}[L]^{-3+a-3b+c}[T]^{-c}$

Comparing the terms of M, L and T on both sides,

$1 + b = 0; \quad -3 + a - 3b + c = 0; \quad -c = 0$

Solving these equations result in,

$a = 0; \quad b = -1; \quad c = 0$

Therefore,

$$\boldsymbol{\pi_5 = \rho_s/\rho_f} \qquad \textbf{(A5)}$$

DIMENSIONLESS VARIABLE, π_6

$\pi_6 = (d_p)(d_h)^a(\rho_f)^b(U)^c$

Substituting the basic dimensions of each variable,

$\rightarrow M^0L^0T^0 = [L][L]^a[ML^{-3}]^b[LT^{-1}]^c$

$\rightarrow M^0L^0T^0 = [M]^b[L]^{1+a-3b+c}[T]^{-c}$

Comparing the terms of M, L and T on both sides,

$b = 0; \quad 1 + a - 3b + c = 0; \quad -c = 0$

Solving these equations result in,

$a = -1; \quad b = 0; \quad c = 0$

Therefore,

$$\boldsymbol{\pi_6 = d_p/d_h} \qquad \textbf{(A6)}$$

DIMENSIONLESS VARIABLE, $\boldsymbol{\pi_7}$

$\pi_7 = (\theta)(d_h)^a(\rho_f)^b(U)^c$

Substituting the basic dimensions of each variable,

$\rightarrow M^0L^0T^0 = [-][L]^a[ML^{-3}]^b[LT^{-1}]^c$

$\rightarrow M^0L^0T^0 = [M]^b[L]^{a-3b+c}[T]^{-c}$

Comparing the terms of M, L and T on both sides,

$b = 0; \quad a - 3b + c = 0; \quad -c = 0$

Solving these equations result in,

$a = 0; \quad b = 0; \quad c = 0$

Therefore,

$$\boldsymbol{\pi_7 = \theta} \qquad \textbf{(A7)}$$

Further simplification of parameters can be carried out using arithmetic operations to obtain final dimensionless (Π) groups as follows:

$\Pi_1 = \pi_1 = h_n$ $\qquad$ $\Pi_2 = \dfrac{1}{\pi_2} = \dfrac{\rho_f U d_h}{\mu_a}$

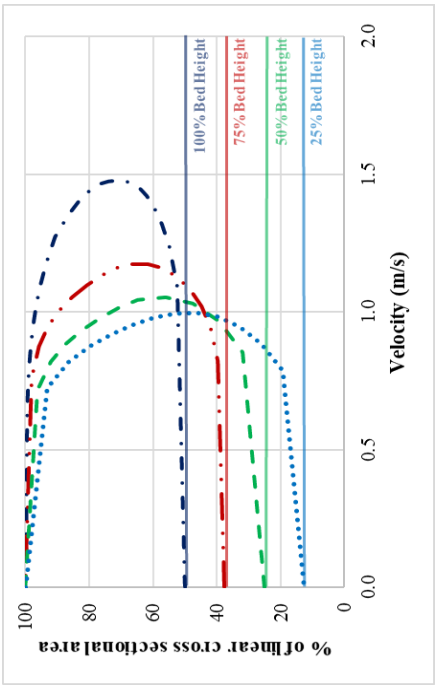
$\Pi_3 = \pi_3 * \pi_4^2 = \dfrac{g d_h}{U^2} * \dfrac{U^2 t^2}{d_h^2} = \dfrac{g t^2}{d_h}$ $\qquad$ $\Pi_4 = \pi_5 = \dfrac{\rho_s}{\rho_f}$

$\Pi_5 = \pi_6 * \dfrac{l^2}{d_p^2} = \dfrac{l}{d_p d_h}$ $\qquad$ $\Pi_6 = \dfrac{(\pi_3)^{-\frac{1}{2}}}{\sin(\pi_7)} = \dfrac{U}{\sqrt{(g.sin\theta d_h)}}$

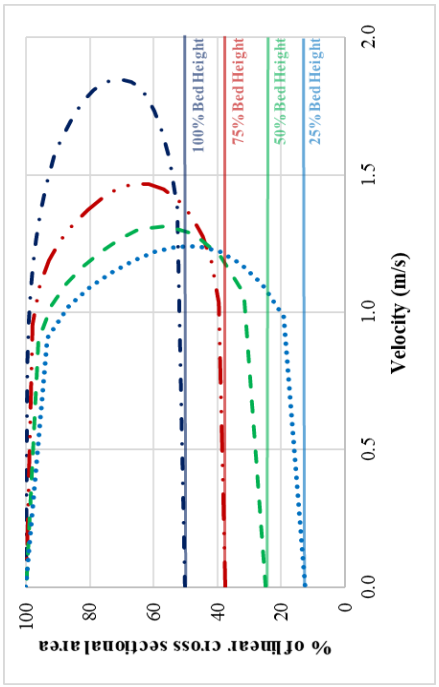
APPENDIX B

VELOCITY PROFILES FOR DIFFERENT FLUIDS AT VARIOUS BED HEIGHTS AND FLOW RATES

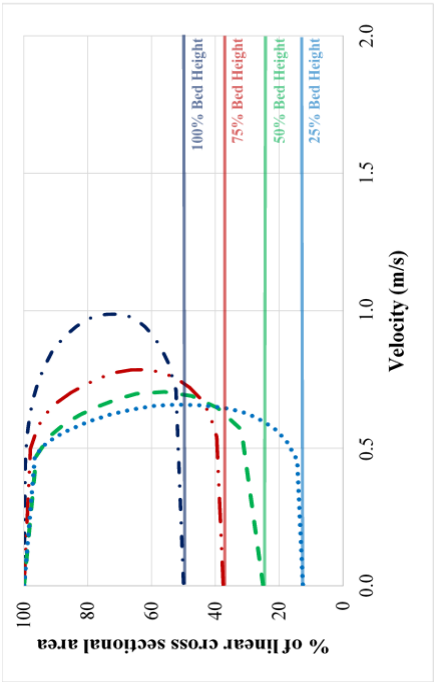
FLUID 1



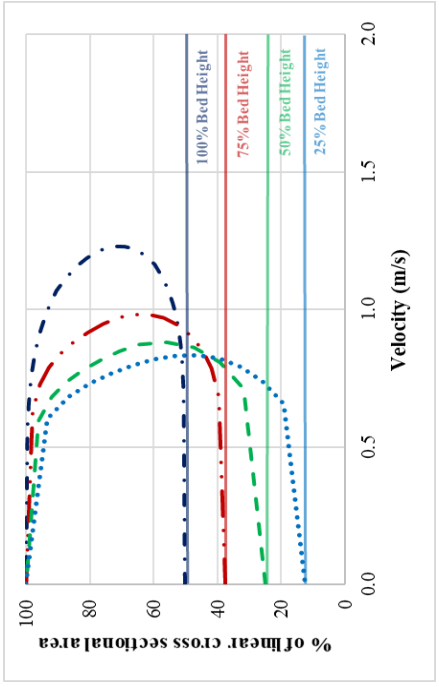
7.57 L/s



9.46 L/s

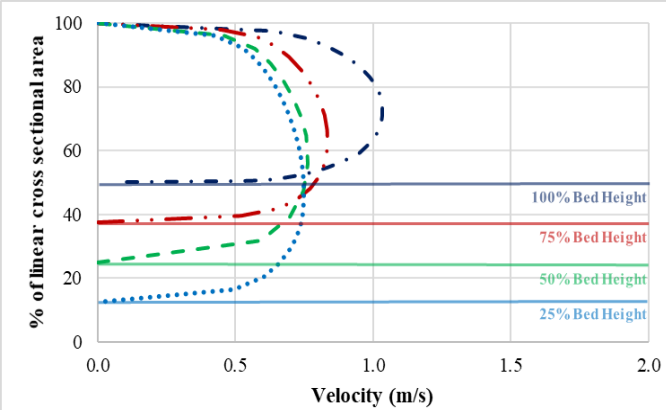


5.05 L/s

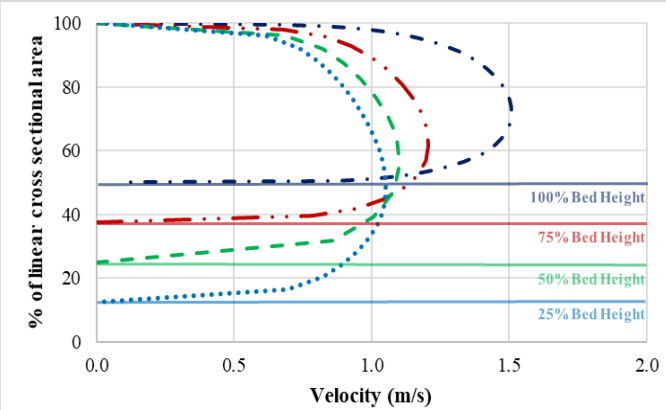


6.31 L/s

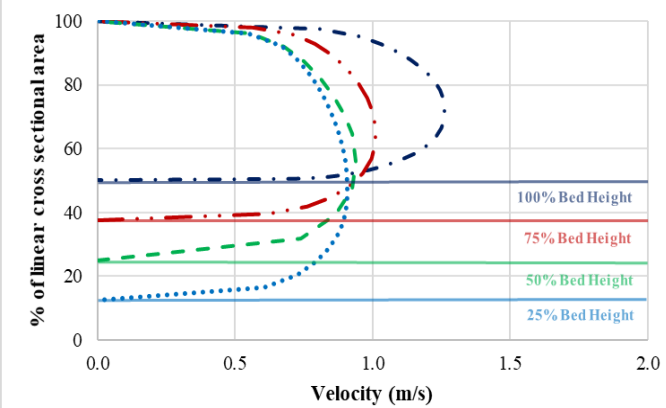
FLUID 2



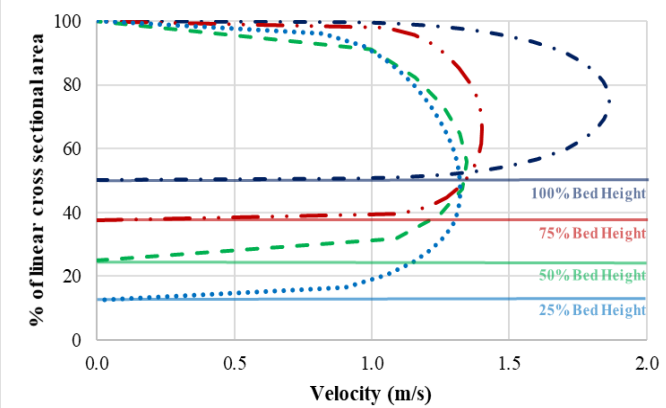
5.05 L/s



7.57 L/s

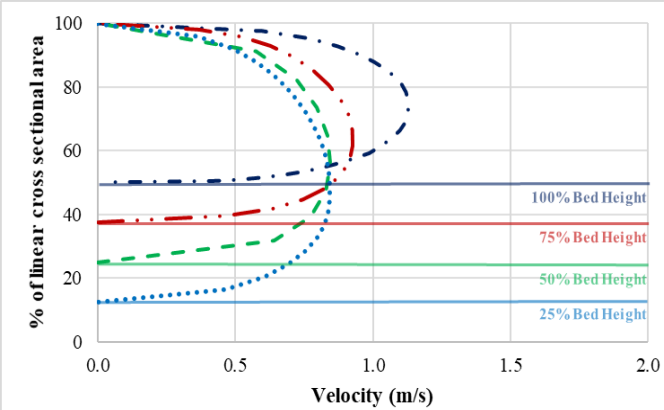


6.31 L/s

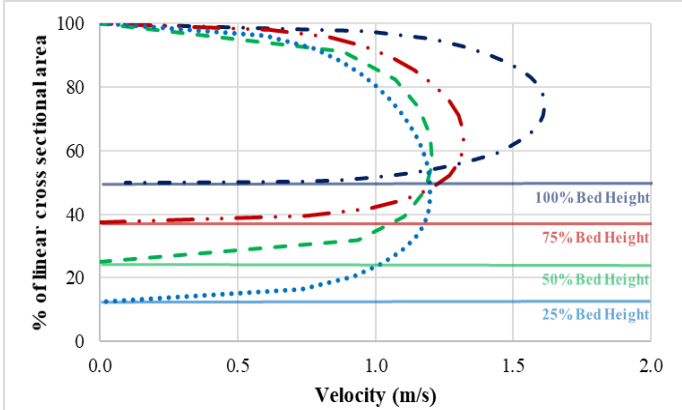


9.46 L/s

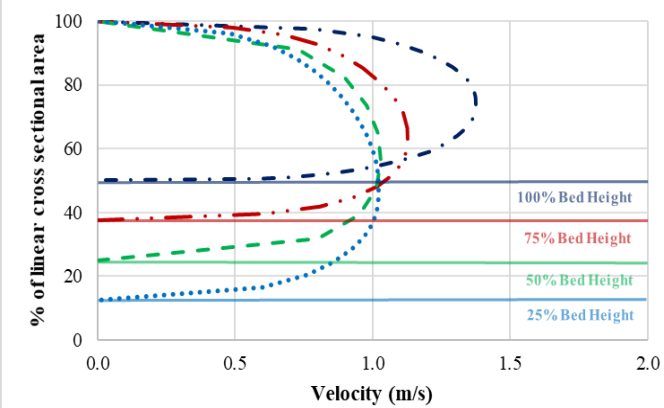
FLUID 3



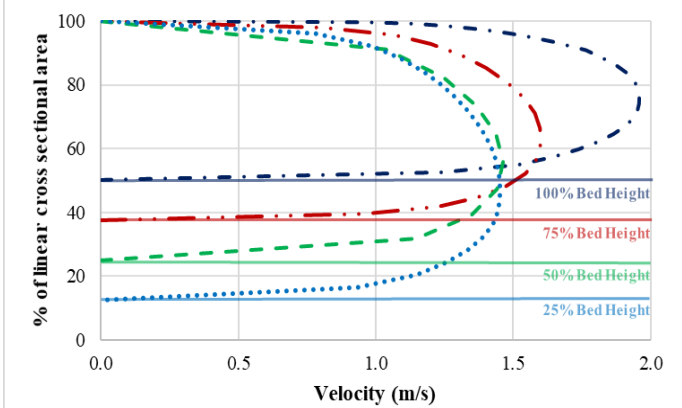
5.05 L/s



7.57 L/s



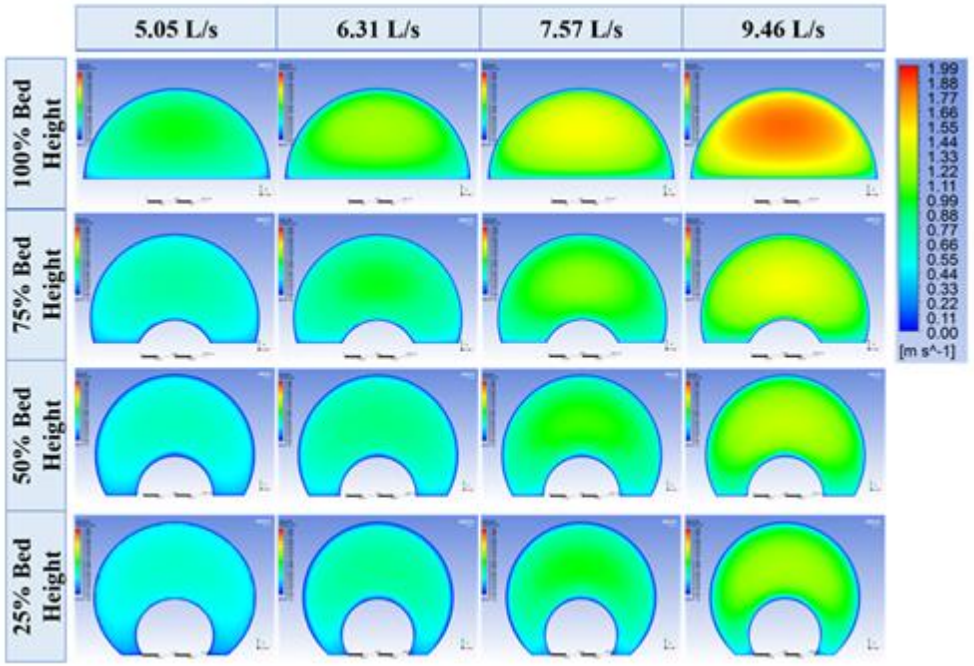
6.31 L/s



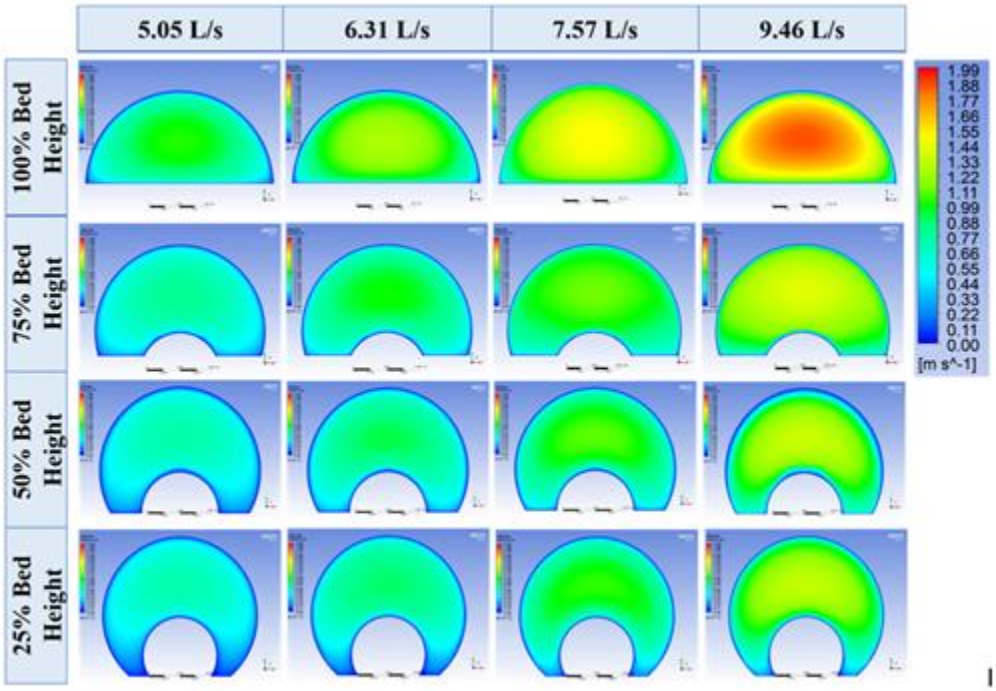
9.46 L/s

APPENDIX C

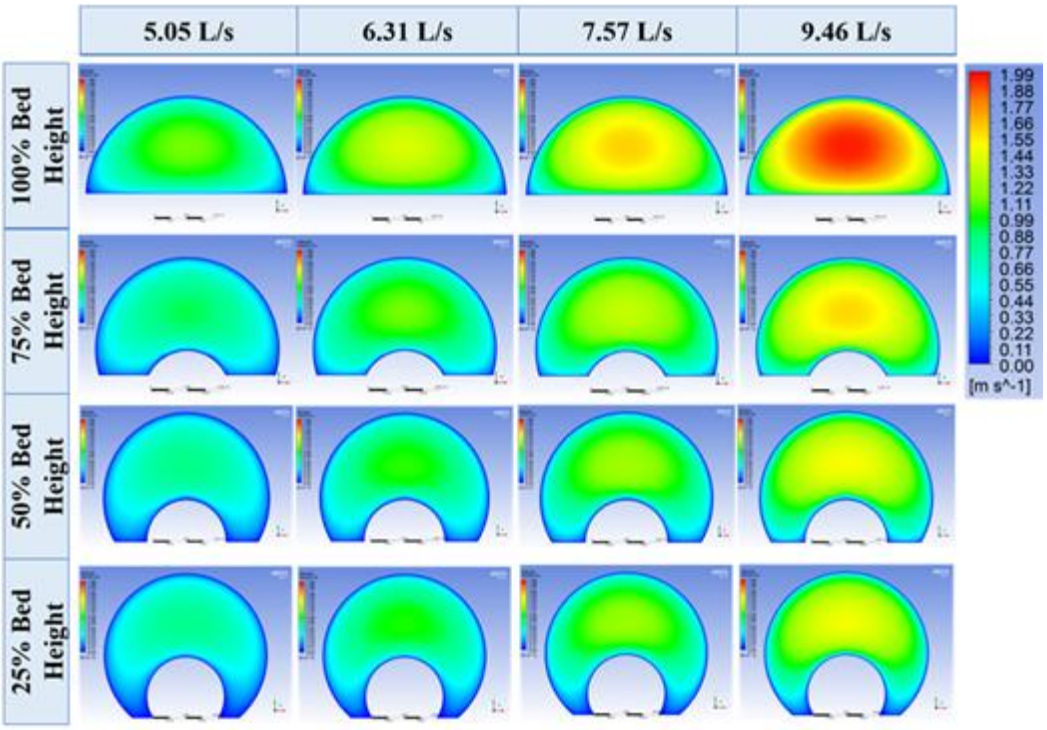
VELOCITY CONTOUR PLOTS – CONSTANT FLUID



Fluid 1



Fluid 2


5.05 L/s
6.31 L/s
7.57 L/s
9.46 L/s
100% Bed Height
75% Bed Height
50% Bed Height
25% Bed Height
1.99
1.88
1.77
1.66
1.55
1.44
1.33
1.22
1.11
0.99
0.88
0.77
0.66
0.55
0.44
0.33
0.22
0.11
0.00
[m s^-1]

Fluid 3

APPENDIX D

VELOCITY CONTOUR PLOTS – CONSTANT FLOW RATE

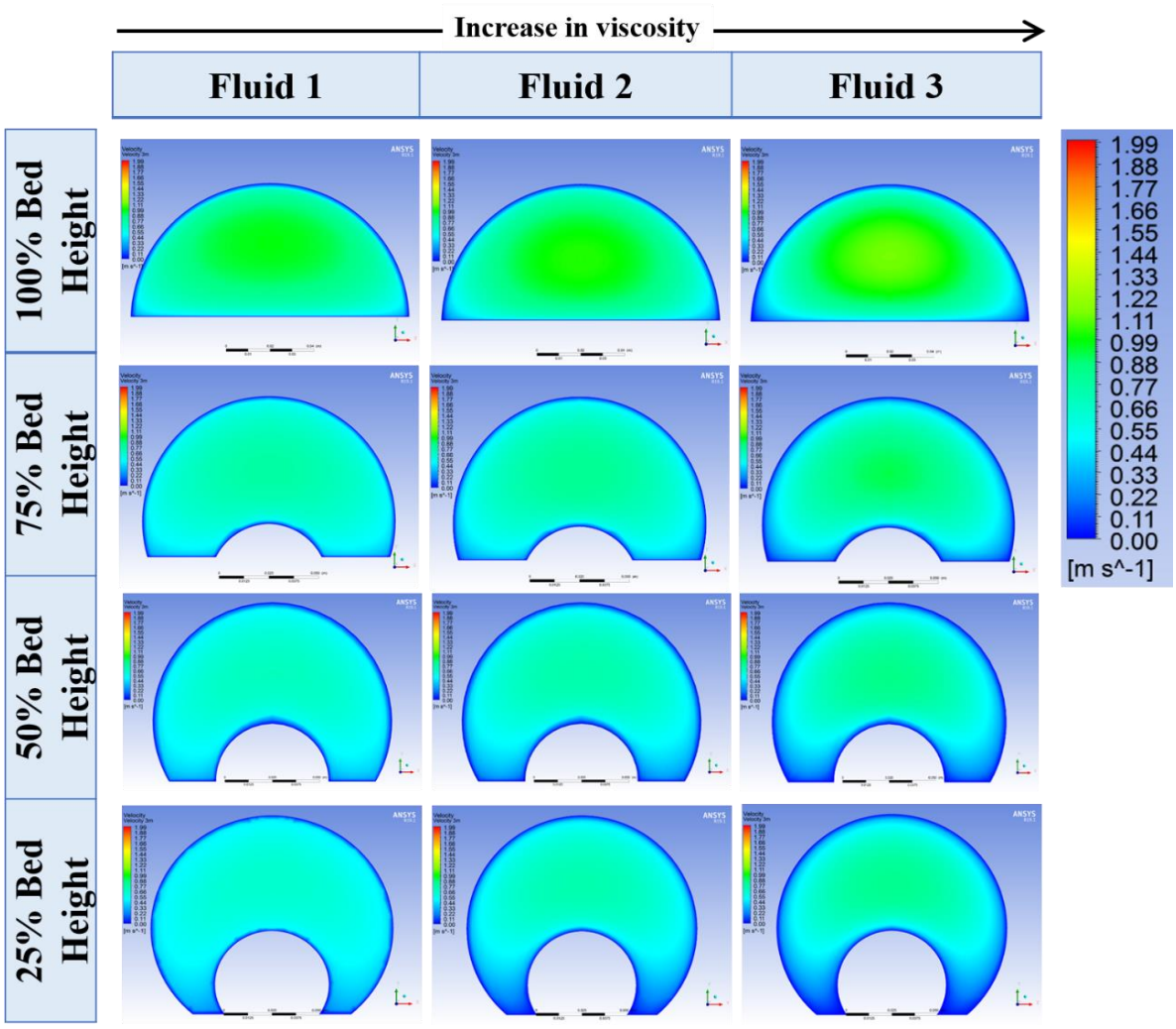


Fig. D1: Velocity contour plots for different fluids with various bed height at 5.05 L/s.

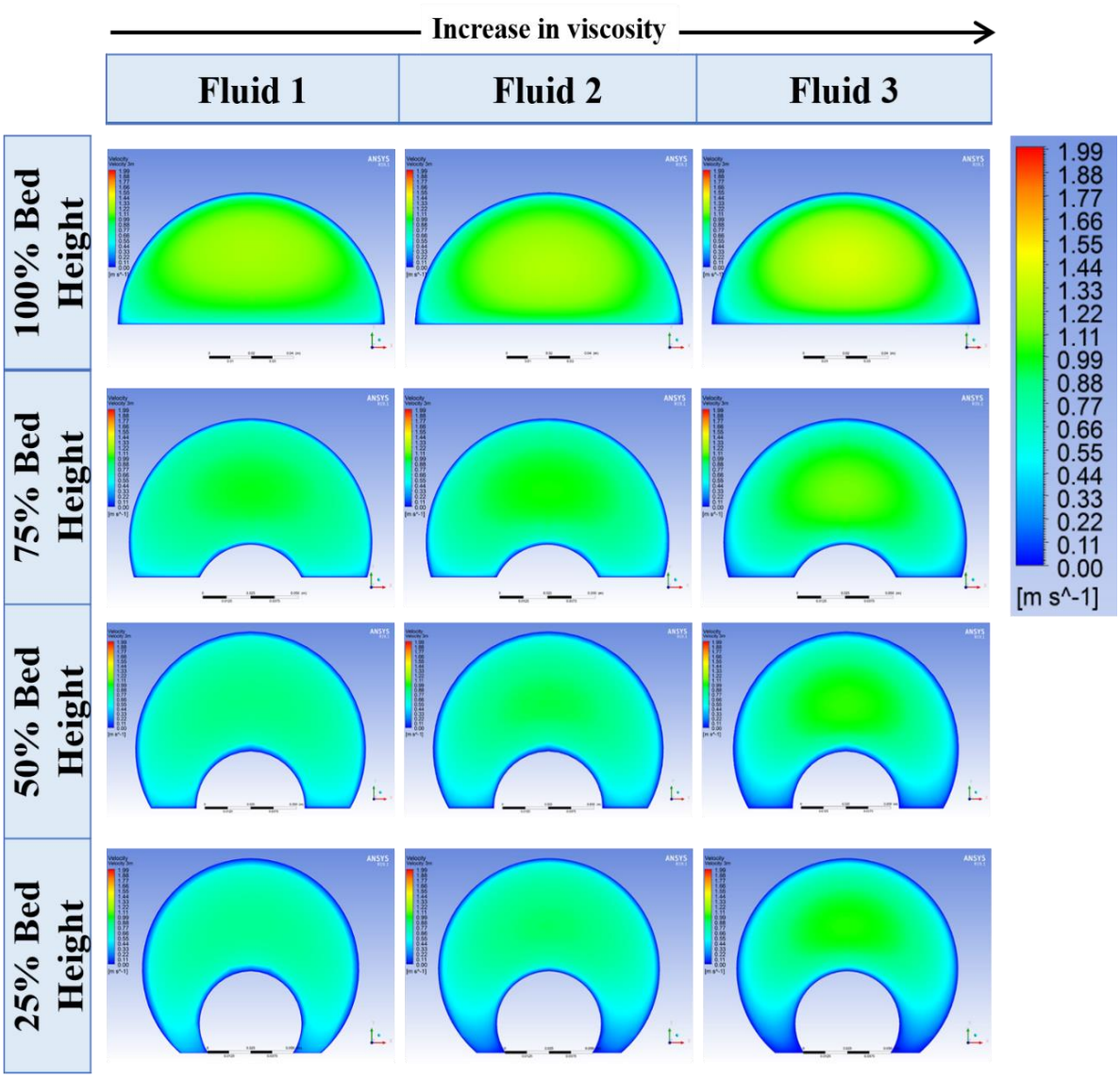


Fig. D2: Velocity contour plots for different fluids with various bed height at 6.31 L/s.

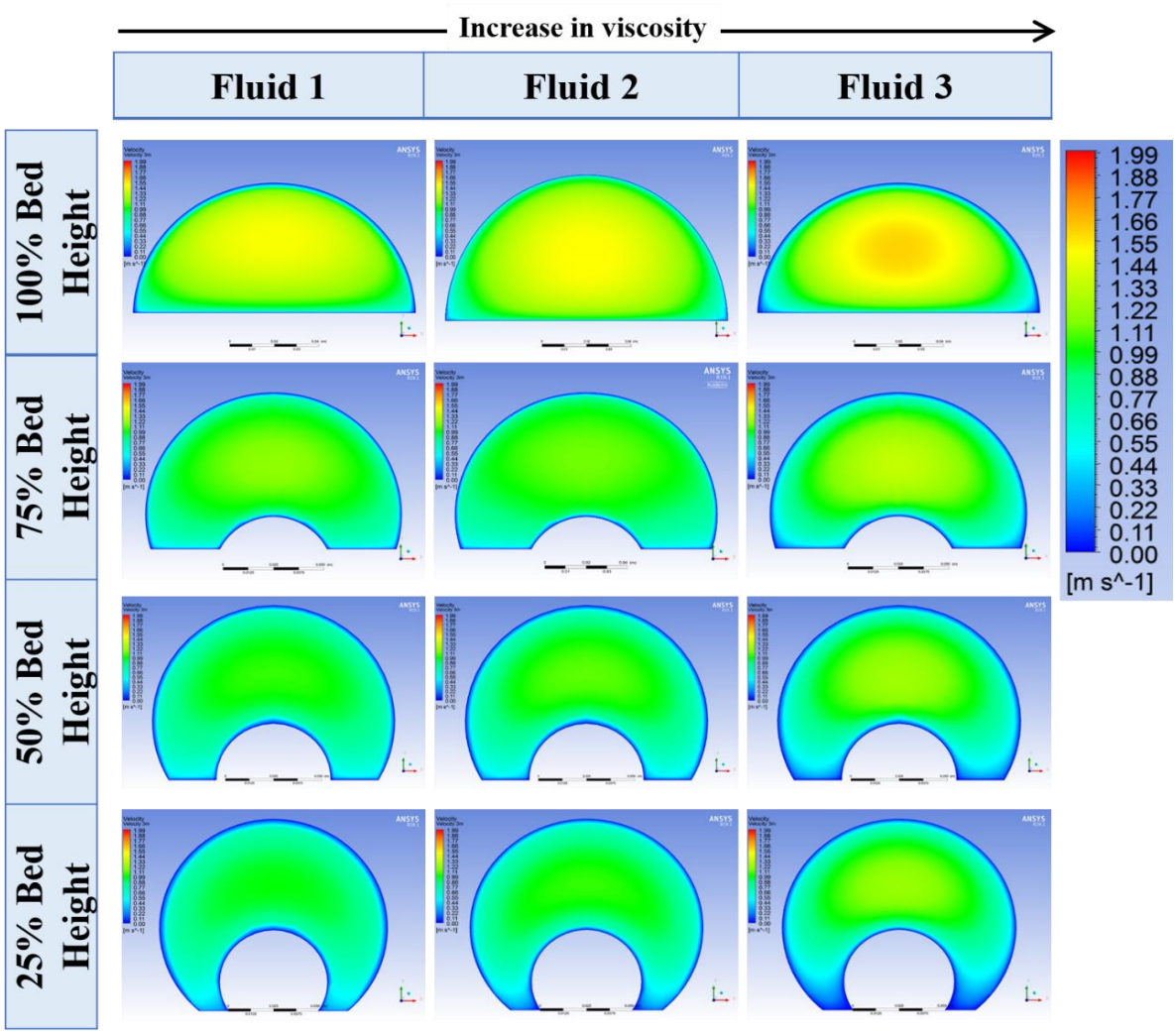


Fig. D3: Velocity contour plots for different fluids with various bed height at 7.57 L/s.

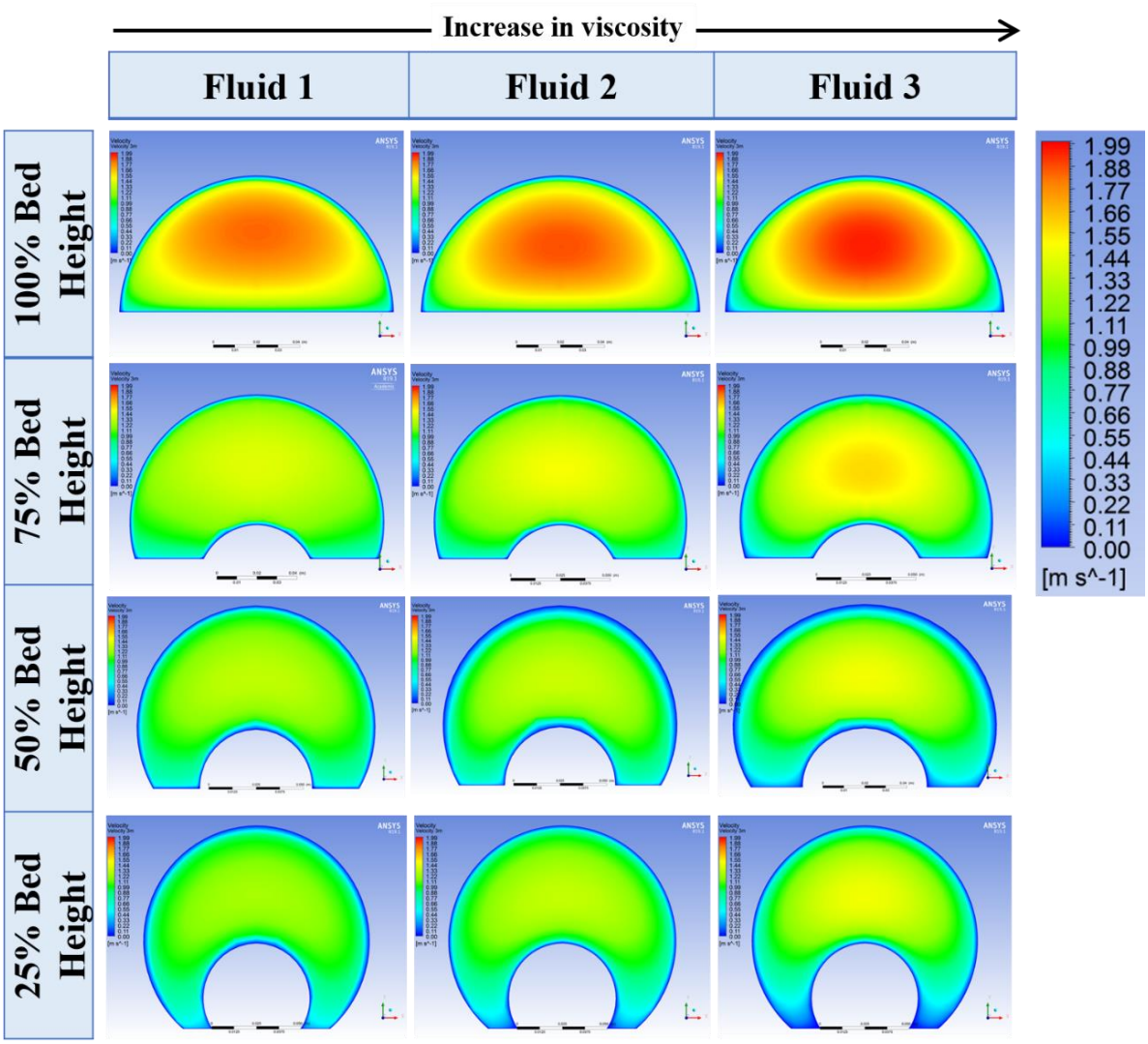
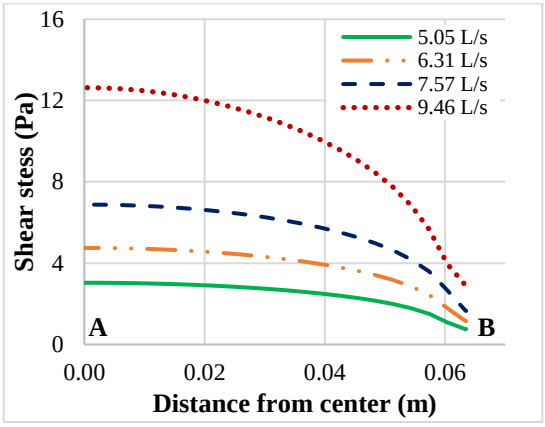


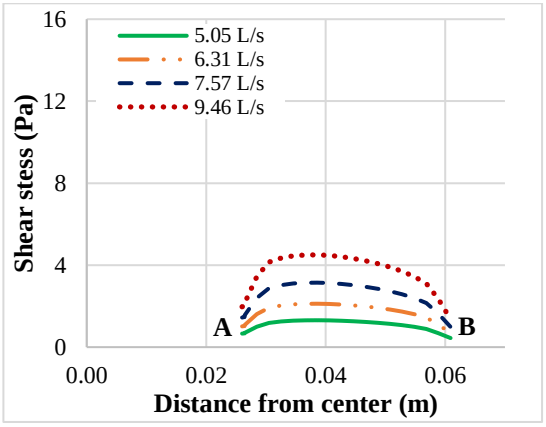
Fig. D4: Velocity contour plots for different fluids with various bed height at 9.46 L/s.

APPENDIX E

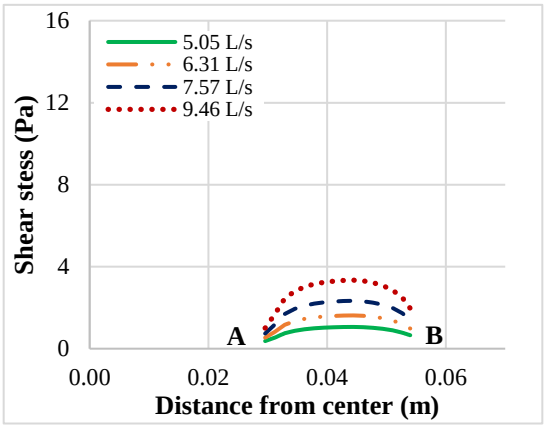
BED SHEAR STRESS PROFILES FOR DIFFERENT FLUIDS



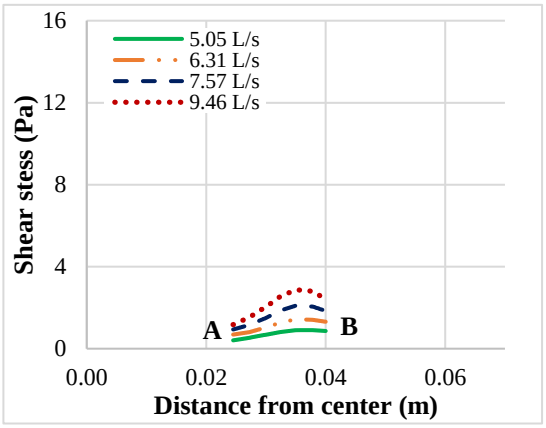
(a) 100% Bed Height



(b) 75% Bed Height

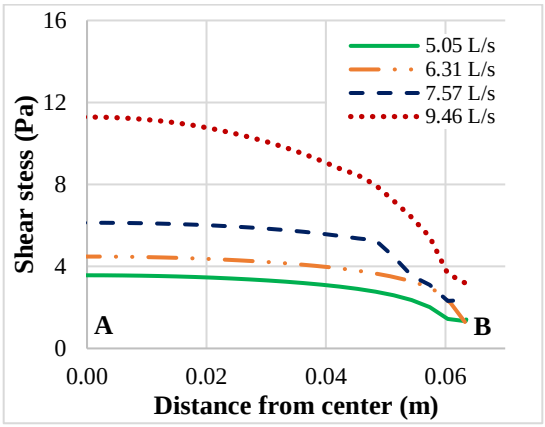


(c) 50% Bed Height

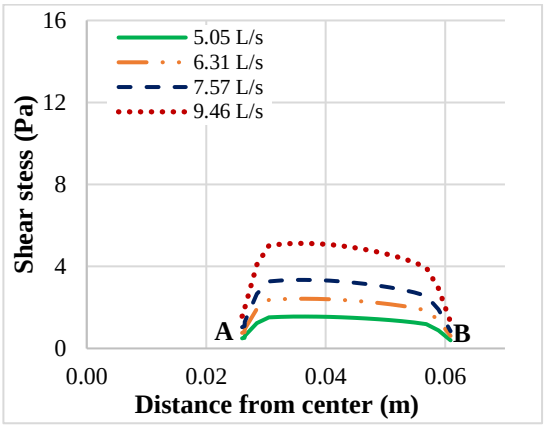


(d) 25% Bed Height

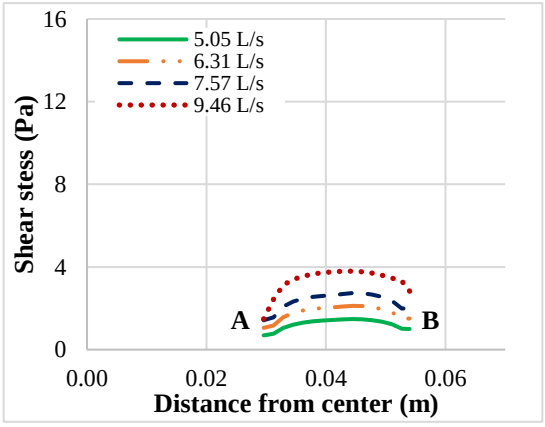
Fig. E1: Bed shear stress profiles for Fluid 1 at various bed heights and flow rates.



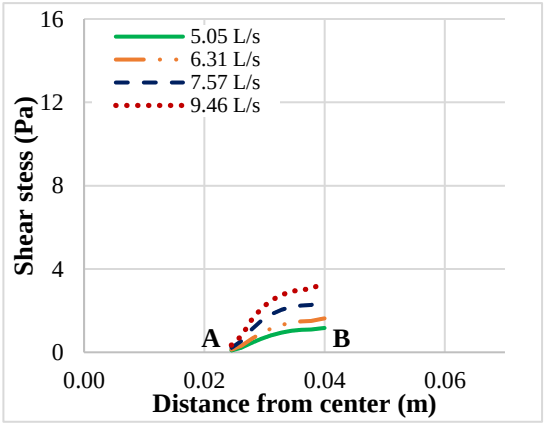
(a) 100% Bed Height



(b) 75% Bed Height

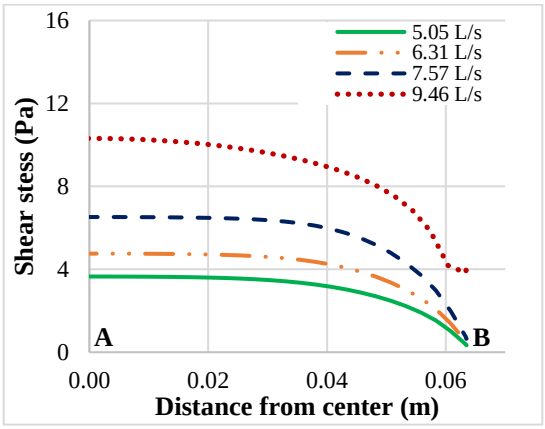


(c) 50% Bed Height

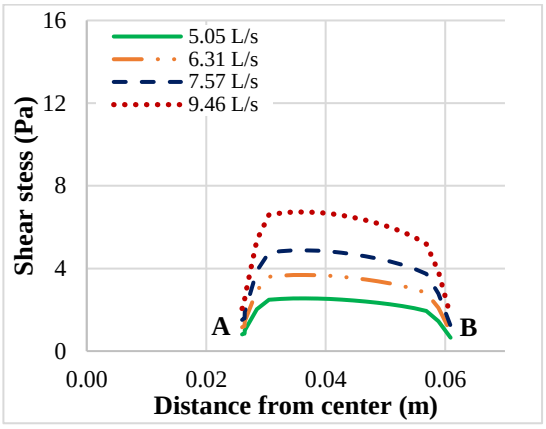


(d) 25% Bed Height

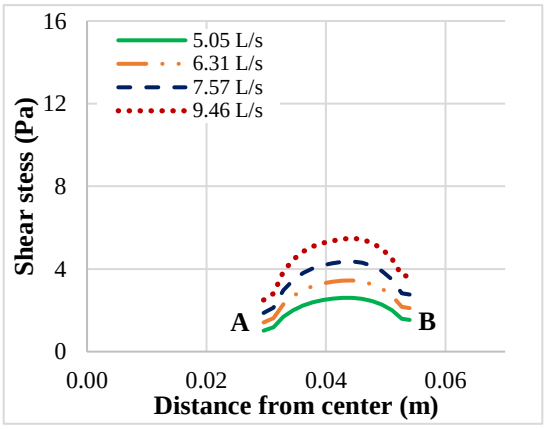
Fig. E2: Bed shear stress profiles for Fluid 2 at various bed heights and flow rates.



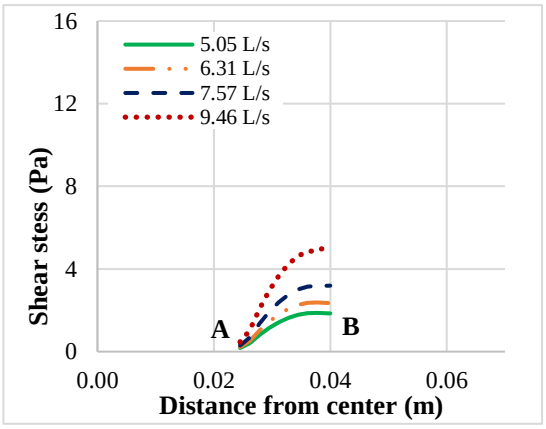
(a) 100% Bed Height



(b) 75% Bed Height



(c) 50% Bed Height



(d) 25% Bed Height

Fig. E3: Bed shear stress profiles for Fluid 3 at various bed heights and flow rates.